

# Journal of Print and Media Technology Research

## Scientific contents

Modelling reflectance factor for special effect  
pigment coatings

*Nina Rogelj and Marta Klanjšek Gunde*

247

Ink adhesion failure during full scale offset printing:  
causes and impact on print mottle

*Hajer Kamal Alm, Göran Ström, Joachim Schoelkopf,  
Cathy Ridgway and Patrick A. C. Gane*

257

Soybean oil based inks for enhanced  
deinkability of litho prints

*Veronika Husovska, Jan Pekarovic,  
Alexandra Pekarovicova and Paul D. Fleming III*

279

Self-supported printed multi-layer capacitors

*Michael James Joyce, Ali Eshkeiti, Paul D. Fleming III,  
Alexandra Pekarovicova and Massood Zandi Atashbar*

285



9 772223 890003

Editor-in-Chief

Gorazd Golob (Ljubljana)

Published by **iarigai**

The International Association of Research  
Organizations for the Information, Media  
and Graphic Arts Industries

[www.iarigai.org](http://www.iarigai.org)

# Journal of Print and Media Technology Research

A peer-reviewed quarterly

## PUBLISHED BY

The International Association of Research Organizations  
for the Information, Media and Graphic Arts Industries  
Magdalenenstrasse 2, D-64288 Darmstadt, Germany  
<http://www.iarigai.org> E-mail: [journal@iarigai.org](mailto:journal@iarigai.org)

## EDITORIAL BOARD

### EDITOR-IN-CHIEF

Gorazd Golob (Ljubljana, Slovenia)

### EDITORS

Timothy C. Claypole (Swansea, UK)  
Edgar Dörsam (Darmstadt, Germany)  
Nils Enlund (Helsinki, Finland)  
Mladen Lovreček (Zagreb, Croatia)  
Renke Wilken (Munich, Germany)  
Scott Williams (Rochester, USA)

### ASSOCIATE EDITOR

Markéta Držková (Pardubice, Czech Republic)

## SCIENTIFIC ADVISORY BOARD

Darko Agić (Zagreb, Croatia)  
Anne Blayo (Grenoble, France)  
Wolfgang Faigle (Stuttgart, Germany)  
Elena Fedorovskaya (Rochester, USA)  
Patrick Gane (Helsinki, Finland)  
Diana Gregor Svetec (Ljubljana, Slovenia)  
Jon Yngve Hardeberg (Gjøvik, Norway)  
Ulrike Herzau Gerhardt (Leipzig, Germany)  
Gunter Hübner (Stuttgart, Germany)  
Marie Kaplanová (Pardubice, Czech Republic)  
John Kettle (Espoo, Finland)  
Helmut Kipphan (Schwetzingen, Germany)  
Björn Kruse (Linköping, Sweden)  
Yuri Kuznetsov (St. Petersburg, Russian Federation)  
Magnus Lestelius (Karlstad, Sweden)  
Patrice Mangin (Trois Rivières, Canada)  
Thomas Mejtoft (Umeå, Sweden)  
Erzsébet Novotny (Budapest, Hungary)  
Anastasios Politis (Athens, Greece)  
Anu Seisto (Espoo, Finland)  
Johan Stenberg (Stockholm, Sweden)  
Philipp Urban (Darmstadt, Germany)

## A mission statement

To meet the need for a high quality scientific publishing in its research fields of interest, the International Association of Research Organizations for the Information, Media and Graphic Arts Industries (iarigai) publishes the peer reviewed quarterly Journal of Print and Media Technology Research.

The Journal is fostering multidisciplinary research and scholarly discussion on scientific and technical issues in the field of graphic arts and media communication, thereby advancing scientific research, knowledge creation and industry development. Its aim is to be the leading international scientific periodical in the field, offering publishing opportunities and serving as a forum for knowledge exchange between all those scientist and researchers interested in contributing to or benefiting from research in the related fields.

By regularly publishing peer-reviewed high quality research articles, position papers, survey and case studies, the Journal will consistently promote original research, networking, international collaboration and the exchange of ideas and know how. Editors will also consider for publication review articles, topical and professional communications, as well as opinions and reflections of interest to the readers. The Journal will also provide multidisciplinary discussion on research issues within the field and on the effects of new scientific and technical development on society, industry and the individual. Thus, it will serve the entire research community, as well as the global graphic arts and media industry.

The Journal will cover fundamental and applied aspects of at least, but not limited to the following fields of research:

### Printing technology and related processes

- ◇ Conventional and special printing
- ◇ Packaging
- ◇ Printed fuel cells and other printed functionality
- ◇ Printing on biomaterials
- ◇ Textile and fabric printing
- ◇ Materials science
- ◇ Process control

### Premedia technology and processes

- ◇ Color management and color reproduction
- ◇ Image and reproduction quality
- ◇ Image carriers (physical and virtual)
- ◇ Workflow management
- ◇ Content management

### Emerging media and future trends

- ◇ Media industry developments
- ◇ Developing media communication value system
- ◇ Online and mobile media development
- ◇ Cross-media publishing

### Social impacts

- ◇ Environmental issues and sustainability
- ◇ Consumer perception and media use
- ◇ Social trends and their impact on media

---

### Submissions to the Journal

Submission details and guidelines for authors can be found on the inside back cover of this issue, as well as downloaded from <http://www.iarigai.org/publications/journal>.

### Subscriptions

<http://www.iarigai.org/publications/journal/order>  
or send your request to [office@iarigai.org](mailto:office@iarigai.org).

---

✉ Contact the Editorial office: [journal@iarigai.org](mailto:journal@iarigai.org)

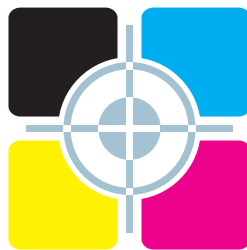
# Journal of Print and Media Technology Research

---

4-2015

---

December 2015



The information published in this journal is obtained from sources believed to be reliable and the sole responsibility on the contents of the published papers lies with their authors. The publishers can accept no legal liability for the contents of the papers, nor for any information contained therein, nor for conclusions drawn by any party from it.

Journal of Print and Media Technology Research is listed in:

Index Copernicus International  
PiraBase and PaperBase (by Smithers Pira)  
NSD – Norwegian Register for  
Scientific Journals, Series and Publishers

## Contents

A letter from the Editor <i>Gorazd Golob</i>	245
Errata	246
Scientific contributions	
Modelling reflectance factor for special effect pigment coatings <i>Nina Rogelj and Marta Klanjšek Gunde</i>	247
Ink adhesion failure during full scale offset printing: causes and impact on print mottle <i>Hajer Kamal Alm, Göran Ström, Joachim Schoelkopf, Cathy Ridgway and Patrick A. C. Gane</i>	257
Soybean oil based inks for enhanced deinkability of litho prints <i>Veronika Husovska, Jan Pekarovic, Alexandra Pekarovicova and Paul D. Fleming III</i>	279
Self-supported printed multi-layer capacitors <i>Michael James Joyce, Ali Eshkeiti, Paul D. Fleming III, Alexandra Pekarovicova and Masood Zandi Atashbar</i>	285
<hr/>	
Topicalities	
<i>Edited by Markéta Držková</i>	
News & more	303
Bookshelf	305
Events	311



## A letter from the Editor

*Gorazd Golob*

Editor-in-Chief

E-mail: gorazd.golob@jpmtr.org

journal@iarigai.org

In front of you it is the last issue of our Journal in 2015. During the last four years of successful publishing of this journal, this title has become very relevant to the progress and consolidation of our extensive scientific and research fields.

I would like to take this opportunity to express my sincere acknowledgement to all the authors, reviewers, editors and *iarigai* – the publisher, and also to our readers and users to whom the Journal represents an important resource and reference of their research activities. Only with your full active contributions, support and cooperation, we can together persist and become more visible and recognized. We want to continue on this path and become even better, more broadly accepted in the wider scientific and research community.

In this issue only four papers are published, however, the total page range is comparable with previous releases. Two of the published papers have increased in volume. Despite the decision of the reviewers and editors to classify them as Research and Original scientific papers, due to the extensive experimental content and comments, some elements of Review papers can be recognised in them. A comprehensive theoretical introduction, which gives a deep insight into the specific area of research, represents important added value to common published papers. All four articles bring important information on research results, presented in different areas – from modelling of reflectance spectra over the study of print mottling, deinkability of soybean based inks to the advances in printed capacitors.

Topicalities section, prepared by Markéta Držková (marketa.drzkova@jpmtr.org), is bringing news on drupa, the top forthcoming event in 2016 for our community, together with an interesting overview on new books published, three doctoral thesis and events announced for next months.

This issue of the Journal is also the last to be published in printed form. From 2016 the Journal will be published digitally for all *iarigai* members, subscribers and other recipients. For a surcharge it will be possible to subscribe to the printed edition of the Journal. The basic structure of the content and format will remain unchanged for one year and during this time we will prepare a revised concept, with design and typographic solutions more adapted to the digital medium. The Journal will also have a new, additional ISSN code. Papers from previous volumes, with embargo of six months, will be published in open access mode. With this decision, the Journal will become even more recognised and hopefully even more widespread among scientists and researchers in our multidisciplinary area.

On the next page you will find a novelty in the Journal, the Errata section is introduced. *Errare humanum est* – to err is human, and our intention is to release revisions to allow a credible publication and use of research results, comments and conclusions. Errors may occur already by the authors or they may have been overlooked or committed by reviewers or editor, often as a result of mistakes in the formatting and conversion of files in processing manuscript into the final form suitable for publication. It is difficult to completely avoid them, however we have to consider them and publish corrections. In this issue corrections are published only for Vol. 4, published in 2015. The publication of the digital archive of papers will be corrected for any known errors, and of course, properly documented.

At the same time, I would like to call on all critical readers and users of the Journal, let us draw attention to errors they encounter, and the results and conclusions with which they disagree, with clear argumentation. Checking of research methods used, published results and the resulting comments and conclusions is one of the bases of scientific research. We will gladly post your letters and other open discussion between the authors, critics, reviewers and editors.

On behalf of the Editorial Board and all active participants and contributors to the Journal of Print and Media Technology Research I wish you a lot of success and excellent publications in the New year 2016!

Ljubljana, December 2015

## Errata

*The following corrections are to be made:*

### 4(2015)1

*Title on the spine:* Journal of Print and Media Technology Research

*instead of* Journal of Print and Media Technoloy Research

### 4(2015)2

*Scientific contents on cover and Contents in preliminary pages (p. 83):*

Effects of awareness to security features on the confidence in banknotes  
Osamu Masuda, Marius Pedersen, Jon Y. Hardeberg 103

Security offset printing with twin colors by means of CMYF separation  
Branka Morić Kolarić, Ivana Žiljak Stanimirović, Ivana Bak 111

*instead of* Security offset printing with twin colors by means of CMYF separation  
Branka Morić Kolarić, Ivana Žiljak Stanimirović, Ivana Bak 103

Effects of awareness to security features on the confidence in banknotes  
Osamu Masuda, Marius Pedersen, Jon Y. Hardeberg 111

### 4(2015)3

*Page 211:* The Figures 10 and 11 are in the right position but their captions are switched.

JPMTR 069 | 1504  
DOI 10.14622/JPMTR-1504  
UDC 53.07 : 535.3 | 667.6

Original scientific paper  
Received: 2015-08-10  
Accepted: 2015-11-04

## Modelling reflectance factor for special effect pigment coatings

*Nina Rogelj<sup>1</sup> and Marta Klanjšek Gunde<sup>2</sup>*

<sup>1</sup> University of Eastern Finland, Institute of Photonics,  
Joensuu, P.O.Box 111, Finland

E-mail: nina.rogelj@uef.fi

<sup>2</sup> National Institute of Chemistry,  
Ljubljana, Hajdrihova 19, Slovenia

E-mail: marta.k.gunde@ki.si

### Abstract

A numerical model to calculate goniometric reflectance factor for effect coatings with interference flakes was developed and analysed here. The model incorporates three parts of the light scattering events; from the front surface of the coating, from pigments inside the coating, and from the coating substrate. In order to validate the model, reflectance spectra were measured at an incident angle of 45° and at reflected angles of -60°, -30°, -20°, 0°, 30° and 65° using a commercial multi-angle spectrometer. Metal lustre coating was used for testing the model. It contains Iriodin 4504 pigment, an interference mica-based pigment coated with iron (III) oxide from Merck. This coating includes all spectral characteristics involved in the model. The thickness of the interference layer on the pigments was adjusted to obtain good matches of interference features between modelled and measured reflectance factor. The influence of surface coverage by pigments and of the pigment orientation distribution on the resulting spectra was analysed. The first parameter represents the fraction of surface area covered with pigments and the second how well the pigments inside the coatings are oriented.

**Keywords:** appearance, scattering, spectrum, multi-angle reflectance, effect coating

## 1. Introduction and background

Surfaces that change their appearance significantly with illumination and viewing directions are becoming increasingly important in several applications, ranging from the purely decorative up to providing various functional purposes. The unique optical impressions of such surfaces give eye-catching effects, angle-dependent interference colours, pearl lustre, or multiple reflection, which characterize the appearance of the so-called gonioapparent effect. A large variety of samples falls into this class, giving angle-dependent effects due to (a) topography of the micro- and macro textures of surfaces, such as leather, textile and other microtextured surfaces, and (b) optical effects coming from metallic, interference and surface-structured flaky pigments applied in coatings, plastics and printing inks, which are mostly used in automotive, decorative and security coatings. The optical properties of such samples spread well beyond solid colour and cannot be described by any straightforward colorimetric measurement. Advanced applications demand production of surfaces with repeatable appearance, which requires controllable production process and possibility to predict the appearance. Several conditions have to be fulfilled for these requirements, such as the possibility to measure the appearance of such products, to identify the causes for differences among them, and to document these details

in a convenient way. We have shown already that goniospectrophotometric space curves, a special representation of the corresponding bidirectional reflectance distribution function (BRDF), could serve as an appearance fingerprint of several types of gonioapparent samples (Klanjšek Gunde and Rogelj, 2013). However, theoretical consideration of this methodology was made originally only on diffraction gratings (Rogelj, Poberaj and Klanjšek Gunde, 2013). For this purpose, the diffraction theory was applied to calculate the BRDF of diffraction gratings. This research is continued herein to analyse the numerical model that will enable reliable prediction of the BRDF of effect coatings, especially of paints or inks containing interference flakes.

BRDF contains spectral radiance coefficients for all possible illumination and viewing directions which could be measured by gonioreflectometry. Most research made so far has been done for metal-effect coatings, interference coatings, and more complex effect coatings. Three different geometries (i.e. combinations of illumination and viewing directions) are good enough for metallic coating (ASTM, 2001), whereas at least five or six geometries are required for coatings adopting the interference effect (Takagi, Watanabe and Baba, 2005). Most complex effect coatings require 1485 geometries (Takagi,

Sato and Baba, 2007). The goniospectrophotometers currently available on the market have 6 (BYK-mac i, BYK Gardner), 19 (MA98, X-Rite) and 98 geometries (GK311/M, Zeiss) (Kirchner and Cramer, 2012).

Effect pigments can be classified into two groups, class (i) pigments that consist of only one optically homogeneous material (substrate-free pigments, e.g. metallic and pearlescent flakes) and class (ii) pigments that have a layered structure and consist of at least two optically different layered material (pigments with layer-substrate structure or multilayered pigments with or without a substrate, e.g. interference flakes). The class (i) pigments give rise to reflection and/or partial refraction from flakes, which in the corresponding coating make metallic or pearlescent effects, respectively. Interference flakes from class (ii) add the effect of interference in thin film layers, which contributes strong angle-dependent colour, which is added to the lustre and brilliance (Pfaff and Reynders, 1999; Maile, Pfaff and Reynders, 2005).

The objective set for this research is to make a good calculation model for BRDF of effect coatings with interference flakes, and to verify it by comparison with goniospectrometric measurements. Most attention was devoted to build the theoretical model that could enable one to vary the optical constituents of effect coatings – i.e. the type of flakes (in terms of refractive index and

absorption coefficient), their pigment-volume concentration, size, average inclination angle inside the coating and the corresponding variance. The optical properties of the substrate were also allowed to vary. Some steps in solving this optical problem were already presented (Germer and Nadal, 2001). They were included here and developed further for the purpose of the application in hand. The first successful and promising results of the research are shown here together with the plans for the future. First, building of the numerical model is explained, and then its application is presented for a coating with layered interference flakes (class (ii)). For this purpose, a suitable sample was selected from a commercial set of samples; its reflectance was measured using handheld goniospectrometer and calculated by the built numerical model. Most parameters of the tested sample were provided by the producer. The most important exemption is orientation of flakes inside coating; it heavily influences the appearance and must be included in the numerical model. However, it is well known that measurement of flake orientation in coatings is far from straightforward (Kirchner and Houweling, 2009; Maile, Pfaff and Reynders, 2005; Pfaff and Reynders, 1999). Contrary, the influence of flake's inclination angle and variance to this angle on the goniometric reflectance is easily analysed by variation of the corresponding parameters in the numerical model. This is one among many advantages of the model.

## 2. Materials and methods

### 2.1 Samples

The Merck Effect Pigments colour card (Merck-Gruppe, Darmstadt, Germany) was taken here as a source of effect coating with different pigments. A representative from the coatings with metal lustre pigments was selected. It contains Iriodin 4504 pigments (MERCK, 2012), which are interference pigments, consisting of mica-based flakes with thin layer of iron (III) oxide ( $\text{Fe}_2\text{O}_3$ ). The coating is applied on a white subsurface; its appearance at measurement conditions is shown in Figure 1.

### 2.2 Measurements

The MA98 multiangle spectrometer (X-Rite, Inc.) was applied for measurements. The device is intended for

analyses of most optically complex coatings, also on curved surfaces. It enables reflectance factor measurements within 19 geometries; two illumination directions,  $45^\circ$  and  $15^\circ$ , combined with 10 and 9 viewing directions, respectively. Four directions at each illumination are out of the plane of incidence, therefore there are 8 off-plane and 11 in-plane geometries. Angular accuracy of the equipment is  $\pm 1.15^\circ$ , its reproducibility on average is  $0.18 \Delta E_{ab}^*$  on reference Series II BCRA tile set, and its repeatability, using 20 measurements at 5 seconds intervals, is maximum  $0.03 \Delta E_{ab}^*$  on white cal plaque (X-Rite, 2010). Measurements are taken at different locations on the sample to achieve average of 2 measurement values. The spectra were measured in the 400–700 nm spectral region with 10 nm increment. Only the in-plane measurements at  $45^\circ$  incident angle were analysed here. This

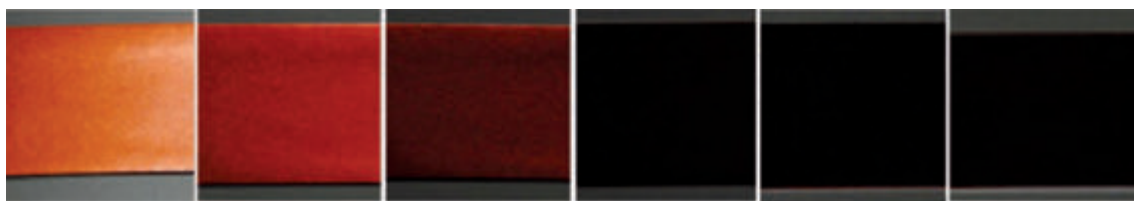


Figure 1: Photographs of the selected sample taken with  $45^\circ$  illumination angle in directions  $-60^\circ$ ,  $-30^\circ$ ,  $-20^\circ$ ,  $0^\circ$ ,  $30^\circ$  and  $65^\circ$  (from left to right) in respect to surface normal; the in-plane geometry is used

gives 6 detection directions,  $-60^\circ$ ,  $-30^\circ$ ,  $-20^\circ$ ,  $0^\circ$ ,  $30^\circ$  and  $65^\circ$ , as measured in respect to the surface normal. While the interference pigments in the selected sample are oriented uniformly and parallel to the substrate, the goniometric reflectance factor is distributed symmetrically around the in-plane direction, therefore, such a simplification is reasonable.

Reflection coefficients for paper substrates, which are used in the numerical model, were calculated from their reflectance factors. The latter were measured using a spectrophotometer Perkin Elmer  $\lambda 1050$ .

### 2.3 Calculations

The numerical model describes the scattering of light impinging onto a special effect pigment coating (Figure 2) at an incident angle  $\theta_i$  from the surface normal. Reflection of scattered light is described using polar angle  $\theta_r$  and azimuthal angle  $\Phi_r$  relative to the normal to the flat surface of the coating. Pigments are assumed to be tilted at an angle  $\theta'_n$ . Orientation distribution function describes how the tilt angle changes from flake to flake; it can be described by many functions. In this paper we use a logistic orientation distribution function  $P$  using  $\theta'_n$  as a mean flake tilt angle and  $\sigma'$  as a standard deviation:

$$P(\theta'_n, \theta'_n, \sigma') = \frac{\exp\left(\frac{\theta'_n - \theta'_n}{\sigma'}\right)}{\sigma' \left(1 + \exp\left(\frac{\theta'_n - \theta'_n}{\sigma'}\right)\right)^2} C \quad [1]$$

In Equation [1],  $C$  is the fraction of the surface area which is covered by pigments, going from 0 (no pigments) to 1 (pigments cover the whole sample area). Other angles in Equation [1] describe the applied geometry as shown in Figure 2.

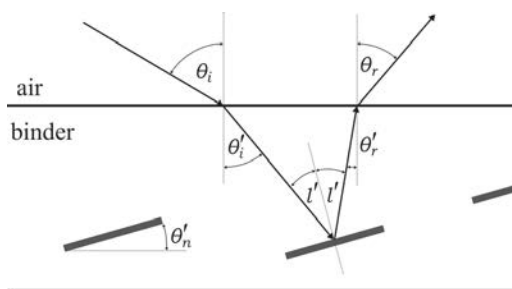


Figure 2: Simplified schematic of light scattering on special effect pigment coating

#### 2.3.1 Numerical model

The numerical model presented in this paper incorporates three models, named here as facet model, flake model, and base model. Each of the models describes

scattering from different level of the coating with special effect pigments:

- scattering from front surface of the coating – facet model
- scattering from special effect pigments inside the coating – flake model
- scattering from substrate of the coating – base model

Scattering from the whole sample is then described using Stokes vector  $S$ :

$$S = (F^{facet}G + F^{flake}G + F^{base})S_0 \quad [2]$$

where  $F^{facet}/F^{flake}/F^{base}$  are the Mueller matrices BRDF for the facet/flake/base model respectively,  $S_0$  is the Stokes vector of the incident light, and  $G$  is the geometrical attenuation factor, which accounts for masking and shadowing of the light at large reflection angles. Its definition and formulation can be found in Torrance and Sparrow (1967). The facet and flake models are treated in similar way and are described in detail in Germer and Nadal (2001), and in Germer, Zwinkels and Tsai (2014). They are used to calculate  $F^{flake}$  and  $F^{flake}$  by following the equation:

$$F = \frac{P}{4 \cos \theta_i \cos \theta_r \cos \theta_n} M \quad [3]$$

using different Mueller matrices,  $M^{facet}$  and  $M^{flake}$ , appropriate angles ( $\theta_i$ ,  $\theta_r$ ,  $\theta_n$  or  $\theta'_i$ ,  $\theta'_r$ ,  $\theta'_n$ ), and orientation distribution function ( $P$ ). The facet model treats the scattering from the front surface as a specular reflection from the aligned facets which have their slopes distributed according to the orientation distribution function. The flake model treats pigments as aligned facets and also takes into account the refraction into and out of the binder, surrounding the flakes. The facet and flake models are presented more in depth in Germer and Nadal (2001), and in Germer, Zwinkels and Tsai (2014), whereas the base model is described in the next subsection.

#### 2.3.2 Base model

Scattering from the substrate is incorporated in the base model. According to this model, light can take four different paths on its way through the coating towards the substrate and back. The paths, along with the corresponding angle notations are schematically represented in Figure 3, and expressed as:

1. transmission through pigments, diffuse reflection from substrate, transmission returning through pigments,
2. transmission through pigments, diffuse reflection from substrate, transmission returning through binder (no crossing of pigments),

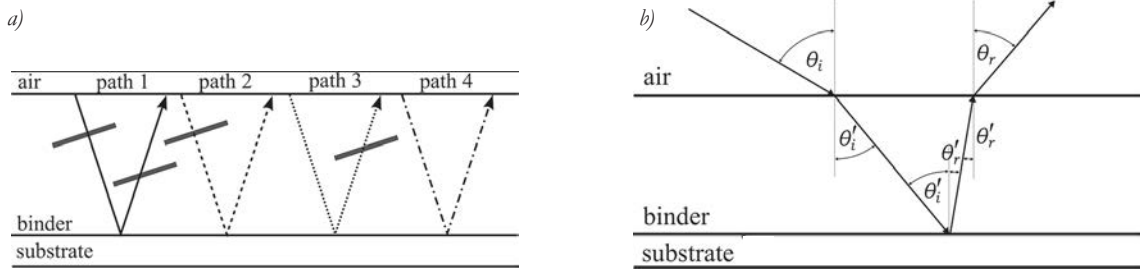


Figure 3: a) Schematic representation of the four different paths the light can follow when undergoing scattering from the substrate, where for simplicity only few pigment flakes are drawn, and b) schematic representation of angles used in the base model

3. transmission through binder (no crossing of pigments), diffuse reflection from substrate, transmission returning through pigments,
4. transmission through binder (no crossing of pigments), diffuse reflection from substrate, transmission returning through binder (no crossing of pigments).

In Figure 3b, only the path 4 is shown. For other three paths, the angles are the same; we only add pigment on the corresponding side(s).

The path 1 will always occur to some extent, being the only possible path in the case of complete coverage ( $C=1$ ), whereas the other three can occur only if  $C < 1$ . Mueller matrices BRDF for the four different paths are calculated as:

$$F^{path1} = \frac{P(\theta_n', \theta_0', \sigma') n_{binder}^2}{4 \cos \theta_i \cos \theta_r \cos \theta_n'} M^{path1} \quad [4a]$$

$$F^{path2} = \frac{P(\theta_n', \theta_0', \sigma') n_{binder}^2}{4 \cos \theta_i \cos \theta_r \cos \theta_n'} (1-C) M^{path2} \quad [4b]$$

$$F^{path3} = \frac{P(\theta_n', \theta_0', \sigma') n_{binder}^2}{4 \cos \theta_i \cos \theta_r \cos \theta_n'} (1-C) M^{path3} \quad [4c]$$

$$F^{path4} = (1-C)^2 M^{path4} \quad [4d]$$

and Mueller matrices are transformed from Jones matrices,  $J^{path}$ , as (Goldstein, 2003):

$$M = UJ \otimes J^* / U \quad [5a]$$

$$U = \frac{1}{\sqrt{2}} \begin{bmatrix} 1 & 0 & 0 & 1 \\ 1 & 0 & 0 & -1 \\ 0 & 1 & 1 & 0 \\ 0 & i & -i & 0 \end{bmatrix} \quad [5b]$$

Jones matrices for the four different paths are calculated as:

$$J^{path1} = \begin{bmatrix} q_{11}^{flake} t_s'^2(l') & q_{12}^{flake} t_s'(l') t_p'(l') \\ q_{21}^{flake} t_s'(l') t_p'(l') & q_{22}^{flake} t_p'^2(l') \end{bmatrix} \quad [6a]$$

$$J^{path2} = \begin{bmatrix} q_{11}^{flake} t_s'(l') & q_{12}^{flake} t_p'(l') \\ q_{21}^{flake} t_s'(l') & q_{22}^{flake} t_p'(l') \end{bmatrix} \quad [6b]$$

$$J^{path3} = \begin{bmatrix} q_{11}^{flake} t_s'(l') & q_{12}^{flake} t_p'(l') \\ q_{21}^{flake} t_p'(l') & q_{22}^{flake} t_s'(l') \end{bmatrix} \quad [6c]$$

$$J^{path4} = \begin{bmatrix} t_s(\theta_i) t_s(\theta_r) r_s''(l') & 0 \\ 0 & t_p(\theta_i) t_p(\theta_r) r_p''(l') \end{bmatrix} \quad [6d]$$

where  $q_{ij}^{flake}$  are elements of Jones matrix for facet model,  $t_s'$  and  $t_p'$  are transmission and  $r_s''$  and  $r_p''$  reflection coefficients for substrate and pigments, respectively. Transmission coefficients for pigments are calculated using the thicknesses of the pigment's layers and their wavelength-dependent refractive indices. The equations are well known and can be found, for example, in Germer, Zwinkels and Tsai (2014).

#### 4.1 Numerical modelling of the samples

The described numerical model was used to calculate the reflectance factor of the selected sample at the conditions used for measurements. This includes six in-plane reflectance directions with 45° illumination and aspecular angles  $-60^\circ, -30^\circ, -20^\circ, 0^\circ, 30^\circ, 65^\circ$  as specified for MA98 multiangle spectrometer. The sample was described with a coating containing flaky pigments in a resinous binder (Table 1). A white paper was used as a substrate. The mica-based flakes, having thin interference layer made of  $Fe_2O_3$  on both sides (Iriodin 4504, Merck) were used. The flakes are described as layer-core-layer where the corresponding thicknesses were adjusted by the best fit to the measured reflectance. Because the flakes cover the entire surface,  $C=1$  was used. Vast majority of flakes were oriented parallel to the substrate, therefore the flake's mean tilt angle was taken to be  $\theta_0' = 0^\circ$ . The refractive index of  $SiO_2$  was used instead of mica ( $KAl_2(Si_3Al)O_{10}(OH,F)_2$ ). The refractive indices

of  $\text{SiO}_2$ ,  $\text{Fe}_2\text{O}_3$  and acrylic pitch (binder) were obtained from the literature (Palik, 1997; Kasarova et al., 2007; Database of AIU Jena, 2015), while the thicknesses of the core material and of the interference layer of flakes

were obtained by the best match between the calculated and measured spectra, based on CIE76 colour difference (Schanda, 2007). The Stokes vector of the incident light for all calculations was that of an unpolarized light.

*Table 1: Specifications of the analysed effect coating; data for the binder, the substrate and the flakes, where  $C$  is the coverage of the substrate by flakes,  $\theta_0$  is the flake's mean tilt angle and  $\sigma'$  is the standard deviation for the orientation distribution of flakes, binder layer thickness was estimated from measurements with caliper and flake's thicknesses were adjusted by the best fit to the measured reflectance while the mean diameter was taken from the Merck Effect Pigments colour cart*

<b>Binder</b>	Material	acrylic pitch
	Layer thickness	600 $\mu\text{m}$
<b>Substrate</b>	Material	white paper
<b>Special effect pigments (flakes)</b>	Materials	$\text{Fe}_2\text{O}_3 + \text{mica} + \text{Fe}_2\text{O}_3$
	Thicknesses	(0.074 + 0.121 + 0.074) $\mu\text{m}$
	Mean diameter	5–50 $\mu\text{m}$
	$C$	1
	$\theta_0$	0°
	$\sigma'$	3°

## 5. Results and discussion

The suitability of the numerical model to describe the goniometric reflectance factor of an effect coating was analysed in four steps. First, the measured reflectance factor was compared to the calculated one for the entire set of illumination–viewing angles. The thickness of the pigment flakes, the mica core and interference layer applied over it, were varied for the best possible match of the reflectance spectra. Second, the influence of the fraction of the substrate surface covered by pigments (parameter  $C$  in the Equation [1]) on the calculated reflectance factor was analysed. Third, the consequences of the orientation distribution function of flakes within coating were analysed. And fourth, the effect of different coloured paper substrates was analysed.

### 5.1 Measured vs. modelled reflectance factor

The calculations were made for the 440–700 nm spectral region because the published values for refractive index and absorption coefficient are limited to this region, and no extrapolation was made. Figure 4 shows the measured and calculated reflectance spectra for all applied illumination–viewing combinations and the corresponding CIELAB  $a^*$  and  $b^*$  colour values (Schanda, 2007) determined from the measured reflectance factor. The parameters used in computations are those from Table 1. The CIELAB values  $a^*$  and  $b^*$  are the largest at 60° reflectance angle and almost linearly diminish when this angle changes towards smaller and then nega-

tive values, where the appearance of the sample is going towards black. This is in accordance with photographs shown in Figure 1.

The measured spectra have a slight increase in reflectance at 440 nm, a valley between 500 and 550 nm, a peak around 630 nm and a decrease at 700 nm. The reader should notice that the measurements, as well as the model, provide reflectance factor and not reflectance. By definition, the reflectance factor is the ratio of radiant flux reflected of a sample in a given direction to that reflected in the same direction by perfectly reflecting diffuser (PRD). This means that some samples can reflect more light in a certain direction than the PRD, resulting in reflectance factor values above 1. The position of peaks and valleys is greatly determined by the thickness of interference layer applied on the mica core of the pigment flakes. The thickness data are not available for the Iriodin 4504 pigment, however, the percentage of each material used in the pigment is specified by the producer. The interference layer thickness and the thickness of the mica core were adjusted, using the percentage information, in order to minimize the colour difference,  $\Delta E_{\text{ab}}^*$ , between the measured and calculated reflectance factor. The CIE76 colour-difference formula was applied for this purpose. Table 2 shows the results obtained for the spectra shown in Figure 4. The spectra show an acceptable match, however, the individual colour differences are quite large. The possible reasons

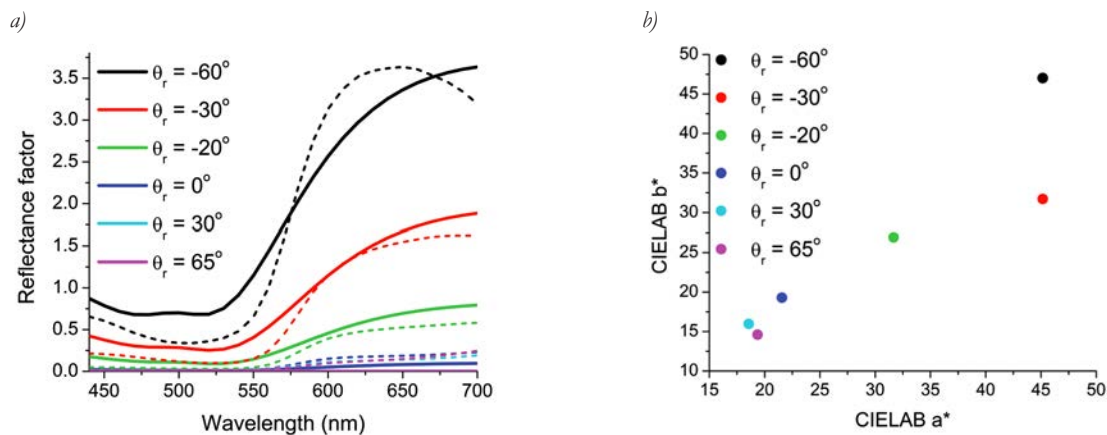


Figure 4: a) Measured (dashed line) and modelled (solid line) reflectance factor obtained for the selected coating sample with interference flakes and (b) CIELAB  $a^*$  and  $b^*$  colour values calculated from the measured reflectance spectra (see also Figure 1 and Table 2); measurement directions are specified in the legend

Table 2: CIE76 colour difference and RMSE between measured and modelled reflectance factor values

Aspecular angle	$\Delta E^*_{ab}$	RMSE
$-60^\circ$	20.58	0.3543
$-30^\circ$	14.76	0.1702
$-20^\circ$	12.32	0.1245
$0^\circ$	17.64	0.0741
$30^\circ$	26.29	0.0952
$65^\circ$	26.27	0.1077

could be insufficient knowledge about the layers thicknesses, substituting optical constants of mica layer for optical constants of  $\text{SiO}_2$ , and insufficient modelling of the roughness of the mica flakes. Alongside the colour difference, Table 2 also shows the root mean square error (RMSE) between measured and calculated spectra. It was calculated as:

$$RMSE = \sqrt{\frac{\sum_{\lambda=440}^{700} (s_{\lambda, \text{measured}} - s_{\lambda, \text{calculated}})^2}{w}} \quad [6]$$

where  $s$  represents reflectance spectra and  $w$  is the number of wavelengths.

## 5.2 Influence of surface coverage

Changing the volume concentration of pigments or their diameter, in general, changes the surface coverage, which is expressed by  $C$  in Equation [1]. Smaller surface coverage means that less of the area is covered with pigments and the substrate has a greater influence on the reflectance of such a sample. The influence of this effect on the reflectance factor spectra was analysed by calculating the reflectance factor spectra for all the applied illu-

mination-viewing geometries using different values of the surface coverage,  $C$ . Figure 5 shows the results for  $C$  values of 0.1, 0.5 and 0.9. Smaller surface coverage results in bigger influence of the substrate, as expected. At wavelength below 530 nm, the reflectance factor in all viewing angles converges to a single value, but their relative separation stays the same as it is at longer wavelengths. The shape and the intensity of the reflectance factor changes with surface coverage. For smaller coverage, the reflectance factor becomes similar to that of the coating substrate alone (see also Figure 10). Therefore, the interference effect caused by the pigments is clearly seen at large enough coverage. This confirms the validity of the used computational model and enables to predict the concentration of flakes that should be used in coating if hiding of the substrate is desired.

The reader should pay special attention to the scale of the reflectance factor in Figure 5. When surface coverage is 1, the interference effect produces reflectance factor values higher than 1. With the smaller surface coverage, the interference effect diminishes and the reflectance factor values slowly became more similar to the reflectance factor of the substrate, meaning that the values go below 1.

## 5.3 Influence of orientation distribution function

The orientation distribution function of flakes is assumed to be a logistic distribution with its mean value,  $\theta_0'$ , and standard deviation,  $\sigma'$ . Since both parameters influence the results, we will analyse how each of them affects the reflectance spectra.

### 5.3.1 Influence of orientation distribution's standard deviation

Here, we assume that the mean tilt angle is  $0^\circ$ , meaning the flakes are parallel to the substrate, and we change

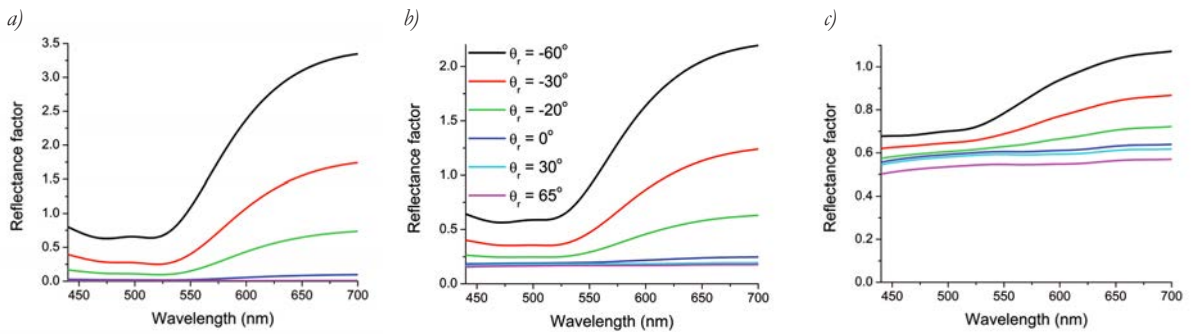


Figure 5: Reflectance factor spectra calculated for the applied illumination–viewing directions using surface coverage a)  $C=0.9$ , b)  $C=0.5$ , and c)  $C=0.1$ ; the legend in the middle graph is applicable to all three graphs

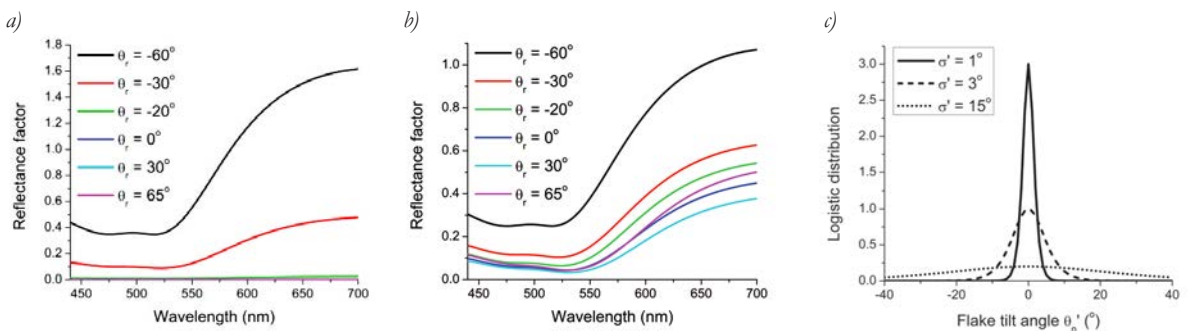


Figure 6: Reflectance factor spectra calculated for the applied illumination–viewing directions (see the legend) using surface coverage  $C=1$ , the flake’s mean tilt angle  $\theta_0'=0^\circ$  and standard deviation of the orientation distribution function equal to a)  $\sigma'=1^\circ$  and b)  $\sigma'=15^\circ$ ; the reader should pay attention to the y axis range of the two graphs; c) orientation distribution function using the standard deviations specified in the corresponding legend

the value of standard deviation. Figure 6 shows the calculated reflectance spectra for the applied sample using standard deviation equal to  $1^\circ$  and  $15^\circ$ . The logistic orientation distribution functions for the variances  $1^\circ$ ,  $3^\circ$  and  $15^\circ$  are also illustrated in the same figure, to show the broadness of the pigment tilt angle in such conditions. Reflectance factor spectra show that smaller variance results in significant reflection only at reflectance angles close to the specular reflection, at  $-30^\circ$  and  $-60^\circ$ . Other angles have very low reflectance factor. When orientation distribution is broader (the standard deviation is bigger), the reflectance factor increases over a wide range of reflectance angles.

A small standard deviation means that almost all flakes are parallel to the substrate, therefore the reflection of the sample is highly directional, and distributed around the specular direction, as a result of scattering on the edges of the flakes. A large standard deviation of the orientation distribution function means that the pigments are randomly oriented, thus reflect in accordance with these directions. The reflectance factor of such a coating becomes highly diffuse, meaning that a wider range of reflection directions reflect similar amount of light.

To analyse how the standard deviation of the orientation distribution function affects the reflectance factor at different reflectance angles, we have analysed the reflectance factor at  $\lambda=650\text{ nm}$  as a function of the applied value of standard deviation. The results are shown in Figure 7. The reflectance factor at  $650\text{ nm}$  is shown for all applied geometries plotted against standard deviation values between  $1^\circ$  and  $40^\circ$ .

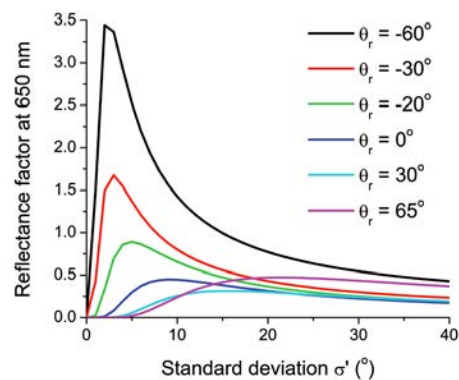


Figure 7: Reflectance factor at  $\lambda=650\text{ nm}$  for specific reflectance angle versus standard deviation of orientation distribution function

The reflectance angles closer to the specular reflection have a quicker rise at small standard deviation and slowly converge to a constant value at larger standard deviation. The reflectance factor at angles furthest away from specular reflection,  $30^\circ$  and  $65^\circ$ , starts to increase at larger standard deviations, and does not show such a high reflectance factor like at angles closer to the specular direction. Such behaviour is in accordance with the logistic distribution function; when standard deviation becomes large enough, all inclination angles become possible.

5.3.2 Influence of orientation distribution’s mean value

Here, we assume that the standard deviation is  $\sigma' = 3^\circ$ , and we change the mean value of the logistic distribution function,  $\theta_0'$ . If the flakes would be surrounded by air, the reflected angle for specular reflection on flakes (noted here as specular reflected angle) would be an addition of incident angle and flake’s tilt angle. Because the flakes are inside a binder, the refraction at binder-air interface has to be also taken into account. The nonlinear relation between flake’s tilt angle,  $\theta_n'$ , and specular reflected angle, is shown in Figure 8a. Flake’s tilt angle can only range between  $-6^\circ$  and  $35^\circ$ , beyond this we would encounter total internal reflection and no light would come from the sample. We can see that a small shift in flake’s tilt angle causes a large shift in specular reflected angle.

Figure 8b shows the reflectance factor at  $\lambda = 650$  nm at different reflectance angles, as a function of the applied mean value, ranging from  $-6^\circ$  to  $35^\circ$ . When we change the mean value, we see that every aspecular angle has its own reflectance factor peak. The position of these peaks is directly related to the specular reflected angle, shown in Figure 8a. The intensity of the peaks, on the other hand, is mainly related to the denominator in Equation [3], where we have cosine of flake tilt angle and reflected angle (Figure 8c). This part of the equation is relatively low for most of the angles, but becomes large in the border range of flake tilt angles, corresponding to aspecular angles  $-60^\circ$  and  $65^\circ$ . This

explains the much higher intensity of reflectance factor peaks for those two aspecular angles in relation to other aspecular angles.

5.4 Influence of the substrate

The influence of the substrate can be analysed when different paper substrates are used. We have used black, magenta, cyan and yellow paper substrate (Figure 9). To show the corresponding effects, we calculated reflectance factor spectra of the effect coating with different surface coverage,  $C$ . Figure 10 is showing the results for  $C = 0.1, 0.5$  and  $0.9$  for reflectance angle  $60^\circ$ . Other parameters used in the calculations were those defined in Table 2. Figure 10 should be compared with Figure 5, where the same parameters were used with white paper substrate.

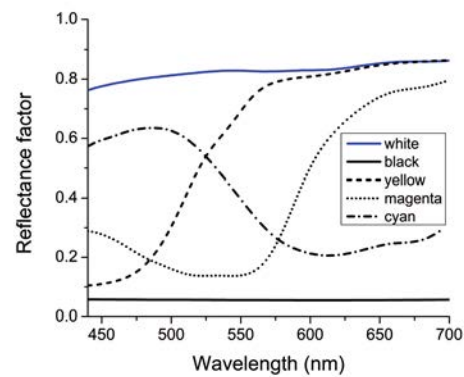


Figure 9: Measured reflectance factor for white, black, magenta, cyan and yellow paper substrates

Even with high surface coverage,  $C = 0.9$ , some differences were obtained in calculated spectra when different paper substrates were applied. Coating on magenta and yellow substrates that have high reflectance factor at  $\lambda > 550$  nm, where the flakes also give high reflectance, give similar but slightly lower reflectance as the white substrate. Cyan and black paper substrates give even smaller reflectance factor values since the reflectance of

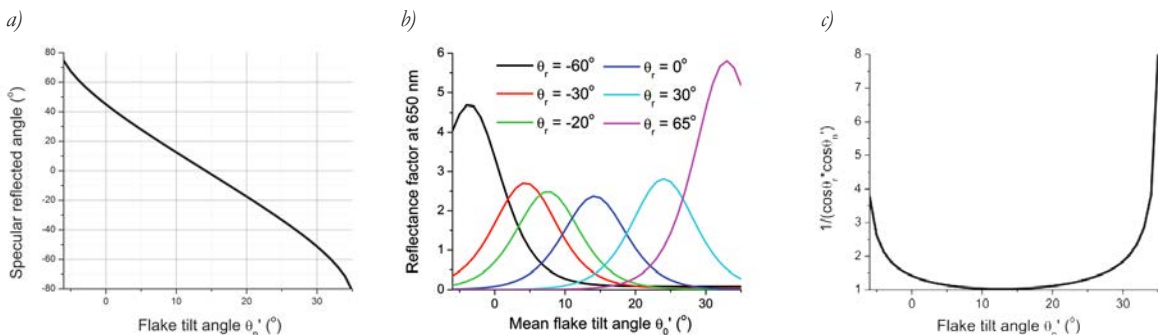


Figure 8: a) The reflected angle for specular reflection on flakes (specular reflected angle) as a function of flake tilt angle, b) reflectance factor at  $\lambda = 650$  nm for specific reflectance angle as a function of orientation distribution’s mean value,  $\theta_0'$ , and c) inverse of cosine of flake tilt and reflected angle versus flake tilt angle

the substrate alone is not high in that region. The small difference is because the interference effect caused by the pigments produces much higher reflectance factor values than the reflection from the substrate. When the surface coverage is getting smaller, the difference among paper substrates becomes larger. This is expected, since

more and more of the substrate is visible and thus it contributes more to the reflectance factor of the entire coating. Not only the reflectance factor intensity changes, but also the shape of the reflectance factor curve starts to change and becomes more and more similar to the reflection of the substrate alone (Figure 9).

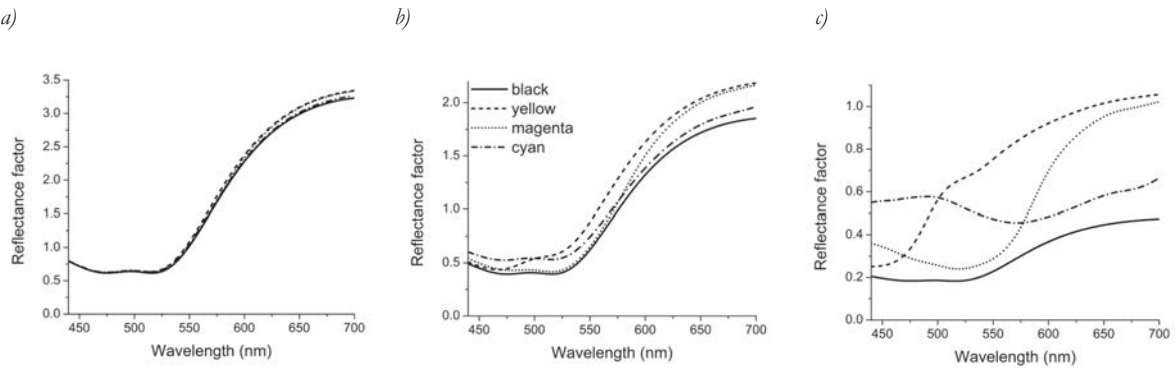


Figure 10: Reflectance factor calculated for the reflection angle  $-60^\circ$  using surface coverage a)  $C=0.9$ , b)  $C=0.5$ , and c)  $C=0.1$  for different paper substrates (the legend in the middle graph applies to all three graphs); other parameters used in the calculation are those from Table 2; scale on y axis is changing for different  $C$  parameter, however, the same  $C$  parameter has the same y axis scale in this Figure 10 as well as in Figure 5

## 6. Conclusions

The focus of this research is on modelling the reflectance spectra of the selected special effect coating with interference pigments, having a  $\text{Fe}_2\text{O}_3$  layer on a mica core. The modelled reflectance factor was validated with measurements of the selected sample at the same goniometric angles that were used in the model. The influence of three important parameters on goniometric reflectance factor was analysed, namely surface coverage, pigment orientation distribution and coating substrate. Surface coverage is directly related to the diameter and volume concentration of pigments for a given pigment thickness, i.e. aspect ratio, and both can be varied in the ink or paint manufacturing process. Depending on this factor, the coating substrate will affect the reflectance factor and influence the appearance of the coating. The pigment orientation distribution is an important factor when applying the ink or paint. Different application processes can distribute pigments with different orientation and standard deviation of orientation, and, as we have shown, this parameter can have great influence on the goniometric reflectance factor. Substrate used for application of the coating also contributes to the overall appearance of the sample, especially if the surface coverage is small. The results of our research show that the model built for such samples provides useful results; therefore it will be developed further. The coating sam-

ple, selected to present the application of the numerical model, includes all types of optical events taken into account in our numerical model. Therefore, this evaluation shows that the model is generally acceptable for effect coatings with both types of flakes, class (i) and class (ii). Moreover, this makes a good ground for further research of problems connected with appearance of gonioapparent samples. Moreover, interference flakes with more layers (multilayered interference flakes) are currently being considered. The entire data will be used to check the possibility of using the numerical model to define the input data for appearance fingerprinting.

The entire research has an ambition to provide a generalized model for goniospectrometric reflectance factor of effect coatings with arbitrary complexity. The numerical model should help in answering the question which spatial resolution is good enough to describe the BRDF of effect coatings. While coatings with all currently known special effects pigments will be considered, the proposed model will provide the reflection spectrum for arbitrary illumination-viewing directions for any combinations of ink/paint preparation and coating application. Such data are important for several purposes of optically complex coatings, being for decorative, security or any other purpose.

## Acknowledgements

The authors acknowledge X-Rite and their country representative, Roman Habicht, for the opportunity to apply the software of the MA98 multi-angle spectrophotometer, and to Hana Eržnožnik and Frenk Šemen at Helios d.d., Slovenia, for measurements on their apparatus.

## References

- ASTM, 2001. ASTM E2175-01, *Standard practice for specifying the geometry of multiangle spectrophotometers*. Conshohocken, PA, USA: ASTM International.
- Database of Optical Constants for Cosmic Dust, 2015. Laboratory Astrophysics Group, University of Jena, Germany. Available at: <<http://www.astro.uni-jena.de/Laboratory/OCDB/>> [Accessed 10 August 2015].
- Germer, T.A. and Nadal, M.E., 2001. Modeling the appearance of special effect pigment coatings. In: Z.-H., Gu and A.A., Maradudin, eds. *SPIE Proceedings* Vol. 4447, pp. 77–86.
- Germer, T.A., Zwinkels, J.C. and Tsai, B.K., eds., 2014. Spectrophotometry: accurate measurement of optical properties of materials. *Experimental Methods in the Physical Sciences*, 46.
- Goldstein, D., 2003. *Polarized Light, Second Edition Revised and Expanded*. New York: Marcel Dekker, Inc.
- Kasarova, S.N., Sultanova, N.G., Ivanov, C.D. and Nikolov, I.D., 2007. Analysis of the dispersion of optical plastic materials, *Optical Materials*, 29(11), pp. 1481–1490.
- Kirchner, E. and Houweling, J., 2009. Measuring flake orientation for metallic coatings. *Progress in Organic Coating*, 64, pp. 287–293.
- Kirchner, E. and Cramer, W., 2012. Making sense of measurement geometries for multi-angle spectrophotometers. *Color Research and Application*, 37(3), pp. 186–198.
- Klanjšek Gunde, M. and Rogelj, N., 2013. Suitability of goniospectrophotometric space curves as appearance fingerprints, *Applied Optics*, 52(12), pp. 2718–2728.
- Maile, F.J., Pfaff, G. and Reynders, P., 2005. Effect pigments – past, present and future. *Progress in Organic Coatings*, 54(3), pp. 150–163.
- MERCK, 2012, *Safety data sheet, Irodim 4504 Lava Red*. Available at: <<http://merck-performance-materials.com/>> [Accessed 10 August 2015].
- Palik, E.D., ed., 1997. *Handbook of Optical Constants of Solids*. San Diego, Chestnut Hill, London: Academic Press.
- Pfaff, G. and Reynders, P., 1999. Angle-dependent optical effects deriving from submicron structures of films and pigments. *Chemical Reviews*, 99(7), pp. 1963–1982.
- Rogelj, N., Poberaj I. and Klanjšek Gunde, M., 2013. Goniospectrophotometric space curves of diffraction gratings and their applicability as appearance fingerprints. *Applied Optics*, 52(34), pp. 8355–8362.
- Schanda, J., ed., 2007. *Colorimetry: Understanding the CIE System*. Hoboken, New Jersey: John Wiley & Sons.
- Takagi, A., Watanabe, A. and Baba, G., 2005. Prediction of spectral reflectance factor distribution of automotive paint finishes. *Color Research and Application*, 30(4), pp. 275–282.
- Takagi, A., Sato, S. and Baba, G., 2007. Prediction of spectral reflectance factor distribution of color-shift paint finishes. *Color Research and Application*, 32(5), pp. 378–387.
- Torrance, K.E. and Sparrow, E.M., 1967. Theory for off-specular reflection from roughened surfaces. *Journal of the Optical Society of America*, 57(9), pp. 1105–1114.
- X-Rite, 2010. *X-Rite MA98: Portable multi-angle spectrophotometers*, X-Rite, Incorporated. Available at: <[https://www.xrite.com/documents/literature/en/L10-372\\_MA98\\_en.pdf](https://www.xrite.com/documents/literature/en/L10-372_MA98_en.pdf)> [Accessed 10 August 2015].

JPMTR 070 | 1503  
DOI 10.14622/JPMTR-1503  
UDC 539.6 – 035.67 : 763

Original scientific paper  
Received: 2015-06-23  
Accepted: 2015-11-17

## Ink adhesion failure during full scale offset printing: causes and impact on print mottle

Hajer Kamal Alm<sup>1</sup>, Göran Ström<sup>1</sup>, Joachim Schoelkopf<sup>2</sup>, Cathy Ridgway<sup>2</sup> and Patrick A. C. Gane<sup>2\*</sup>

<sup>1</sup> Innventia AB,  
BOX 5604, SE-114 86 Stockholm, Sweden

<sup>2</sup> OMYA Development AG, P.O BOX: 32,  
CH-4665 Oftringen, Switzerland

\* (also) Aalto University, School of Chemical Technology,  
P.O. Box 16300, FI-00076 Aalto, Finland

E-mails: hajer.kamal@innventia.com  
goran.strom@innventia.com  
joachim.schoelkopf@omya.com  
cathy.ridgway@omya.com  
patrick.gane@omya.com

### Abstract

The printing plate used in offset lithography is designed to accept ink on image areas and reject ink on non-image areas. In order to reject ink in conventional offset, fountain solution is needed to form a weak boundary layer between the plate and the ink. Paper and coated paper in particular are designed to accept ink and absorb ink oil and fountain solution. The latter is often transferred to the paper surface through the rubber blanket and its absorption or subsequent displacement is essential for final ink transfer to the surface. There are strong demands on the uniformity of the paper surface, including in respect to absorptivity, both in structure and chemistry, in order to gain a print of high quality. If this is not the case, the ink film thickness may be non-uniform; subsequently, ink adhesion may even fail completely, leaving white spots on the paper surface in the print. This gives rise to print mottle, a severe print quality defect.

The aim of this paper was to study the quality of prints from a full scale offset printing trial made on pilot coated paper, with attention given to ink-surface adhesion. Seven calcium carbonate pigment based coatings with different contents of pigment dispersing agent were included in this study. The work showed that a moderate over-dosage of dispersant significantly increased the ink adhesion failure and print mottle, mainly on prints from the later print units and especially at high fountain feed levels. These findings demonstrate the fundamental impact of fount level, surface chemistry and coating formulation on ink adhesion and thus also print mottle.

**Keywords:** coated paper, coating permeability, offset print quality, water induced print mottle, uncovered area, polyacrylic dispersant

## 1. Introduction

The principal function of fountain solution in conventional offset printing is to prevent ink to be transferred to the non-image areas of the printing plate (MacPhee, 1979; Kipphan, 2001). The fountain feed level is a delicate control issue for the printer. Too low a feed volume will cause scumming, i.e. the non-image areas will take up ink and start to print. Too high a feed will give problems with poor ink transfer and print quality defects will appear. A minimum thickness of the fountain film is considered to be around 40 to 80 nm (see Discussion for details), which is well below the range of 0.5–1 µm which has been reported as a normal average thickness (MacPhee, 1979). However, the non-image area of the plate is not mirror-smooth, a press design feature is applied to ensure satisfactory fount transfer, and so sufficient fountain feed is needed in order to assure that the water film on elevated areas also has an appropriate thickness.

Both ink and paper must be compatible with fountain solution in order to assure ink transport in the press and good print quality. The ink must be able to incorporate fountain solution in a water-in-oil emulsion (MacPhee, 1979; Fadner and Doyle, 1985). Also the paper needs to cater for water that has been deposited on its surface when the paper comes into contact with water rich regions on the rubber blanket. The water is first hydraulically impregnated into the paper in the nip in a process controlled by the paper permeability and then subsequently capillary absorbed by the top layer of the paper during the time that elapses between two nips (Aspler, 2006). Direct measurements of water uptake by coated papers during heatset offset printing have been reported by Tåg et al. (2010, 2011). They used near infra-red probe spectroscopy and confirmed a significant water uptake which was influenced by coating smoothness and

capillarity. Due to the high speed of the printing process, the controlled uptake of water into ink and paper must be fast. Compact areas of the paper surface have a low capability to remove larger water volumes fast enough from the surface and this will give problem with ink transfer to the paper.

Print mottle is a perceived uneven print density and a common and severe print defect on coated papers. The amount of wet ink transferred to the paper is very low, less than  $1 \text{ g} \cdot \text{m}^{-2}$  (MacPhee and Lind, 1991) and after drying when the ink oil has depleted from the ink film (Ström and Gustafsson, 2006), the thickness of the dry ink film (i.e. pigment and binder) is in the order of half a micrometre or less (Ström and Karathanasis, 2008). Thus, it is easy to understand that a very small variation in ink film thickness and small spots where the ink has failed to adhere to the surface will result in a mottled low quality print.

There are two principal types of print mottle. Back trap mottle (BTM) is due to variation in ink film thickness. This mottle type has been subjected to scientific studies in both laboratories and on printing presses for half a century, with significant breakthroughs seen during the last 10–15 years (Ozaki, Bousfield and Shaler, 2008; Rajala and Koskinen, 2004; Xiang et al., 2000; Shen et al., 2005; Xiang et al., 1999; Isoard, 1983). BTM is basically due to an uneven depletion of ink oil by transfer into the coating, which in turn is due to a non-uniform pore structure and/or surface chemistry of the coating. This results in an ink film on the paper with local variations in thickness and viscosity. This gives an uneven build-up of ink on the non-image areas of the rubber blanket and non-uniform ink transfer (back trap) in subsequent print units where the previous printed area meets the non-image area of the following rubber blanket, and finally a non-uniform ink film thickness on the paper that exits the printing press.

The other principal type of mottle is water interference mottle (WIM) (Plowman Sandreuter, 1994). Only very little scientific work in this area have been reported (Ström and Madstedt, 2009; Lie and Kolseth, 2007). The common belief is that it is due to ink refusal caused by too high a fountain solution feed rate. We became interested in this research area after a laboratory study on ink adhesion (Kamal et al. 2010; Kamal Alm et al., 2010), where we realised that ink adhesion failure could have

several origins. Not only fountain solution feed was important but also paper properties and the interaction between fountain solution and paper coating.

The laboratory work (Kamal et al. 2010; Kamal Alm et al., 2010) showed that an excess amount of sodium polyacrylate in the coating colour affected the coating properties and the interaction between ink and the paper coating. The coatings became more polar and interacted more strongly with water. This resulted in slower ink setting and reduced ink–paper coating adhesion, especially in the presence of applied water/dampening solution (to mimic fountain solution during offset printing) which are identified as contributory factors in ink piling and print mottle (Purfeerst and Van Gilder, 1991). The work showed that ink adhesion failure resulted in white spots in the print and suggested that the ink failure was due to two different mechanisms, the well-known ink refusal, which is an ink transfer failure, and a new mechanism, which we refer to as ink-lift-off. The latter mechanism suggests that the ink is transferred to the paper surface but removed in a subsequent print nip due to poor ink-surface adhesion (Kamal Alm et al., 2015).

In order to verify if the findings from the laboratory study had any relevance in industrial printing, we designed a special pilot coating trial and printed the coated papers in full-scale sheet-fed offset with a layout designed for our aims. The results are reported in two articles. The first (Kamal Alm et al., 2015) focuses on the impact of paper coating properties gained from the size distribution of the pigment, type of latex binder, calendering and one dosage of additional dispersant on ink adhesion failure. The white spots that were a result of ink adhesion failure were analysed in detail, the unprinted surfaces were inspected with scanning electron microscopy (SEM) and a mechanism was proposed. Now, the second report, i.e. this paper, focuses on paper properties that arise from the use of high amounts of dispersant since this appears to be a key factor, and especially since paper mills often add in extra dispersant(s) to the colour in order to assure that it will perform well on the coater following, for example, pH shock in the case of calcium carbonate, arising frequently from the use of acidic binders or microbiological contamination on the machine. Both reports focus on fountain solution/water feed in addition to paper properties on ink adhesion and print quality. The present paper additionally discusses print quality properties in more detail.

## 2. Materials and methods

### 2.1 Coating colour formulations

Seven different coating colours were formulated. The coatings were prepared according to the formulations in Table 1. The same pigment, a ground calcium car-

bonate (GCC) with mass fraction of 90 % of the particles being less than  $2 \mu\text{m}$ , was used in all formulations. The GCC pigment (Hydrocarb 90, supplied by OMYA) was delivered in the form of dispersed slurry where polyacrylate (PA) dispersant had been used during its

production. The binder used in all formulations was a styrene-butadiene latex (DL920 supplied by STYRON).

The additional polyacrylic dispersant used for excess dosing was Dispex N40 (supplied by BASF), a fully sodium neutralised dispersant (NaPA). The NaPA solution used in the experiment consisted of diluted commercial product, in which only water had been added. A further dispersant solution was also prepared, a partially calcium neutralised (NaCaPA). In the NaCaPA solution a calcium to acrylate ratio ( $[Ca^{2+}]/[A^-]$ ) of 0.3 was targeted. The ion-exchange from sodium to calcium ions was made using calcium nitrate tetrahydrate (supplied by Merck). The calcium salt was first dissolved in water, and then carefully added to the dilute NaPA solution. The thus prepared dilute PA solutions contained 5 % active component, i.e. 5 % acrylate. The solutions were pH adjusted to 10.5 with a NaOH solution (mass fraction of 10%) before being added to the pigment slurry, followed by binder addition and additional water to reach a target solid content of 67 %. The coating colours were finally adjusted to pH 8.8. In three of the seven prepared coating colours, the diluted sodium polyacrylate (NaPA) was added in different dose amounts. In one of the formulations (Ref) no additional dispersant was added. In the remaining three formulations the NaCaPA with partial calcium neutralisation was applied as an additive to the pigment slurry.

## 2.2 Pilot coating

The coating colours were coated on pre-coated wood-free fine paper (Magnostar 80  $g \cdot m^{-2}$  supplied by Sappi). Both sides of the industrially pre-coated base paper were top-coated with approximately  $10 g \cdot m^{-2}$ . The papers were coated with a blade coater at a speed of  $1500 m \cdot min^{-1}$  (Modular Combi Blade (MCB) manufactured by Voith Paper). For additional process parameters see Appendix.

The coated papers were supercalendered (SK 14/12-90 manufactured by Bruderhaus Maschinen GmbH) and

passed through 11 nips, each with a linear nip-pressure of  $120 kN \cdot m^{-1}$  and a line speed of nearly  $300 m \cdot min^{-1}$ . The temperature of the calender rolls was kept constant at  $90 ^\circ C$  and the papers were calendered to reach 69 % gloss (measured with TAPPI Standard T480). Further process parameters can be found in Appendix.

## 2.3 Full scale printing

The coated papers were printed 4 weeks after being coated with a sheet-fed offset printing press (Manroland R 706 LITLV supplied by Manroland sheet-fed GmbH, Germany). For more details of the press set-up, please see Appendix.

The printing order was black (K), cyan (C2), magenta (M), yellow (Y), cyan (C5) and cyan again (C6) as shown in Figure 1. Only the cyan printed areas were evaluated.



Figure 1: The ink sequence used during the printing trial

The print layout seen in Figure 2 shows a total of six cyan areas, three of which are printed in fulltone (first column) and three areas are printed in 50 % halftone (second column). Each area is printed only once at either C2 (first row in Figure 2), C5 (second row) or C6 (third row), respectively.

The positions of the printing units influence the amount of fount being put onto the paper surface, prior to it being printed. Significantly more fount will be put onto the paper printed at C6 compared to the fount amount on a paper printed at C2. Also the prints from C2 may suffer from back trap mottle caused by the subsequent 4 blanket cylinders (M, Y, C5 and C6), whereas prints from C6 do not risk that as it is the last printing unit in the press.

Table 1: Coating colour formulations

Sample	GCC [pph]	SB latex [pph]	Excess PA dosage [pph]	$[Ca^{2+}]/[A^-]$
Ref	100	11	0	0
0.2 NaPA	100	11	0.2 NaPA	0
0.2 NaCaPA	100	11	0.2 NaCaPA	0.3
0.4 NaPA	100	11	0.4 NaPA	0
0.4 NaCaPA	100	11	0.4 NaCaPA	0.3
0.8 NaPA	100	11	0.8 NaPA	0
0.8 NaCaPA	100	11	0.8 NaCaPA	0.3



Figure 2: Print layout used in the printing trial

A normal fountain feed would be 30–50 %, whereas the feed of 70 % used during most of the trial runs was chosen to show the impact of high moisture, i.e. at very humid conditions, on the print quality. The fountain solution used during the printing process contained two dampening additives, 4 % isopropyl alcohol and 5 % Substifix (supplied by Huber group). For two trial runs using uncalendered papers, a lower more normal fountain feed (30 %) was used. These two uncalendered trial runs were the reference and the coating with 0.8 pph NaCaPA. The rubber blankets were inspected and cleaned between each trial run. No wet pick could be observed for any of the coating formulations.

## 2.4 Characterisation of the coating colours

The coating colour viscosities for the seven prepared formulations were determined using a Brookfield viscometer at a rotation rate of 20 and 100  $\text{min}^{-1}$  using spindle #3. The pH and temperature were held constant at  $8.8 \pm 0.1$  and  $27.0 \pm 0.6$  °C, respectively.

## 2.5 Characterisation of the paper surface

### 2.5.1 Topography

The surface topography of the unprinted coated papers was analysed using two measuring devices, Parker Print Surf (PPS (ISO 8791-4:2007), supplied by Lorentzen &

Wetretre, Sweden) and OptiTopo (supplied by Innventia AB, Sweden). The PPS instrument is sensitive to roughness within the range of 0.6–6.0  $\mu\text{m}$  whereas the OptiTopo can detect smaller variations in the topography than the PPS instrument. The OptiTopo is an optical instrument that determines the topography in  $\mu\text{m}$ , given as a standard deviation from a mean plane of the sample using image analysis of two images taken of the exactly same area on the sample. The two images differ only by the illumination direction during the acquisition of the images (Barros and Johansson, 2005). The topography is then computed with a photometric stereo technique (Hansson and Johansson, 1999). Before the topography variations are computed using frequency analysis, a band-pass filter is applied to eliminate both the finest-scale and largest-scale variations. The bandwidth of the filter used was 0.01–0.5 mm.

### 2.5.2 Contact angles

The apparent contact angle and volume absorption of water on the coating surface were measured using the Fibro-DAT instrument (supplied by Fibro System AB, Sweden). The instrument places a droplet of deionized water onto the sample surface and then records the height and base diameter of the droplet as a function of time, together with the contact angle. The values after 0.5 s are reported. The contact angle measurements were performed 12 months after the coating trial, during which the papers were stored in boxes in a non-conditioned storage room.

### 2.5.3 Permeability analysis

The permeability of tablets made of compressed and dried coating colour was determined gravimetrically using a permeability apparatus (Schoelkopf, Gane and Ridgway, 2004) developed by Omya International AG, Switzerland. Tablets were formed by filtration of the coating colour under pressure (15 bar). The coating colours analysed were formulated according to those shown in Table 1. The coatings were filtered through a fine membrane filter (0.025  $\mu\text{m}$ ) supported by two coarser metal meshes. The time required to form a tablet of a certain height depends both on the solids content of the sample, the water retention properties and the size and packing characteristic of the solid particles in the sample. The tablets obtained had a diameter of 4 cm and a thickness of 1–2 cm was attained. The tablet forming procedure took 3–5 h. The tablets were then dried in an oven (60 °C) overnight.

Before the permeability measurements could be performed, the tablets needed to be further prepared. The dried tablets were cut and ground into blocks, see Figure 3, with a cross sectional area of about 1  $\text{cm}^2$ . The blocks were then embedded in resin and left to cure overnight at room temperature. The absorbing

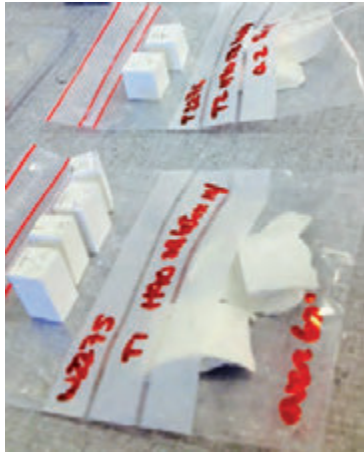


Figure 3: Blocks of compressed coating colour

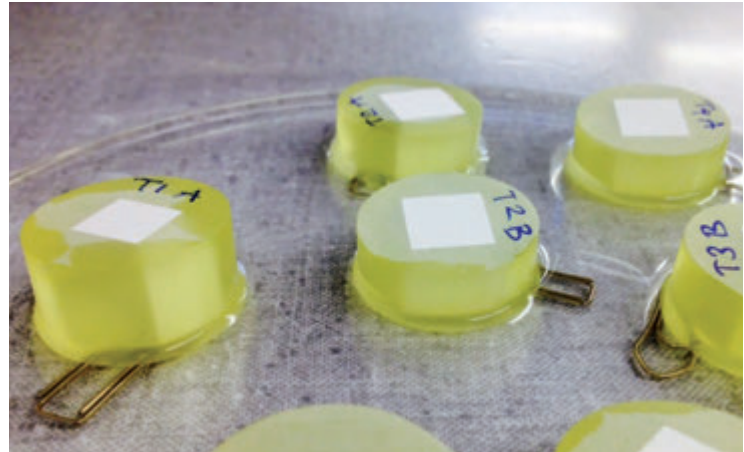


Figure 4: Coating colour blocks embedded in resin and left to imbibe hexadecane

surfaces of the embedded blocks were then carefully ground to ensure full removal of excess resin from the surface. When the resin had dried, the now embedded blocks were placed in a glass dish with hexadecane (ReagentPlus Solvent Grade (99 % purity) supplied by Sigma Aldrich), see Figure 4, and left there until the entire block was saturated with hexadecane, which took roughly one week.

The permeability measurement was performed by placing the embedded sample in the permeability apparatus. Hexadecane was injected into the permeability cell and the sample chamber was then kept pressurised at 7 bar using nitrogen gas. The permeability apparatus was mounted over a micro balance and during the permeability analysis the permeated hexadecane was collected in a sampling dish, placed on the balance, so that the mass of hexadecane as a function of time could be noted (measurements took  $\sim 5$  days). This analysis returned the volume rate of the hexadecane flow, and using Darcy's law (Equation [1]) the permeability, in terms of Darcy's permeability constant ( $k$ ), could be derived (Schoelkopf, Gane and Ridgway, 2004).

$$Q = \frac{-kA\Delta P}{\eta l} \quad [1]$$

where  $Q$  is the volume flow,  $k$  is the permeability constant,  $A$  is the cross sectional area,  $\Delta P$  is the pressure difference,  $\eta$  is the viscosity of the liquid, and  $l$  is the length of sample.

#### 2.5.4 Pore structure analysis

The pore structure of the coating colour tablets, generated for the permeability analysis described above, was evaluated. The pore volume intrusion was analysed on 1.5–2.0 g sample material using a Micromeritics Autopore IV mercury porosimeter (Micromeritics Instrument Corporation, Norcross, GA, USA). The mercury porosimetry method is based on the intrusion

of the non-wetting liquid mercury into the sample under pressure. The pressure required to intrude mercury into the sample structure is then inversely proportional to the pore size, and therefore this technique yields pore size according to the Young-Laplace equation [2].

$$D = \frac{1}{P} \cdot 4\gamma \cos \theta \quad [2]$$

where  $D$  is the diameter,  $P$  is the pressure,  $\gamma$  is the surface tension of mercury, and  $\theta$  is the contact angle of mercury in contact with the sample.

The maximum applied pressure of mercury was 414 MPa, equivalent to a Laplace throat diameter of 4 nm. The equilibration time at each of the increasing applied pressures of mercury was set to 30 seconds. It is vital that the mercury intrusion measurements be corrected for the compression of mercury, expansion of the penetrometer and compressibility of the solid phase of the sample. This is performed conveniently using the software Pore-Comp (a software program developed by and obtainable from the Environmental and Fluids Modelling Group, University of Plymouth, U.K.), in which the Pore-Comp equation [3] (Gane et al. 1996) is applied:

$$V_{\text{int}} = V_{\text{obs}} - \delta V_{\text{blank}} + \left[ 0.175(V_{\text{bulk}}^1) \log_{10} \left( 1 + \frac{P}{1820} \right) \right] - V_{\text{bulk}}^1 (1 - \Phi^1) \left( 1 - \exp \left[ \frac{(P^1 - P)}{M_{\text{ss}}} \right] \right) \quad [3]$$

where  $V_{\text{int}}$  is the volume of intrusion into the sample,  $V_{\text{obs}}$  is the volume of intruded mercury,  $\delta V_{\text{blank}}$  is the volume change during blank run,  $V_{\text{bulk}}^1$  is the sample bulk volume at atmospheric pressure,  $P$  is the applied pressure,  $\Phi^1$  is the porosity at atmospheric pressure,  $P^1$  is atmospheric pressure, and  $M_{\text{ss}}$  is the Bulk modulus of the solid sample.

## 2.6 Characterisation of print quality

### 2.6.1 Print density

The print density of cyan fulltone areas was measured with a reflection densitometer (Techkon supplied by SpectroDens) which records the amount of light reflected by the studied surface over an exposure wavelength range of 500–520 nm. The densitometer returns the print density as a logarithmic ratio between the light reflected by white (unprinted) paper and the light reflected by the print. The print density reported in this study is the average print density of 10 measurements.

### 2.6.2 Print gloss

The print gloss at an angle of 75° (according to TAPPI Standard T480 using a ZLR 1050M glossmeter supplied by Zehntner) of cyan fulltone areas was detected and the stated results are an average of 20 measurements.

### 2.6.3 Uncovered area

The uncovered area (UCA) on printed areas was quantified with the STFI mottling (Johansson and Norman, 1996) image analysis software. The prints are scanned

(Perfection v750 Pro scanner with a maximum optical resolution of 4800 dpi × 6400 dpi supplied by Epson) and saved as grey-scale images. The software uses light reflectance shown in the grey-scale image. The images are calibrated with respect to reflectance, by determining a reflectance threshold (relative to the mean reflectance level of the image), and UCA is then computed by including all areas with a higher reflectance than the threshold as those contributing to the computed UCA. The resolution of the analysed images was 600 dpi, which represents a pixel size of 42.3 μm. The UCA reported is an average of 10 analysed areas (4.3 cm × 4.3 cm).

### 2.6.4 Print mottle

The occurrence of print mottle was also evaluated using the STFI mottling software. The software determines print mottle by detecting the spatial change in light reflectance in grey-scale images. The images are calibrated to reflectance and the output data from the mottle analysis is the coefficient of variation (COV) in reflectance, divided into spatial wavelength bands. Values of variation over 1% are considered to be of importance. Print mottle was analysed on 10 areas (4.3 cm × 4.3 cm) of each sample.

## 3. Results

### 3.1 Viscosity of coating colour

The Brookfield viscosity increased upon addition of polyacrylate (PA) dispersant, see Figure 5. Excess dispersant leads to the presence of free water-soluble polyacrylate in the suspension (Loiseau et al., 2005), which leads to induced pigment and binder agglomeration, which is manifested by increased viscosity related primarily to depletion flocculation (Husband, 2000).

The viscosity increase was seen to be higher in the coating formulation where partially calcium neutralised dispersant had been added, in particular at the highest dosage. The detrimental impact of high levels of bound calcium ions on the dispersing effect of polyacrylate has also been shown by Järnström (1993). It is known that calcium ions interact strongly with sodium polyacrylate (Stenius, Järnström and Rigdahl, 1990) during the formation of Ca-polyacrylate complexes which are solu-

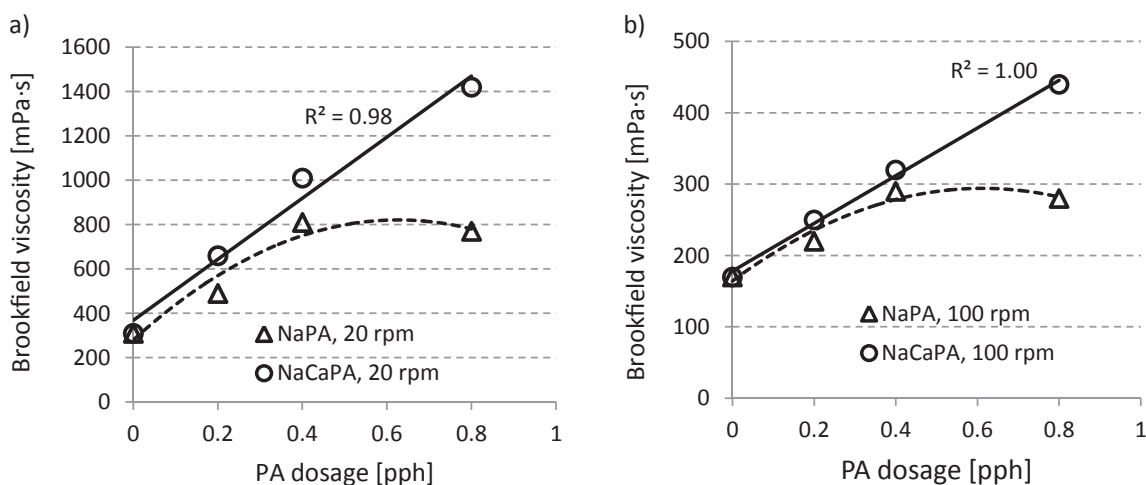


Figure 5: The Brookfield [mPa·s] viscosity as a function of increasing amounts of NaPA and NaCaPA dosage at a rotation rate of a) 20 rpm and b) 100 rpm

ble at low Ca to PA ratio but form colloidal particles at and above a certain ratio. This ratio, also referred to as seed point, decreases with the polyacrylate concentration (Kamal Alm et al., 2010). It is reasonable to assume that a water-soluble Ca-PA complex gives a lower contribution to the viscosity increase than a water-soluble polyacrylate without Ca since its dissociation is impeded and so the charge density is reduced by incorporating calcium ions. Thus, the stronger viscosity increase in the suspensions where partly calcium neutralised dispersants had been used is likely due to formation of colloidal Ca-PA particles and/or particulate agglomeration. The drop in the viscosity at 0.8 pph NaPA is then expected to be due to a reduction in  $\text{Ca}^{2+}$  concentration due to the high excess of PA, and thus also a reduction of colloidal Ca-PA particles.

### 3.2 Properties of the paper surface

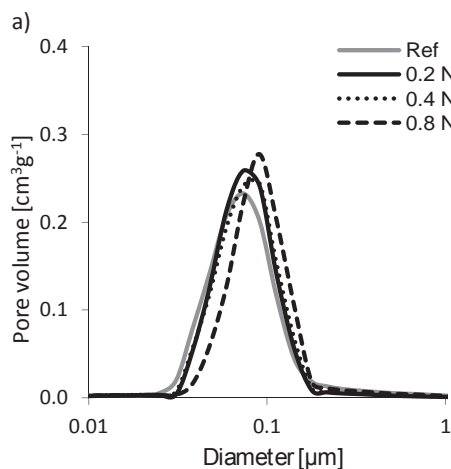
The paper surfaces studied here were from the pilot coated series, and both calendered and uncalendered papers were included.

#### 3.2.1 Topography

The different formulations had no impact on the surface roughness, while calendering, as expected, reduced the roughness. The mean values of 10 measurement points on every formulation included in this study, on both calendered and uncalendered surfaces, are given in Table 2.

Table 2: The mean of all surface roughness values measured with PPS and OptiTopo  $\pm$  standard deviation

Sample	PPS [ $\mu\text{m}$ ]	OptiTopo [ $\mu\text{m}$ ]
Calendered	$0.59 \pm 0.04$	$0.21 \pm 0.04$
Uncalendered	$1.56 \pm 0.11$	$0.53 \pm 0.05$



These roughness results match our previous findings (Kamal Alm et al., 2010), where high (0.8 pph) dosage of polyacrylate had no effect on topography. In this study we have confirmed that this is the case also for lower additions. Thus, the aggregation of coating pigments and/or binder, induced by additional polyacrylate, had little or no impact on the surface roughness at the scale measured.

#### 3.2.2 Contact angle

The contact angle between a water droplet and the coated paper surface was analysed using the Fibro-DAT instrument. The average contact angles of 8 droplets from each sample were collected. Relatively small differences in contact angles were obtained, but no reliable systematic change could be observed. The contact angles for the calendered samples varied between  $87\text{--}92^\circ$  and for the uncalendered samples it varied between  $83\text{--}92^\circ$ , the highest standard deviation for these results being  $\pm 3$ .

#### 3.2.3 Pore structure and permeability

The porosity of the dried coating colour tablets was determined by mercury porosimetry. This analysis returns the pore volume of the dried coating structures, see Figure 6a and 6b for the NaPA and NaCaPA containing formulations, respectively. Increasing dosage of NaPA resulted in a slight increase in pore size and pore volume. The dosing of NaCaPA, however, had a more complex effect on the pore size and volume distribution of the coating structure. A dosage of NaCaPA with 0.2 pph had the largest effect on the pore size and the most marked increase in pore volume, both of which increased significantly at this dosage. This is because the dispersing effect of polyacrylate sharply deteriorates in the presence of free calcium ions, especially at low excess polyacrylate dose (Järnström, 1993) and the depletion effect dominates. Hence, the flocculation of

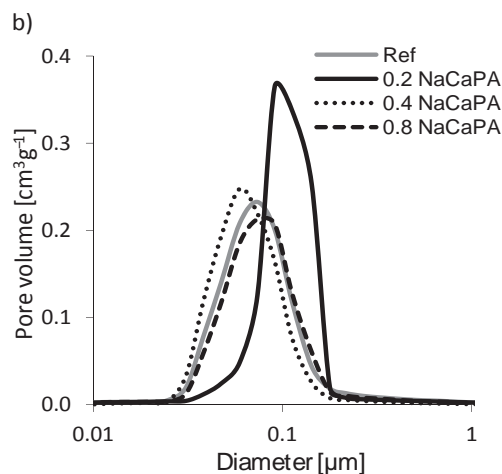


Figure 6: The pore volume [ $\text{cm}^3 \cdot \text{g}^{-1}$ ] of dried coating colours containing a) increasing amounts of NaPA and b) increasing amounts of NaCaPA

pigments, binder and PA is more severe upon initial excess dosage levels of PA in the presence of  $\text{Ca}^{2+}$  ion compared to higher PA ratio levels, and the pore size therefore increases. Once the initial flocculation is overcome by increased addition of NaCaPA, the trend from dispersed to further flocculation due to charge density increase follows roughly that of the NaPA (Figure 6b versus Figure 6a).

The liquid permeability of the dried coating colour structures is shown in Figure 7. The permeability of the sample containing excess NaPA was significantly higher than for the ones containing excess NaCaPA, with the exception of the sample with the lowest excess of NaCaPA (0.2 pph). These results coincide with the porosimetry results, where the pore volume and pore size of the sample with 0.2 pph excess NaCaPA was in fact significantly higher than for the other coating formulations.

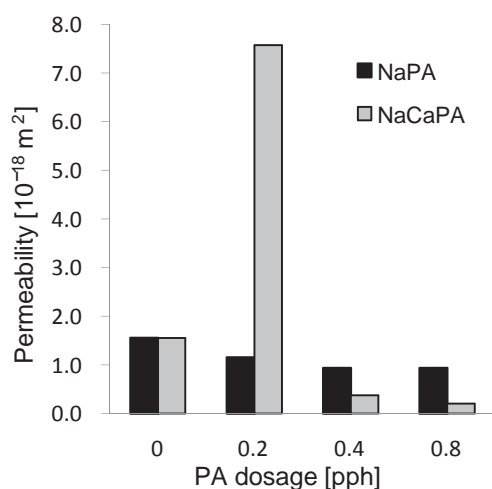


Figure 7: The permeability [ $10^{-18} \text{ m}^2$ ] through compressed tablets of ground calcium carbonate

An inspection of the surface structure of the coated papers using SEM showed a significant non-uniformity in porosity with frequent occurrence of compacted/closed areas, in particular for calendered samples, which have been reported previously (Kamal Alm et al., 2015).

### 3.3 Print quality

Print variability is often seen when printing the cyan colour since the human eye is sensitive to cyan, but also since the cyan inking unit in a multicolour press often is placed early in the print colour order. In addition, cyan is often printed using a relatively low film weight, which leads to a significant visual disturbance when the ink film thickness varies. The results presented here are, therefore, only from cyan printed areas in three different units (C2, C5 and C6) on calendered and uncalendered

papers printed with a fountain solution feed of 70 %, which in this study is referred to as the standard high level feed (SF).

Areas printed at C2 have been wetted by fount once (in the K printing unit) before it was printed in C2 and the print will be subjected to four back traps before it leaves the press. Areas printed in C5 have been wetted four times and will be subjected to one back trap before leaving the press, whereas areas printed at C6 have been wetted five times with fountain solution and are not subjected to back trap.

#### 3.3.1 Print density

The average cyan print densities of the seven different papers printed at C2, C5 and C6 were 1.44, 1.24 and 1.43 with standard deviation  $\pm (0.05-0.10)$  on the calendered and 1.44, 1.39 and 1.41 with standard deviation  $\pm (0.08-0.17)$  on the uncalendered papers, respectively. Thus, the print density did not vary much between the different papers within each print unit. However, the print density decreased somewhat for almost all calendered trial runs in the 5<sup>th</sup> print unit (C5) when compared to prints from the two other cyan printing units.

#### 3.3.2 Print gloss

Figure 8 shows print gloss measured at an angle of 75°. Calendered papers returned values around 77 %, while uncalendered gave values around 60 %. The difference between the formulations and print units was small. This was expected since excess PA had no effect on the specular reflecting size component of the coating topography.

#### 3.3.3 Uncovered area

Light microscope images of a print suffering high levels of UCA were acquired. Figure 9 shows an overview image of a print with a high amount of UCA, and a close-up of such an area.

The amounts of UCA on fulltone prints from all cyan print units are shown in Figure 10. The UCA found on prints from C2 was minor in comparison to the quantity of UCA found on prints from the two following print units (C5 and C6). The majority (90 %) of the uncovered areas identified were small (squares of side 1–3 pixels, equal to 42.3–126.9  $\mu\text{m}$ ). The average standard deviation of the UCA found in C2, C5 and C6 was  $\pm 0.003$ ,  $\pm 0.092$  and  $\pm 0.012$  %, respectively, which roughly corresponds to a coefficient of variation of 10 %.

For prints on calendered papers (Figure 10a and 10b), excess dosage of NaPA or NaCaPA, up to 0.4 pph, increased the quantity of UCA. Generally, more UCA was found on the paper coatings with dosed NaCaPA

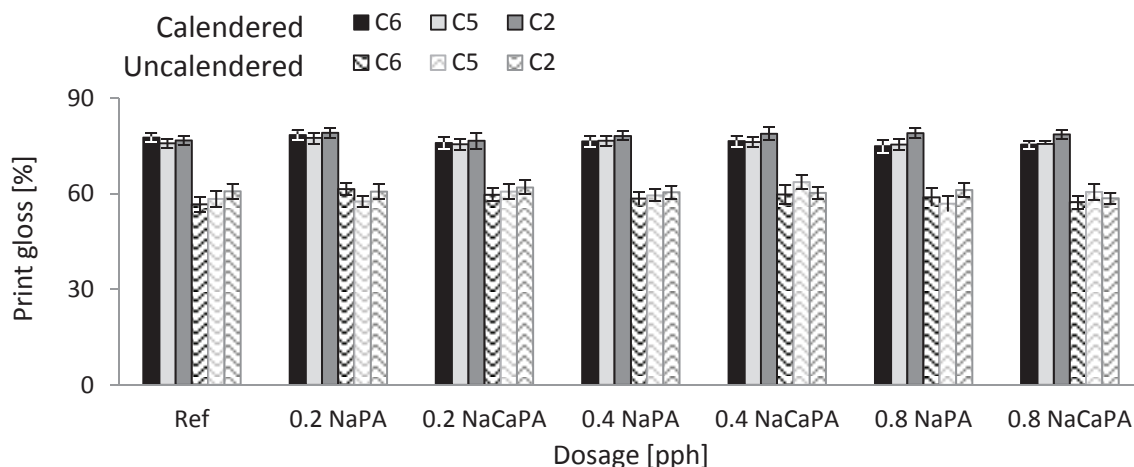


Figure 8: Print gloss at 75°

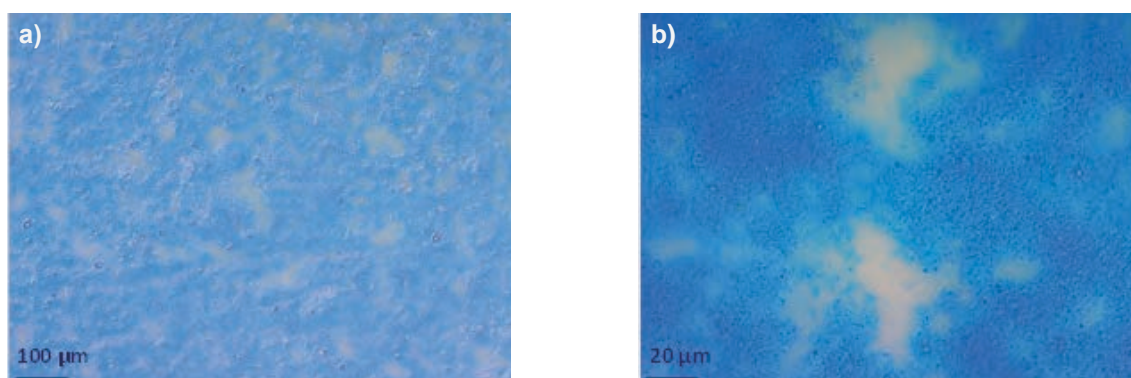


Figure 9: A micrograph image of a print a) with high amounts of UCA and b) UCA adjacent to ink covered areas on a print, at high magnification

compared with NaPA, especially at the lowest excess dosage of 0.2 pph. The highest polyacrylate dosage level, however, is seen not to influence the occurrence of UCA to the same extent as the lower and medium dosage levels.

Also print on uncalendered paper returned higher UCA when additional PA had been added to the coating colour (Figure 10c and 10d). For prints in C5 and C6, maximal UCA was reached already after the lowest dosage of PA. UCA on prints from C2 showed a steady increase with dosage of NaPA and reached a significantly high value at the highest dosage.

The general picture can be summarised as:

- Excess of dispersant leads to an increase in UCA with a maximum at 0.2–0.4 pph excess dispersant.
- The ratio of PA to  $\text{Ca}^{2+}$  is seen as critical in calcium carbonate-containing coating colours.
- Uncalendered papers showed roughly the same amount of UCA on the fifth and sixth units while calendered papers showed significantly higher UCA on prints from the fifth unit.

### 3.3.4 Print mottle

The print mottle was measured in two wavelength classes, and the results are given in Figure 11. The larger wavelength class which starts at 0.25 mm shows much higher values than the smaller and most often used wavelength class, which starts at 1 mm. This means that a significant amount of the non-uniformity in print density comes from small sizes, which is reasonable in this case since the majority of the UCA detected was made up from small white spots. Only a small effect on the mottle value related to PA dosage was seen on prints from C2, but a rather limited addition of dispersant had a significant impact on mottle in prints from C5 and C6, where prints from C5 showed the highest values.

Addition of NaCaPA had a more severe impact on the mottle than NaPA, independent on whether the papers were calendered or not. For calendered papers, the print mottle decreased at the highest addition of NaPA or NaCaPA, but this was not as pronounced for the uncalendered papers.

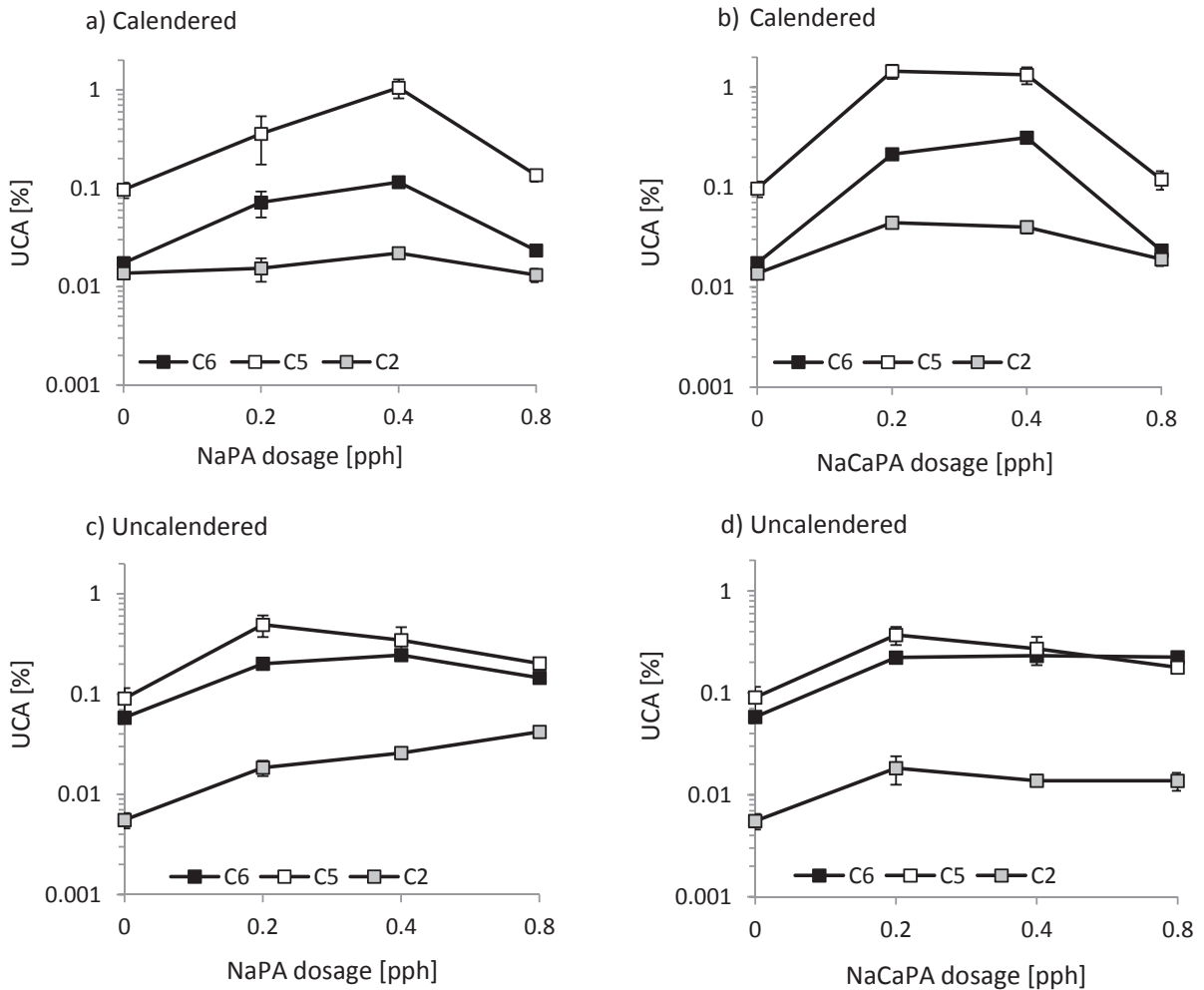


Figure 10: Amount of UCA [%] found on calendered (a, b) and uncalendered (c, d) papers printed at C2, C5 and C6 as a function of NaPA (a, c) and NaCaPA (b, d) dosage [pph], respectively

The print mottle on 50 % halftone prints was also analysed in the same manner as the fulltone prints. Figure 12 shows print mottle of fulltone and halftone prints in the same graph. Increasing PA dosage leads to impaired print quality mainly on prints from C5 and C6. The calendered papers show a clear maximum in print mottle, which indicates the detrimental effect of excess PA dosage when considering print quality. This is also observed on prints on uncalendered papers coated with coating formulations containing NaCaPA.

The detrimental print mottle maximum occurs at higher dispersant dose for the halftone prints compared with the fulltone ones. This endorses the hypothesis that trapped fount can escape sideways slightly better in the halftone print than when trapped under a fulltone ink layer, and so water interference mottle in the halftone is somewhat less severe.

### 3.4 Impact of fountain feed on UCA and print mottle

For two trial runs the level of fountain feed was reduced from 70 %, which was the standard feed (SF), to 30 %, referred to as reduced feed (RF). Two uncalendered papers were printed, i.e. the reference and the one with 0.8 pph NaCaPA. Figure 13 shows that UCA becomes significantly reduced upon reducing the fountain feed. However, also at the lower feed, the dosage of 0.8 pph NaCaPA still had a significant impact on UCA in prints from C5 and C6, since it was about three times higher compared to the reference. Also the print mottle values were reduced when the fountain feed was reduced, as shown in Figure 14. The mottle values were low also for the paper containing the top level of 0.8 pph NaCaPA. The print quality deteriorating effect of excess PA was, therefore, more evident for the standard (high) fountain level used during these trials.

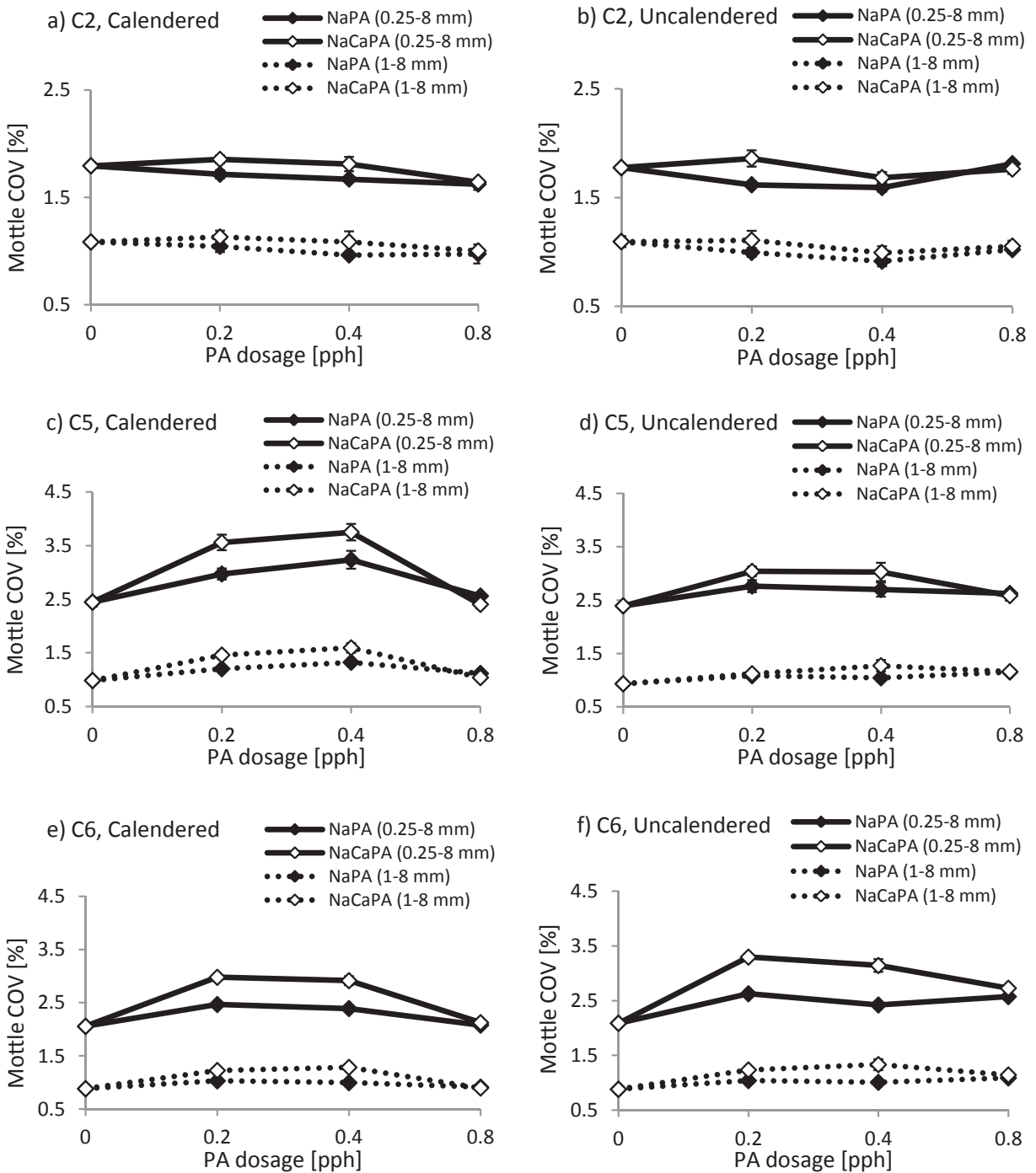


Figure 11a–f: The print mottle COV [%] in two wavelength classes, 0.25–8 mm (solid lines) and 1–8 mm (dashed lines), for the fulltone prints on calendered (left column) and uncalendered (right column) papers from the three print units, where solid symbols are papers with addition of NaPA, while open symbols are with addition of NaCaPA

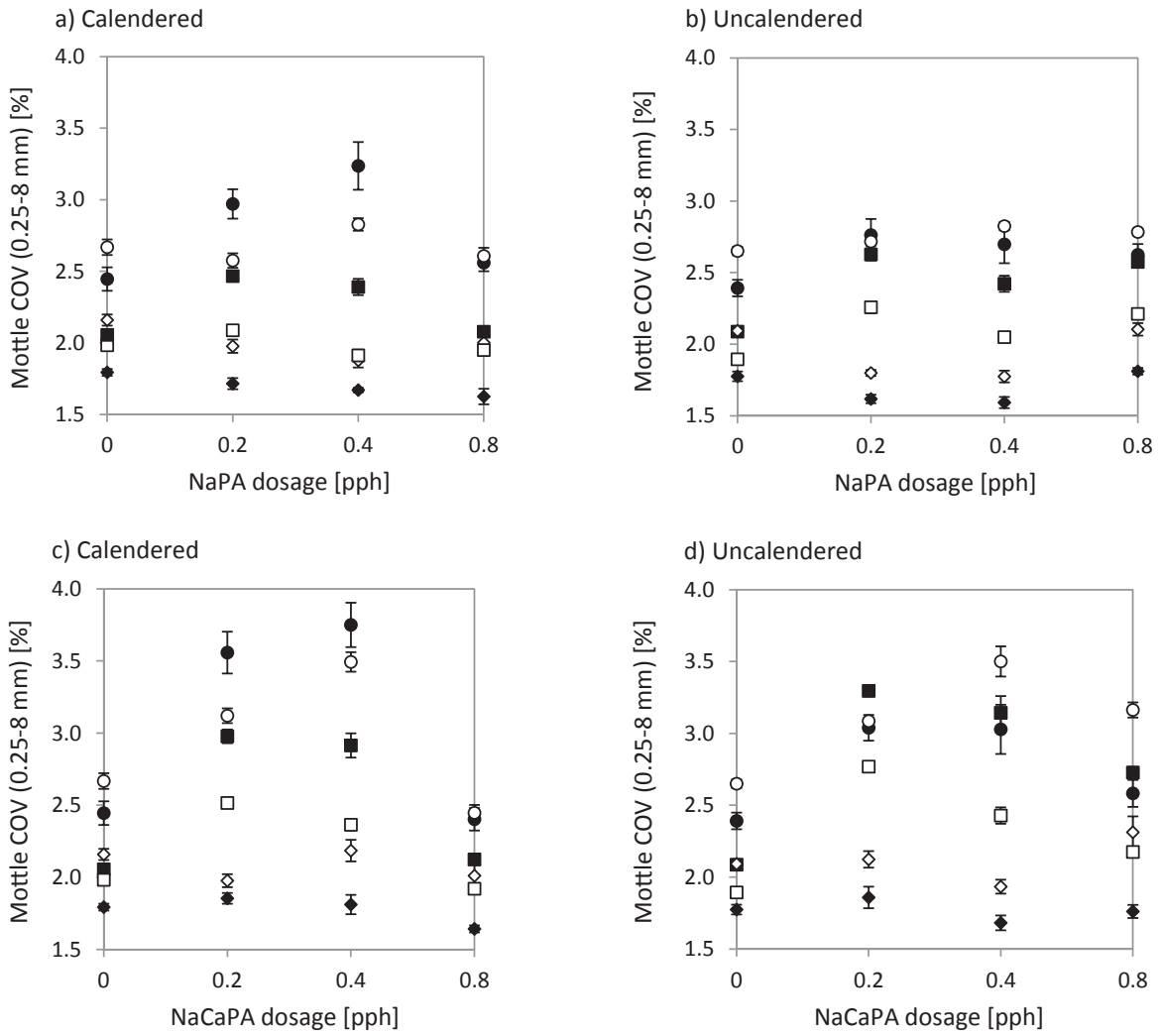


Figure 12a–d: The print mottle COV [%] in fulltone (closed symbols) and halftone (open symbols) on prints printed at C2 (◆ ◇), C5 (● ○) and C6 (■ □), respectively, on a) calendered paper with excess dosage of NaP, b) uncalendered paper with excess dosage of NaPA, c) calendered paper with excess dosage of NaCaPA, d) uncalendered paper with excess dosage of NaCaPA

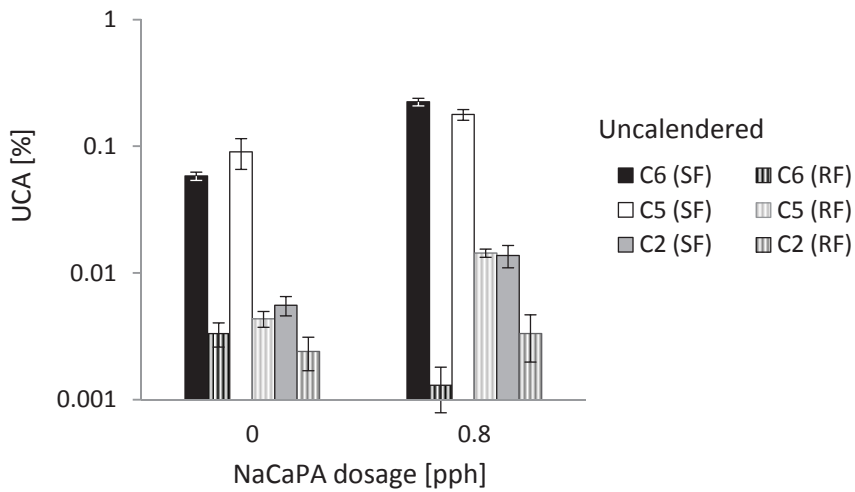


Figure 13: Amount of UCA [%] on fulltone prints printed at C2, C5 and C6, respectively, when two (SF and RF) fountain feed levels were used

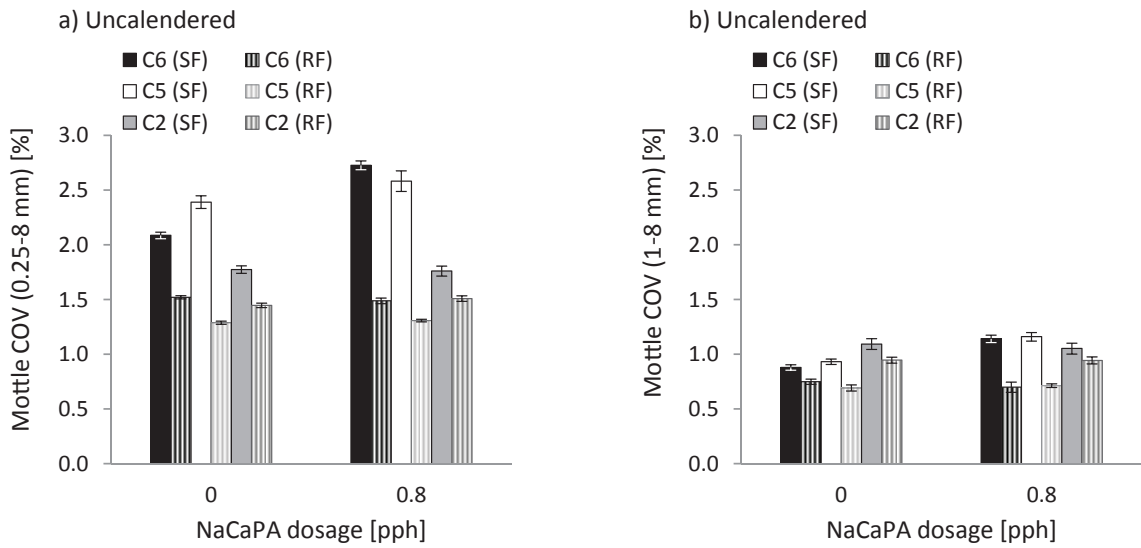


Figure 14: Print mottle COV [%] on fulltone prints printed on uncalendered paper at C2, C5 and C6, respectively, when two fountain feed levels were used, SF (solid bars) and RF (striped bars), for two wavelength classes a) 0.25–8 mm and b) 1–8 mm

#### 4. Discussion

##### 4.1 Coating structure and surface chemistry

The presence of excess NaPA has a significant impact on local pore structure and surface chemistry of the

coating layer, and these in turn appear to be key factors for ink adhesion. Compact areas within the surface layer of the coating have been identified (Kamal Alm et al. 2015) and an example of such an area is shown in

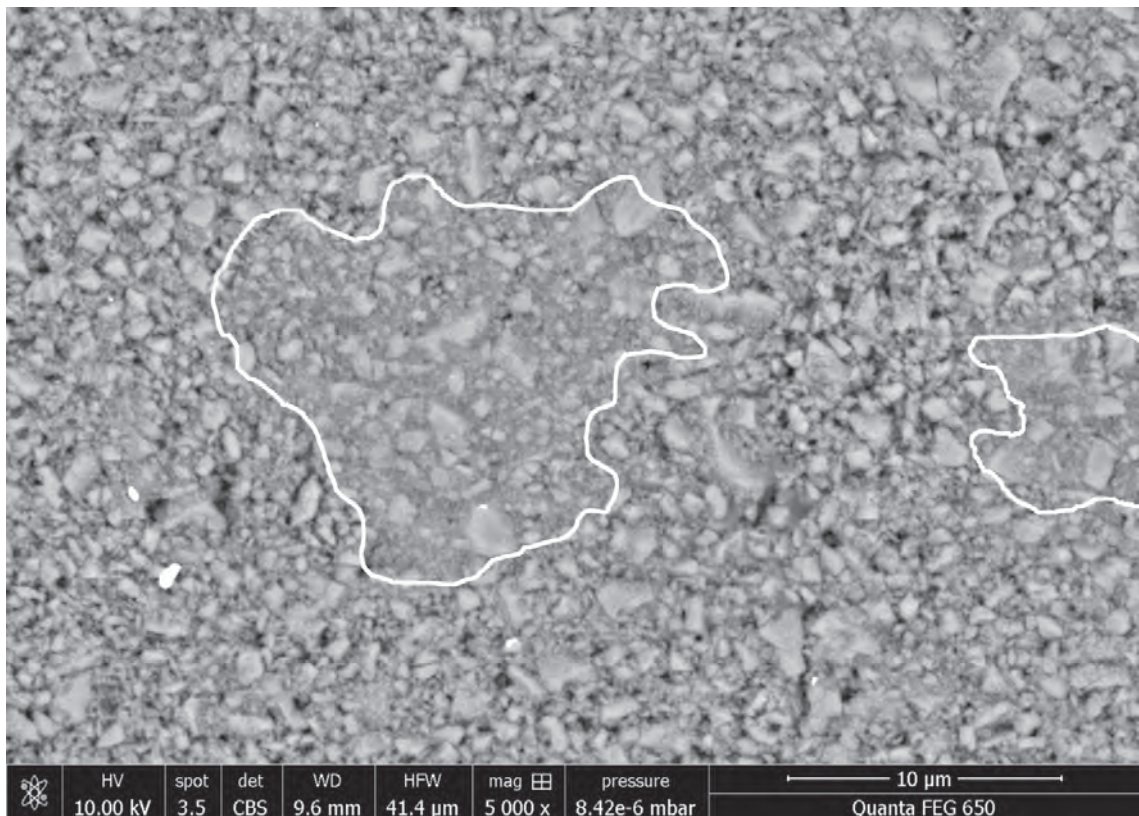


Figure 15: Scanning electron microscope image of an area of the coating with compact spots, which are indicated by the white boundary line

Figure 15. The compact spots occurred more frequently on papers with high amount of UCA and contained more NaPA than open areas. Data on this relation effect have been reported in a recent publication (Kamal Alm et al., 2015), in which focus was given on the relation between paper properties and the ink adhesion failure mechanism, while this paper focuses on the overall printability.

Literature data comparing the surface chemistry of calcite with adsorbed NaPA and that of calcium carbonate coatings with excess dispersants added have shown that adsorption of NaPA makes the surface more hygroscopic, more polar and the pore structure absorbs water faster (Koivula, Kamal Alm and Toivakka, 2011; Kamal Alm et al., 2010). For model systems of freshly cleaved calcite surfaces Koivula, Kamal Alm and Toivakka (2011) showed that the water contact angle on clean calcite surface was around 50°, while it decreased to about 30° for a calcite surface covered by adsorbed NaPA.

The value decreased even further when tested in a more humid environment. The findings were supported by data from vapour sorption isotherms, which showed strong increase in adsorbed vapour when the relative humidity exceeded 50 %. Also reported was the surface energy of calcite with adsorbed NaPA. The total surface energy was 46.8 mJ·m<sup>-2</sup> with the Lifshitz–van der Waals part being 21.4 mJ·m<sup>-2</sup> and the acid-base part being 25.5 mJ·m<sup>-2</sup>. The Lifshitz–van der Waals contribution to the surface tension of water is 21.8 mJ·m<sup>-2</sup> (Fowkes, 1980), which is very close to the value found for an adsorbed layer of NaPA. This suggests that the layer in a moist environment is a mixed layer of water and NaPA. Layers of polyacrylate are indeed both hygroscopic, hydrophilic and polar.

In a coating layer, the situation becomes different since the calcium carbonate surface is not as pure as was studied for the calcite, and one must consider that partially hydrophobic polymer latex with surface active agents has also been added. Moreover, the typical coating layer is microrough, porous and chemically heterogeneous, all of which makes the interpretation of contact angle difficult. In addition, the contact angles of the pilot coated papers were measured some 12 months after coating and cannot be used in the discussion since, amongst many factors, mobile components of the coating migrate to the surface and act to render it hydrophobic (Lindenmark et al., 2010). Instead, we refer to earlier work conducted at our laboratory. These measurements showed a decrease in the advancing water contact angle of 10°, from 86° to 76°. Even though the decrease in contact angle is moderate it has a significant impact on wettability, since the cosine value of the contact angles goes from 0.07 to 0.24. It is the cosine value of the contact angle, which reflects the wettability linearly.

The water absorption, as observed in the contact angle measurements, occurring within the first 8 ms from contact we refer to as “instantaneous absorption”, and it was seen to change from 0 to 10 cm<sup>3</sup>·m<sup>-2</sup> upon introducing 0.8 pph extra polyacrylate. The surface energy of the coated layer, as calculated from the advancing contact angle, was around 44 mJ·m<sup>-2</sup> and the acid-base part had increased from around 1 to 2.5–3 mJ·m<sup>-2</sup> upon addition of extra NaPA. This can be seen as a significant increase, since the advancing contact angle, which was used in the calculations, is strongly influenced by the low energy areas of the heterogeneous surface, in this case areas with high amount of latex.

The data for calcite, and the fact that polyacrylate is concentrated within compact areas, suggest that the compact spots may be more polar than the average polarity of the coating layer.

#### 4.2 Ink adhesion failure mechanisms in offset printing

Water on hydrophilic surfaces has a significant importance for ink transfer in offset printing. Non-image areas of the printing plate are hydrophilic and fountain solution is applied to prevent ink adhering to these areas. The mechanism that inhibits the ink adhering to non-image areas was earlier believed to be a result of adhesion failure at the ink/fountain solution interface (Kato, Fowkes and Vanderhoff, 1982). However, the general belief today is that a cohesive split of the fountain solution layer, rather than a weak interface, is what actually prevents ink transfer onto non-image areas during the printing process (McGill, 1977; Shen, Hutton and Liu, 2004).

According to the Stefan equation [4] (Stefan, 1874), the force needed to split a liquid film depends on the splitting velocity, but, more importantly for this application, it is inversely proportional to the third power of the film thickness and proportional to viscosity of the film.

$$\frac{F}{A} = \frac{C\eta v}{t^3} \quad [4]$$

where  $F$  is the force,  $A$  is the plate area,  $C$  is the constant,  $\eta$  is the viscosity of liquid,  $v$  is the velocity at plate separation, and  $t$  is the film thickness or distance between plates.

MacPhee (1979) used this as a starting point to discuss ink transfer in offset printing and showed theoretically that for a configuration of non-image area/fountain solution/ink/ink roller, splitting will occur in the ink layer when the thickness of the fountain layer is low, but once it exceeds a certain value splitting will occur within the fountain solution film. The critical thickness depends on the viscosities of the two liquids as well as the thickness of the ink film and can be calculated using Stefan's equation. A calculation using industrial-like conditions

suggests that the critical fountain solution film thickness is around 40 to 80 nm, below which ink transfer to the non-image areas of the printing plate is likely to occur. The calculation is based on an ink film thickness of 2  $\mu\text{m}$  and a ratio of ink viscosity to fount viscosity between  $2 \cdot 10^4$  and  $10^5$ .

A similar approach can be used for the appearance of spots without ink, i.e. UCA on a moist paper surface due to ink transfer failure, also referred to as ink refusal. UCA is a consequence of areas on the coating surface where the absorption rate of fount is low compared to the printing speed, which results in ink transfer failure. This takes place when the thickness of the fount layer on the paper surface has surpassed the critical thickness required for ink transfer, according to Stefan's equation and the discussion above.

Ink-lift-off, on the other hand, means that the ink has been transferred to the paper, but due to low adhesion to the surface it has been lifted off by the rubber blanket in the subsequent print unit(s). The theoretical explanation for the phenomenon is that ink first is transferred to the paper because the moisture on the paper surface is not sufficient to give ink refusal. The ink is then lifted off by the rubber blanket in the subsequent print nip because the cohesive strength in the ink film has increased, i.e. since the physical state of the ink film has changed, the ink film thickness is now less and its viscosity is higher. The ink film thickness has decreased because the ink film transferred to the paper is thinner than the ink film on the rubber blanket prior to transfer, since splitting normally occurs in the middle zone of the ink film. The ink that is built-up on the non-printing parts of the subsequent rubber blanket(s) has previously been on the paper where ink oil has depleted and its viscosity is higher compared to fresh ink that has been deposited on the printing areas on the rubber blanket from the printing plate.

Given the description above, when ink is transferred to the paper in the 5<sup>th</sup> unit, the ink film is thick, which results in a cohesive failure within the ink film and thus ink transfer. Subsequently, when this ink meets the rubber blanket in the 6<sup>th</sup> unit, the ink film is thinner and it joins together with ink on the rubber blanket, which has high viscosity. The cohesive strength of the ink film is now higher. If it is higher than the strength between the paper and the ink film, the ink will be lifted off from the paper and transferred onto the rubber blanket. The strength between the ink film and the paper surface is strongly affected by the coating structure and surface chemistry, e.g. polar character and moisture on the surface, which definitely will have impact on the strength. This effect relies on the large roles being played by permeability and capillarity, respectively, as large connected pores facilitate transport of fountain solution away from the surface only when external pressure is

applied in the nip in contrast to closed areas, and finer pores act between units to remove water by their high capillarity. Calendering will thus be critical since it not only smoothens the surface and reduces the pore size, but also induces compacted/closed areas. An excess of dispersant will make the surface more polar, which enhances adsorption, and so retention, of water molecules and formation of water-containing surface layers.

Another phenomenon that occurs in the presence of excess dispersant, not studied independently here but reported by Loiseau et al. (2005), is the formation of colloidal Ca-PA particles. They are formed at moderate excess of polyacrylate but not at high excess due to a too low concentration of calcium ions in solution following the initial chelation by the dispersant at lower dose. These particles may further densify compaction spots under severe calendering within the coating, and so further reduce transport of fount from these spots. Additionally, or alternatively, it is this condition of colloidal CaPA that we see creates the greatest disruption of the coating pore structure, and so a likely non-uniformity in surface chemistry between pigment and binder-rich areas. The fact that UCA is greater when NaCaPA is added compared with NaPA, and the decrease in UCA at high dosages of extra dispersant suggests that the colloidal Ca-PA complex has a significant importance for the overall mechanism.

More details on the mechanism of ink adhesion failure can be found in our previous paper from this printing trial (Kamal Alm et al., 2015). For instance, it was concluded that compact areas in the coating, which have very low permeability after calendering, had a large impact on ink adhesion failure and UCA. In the present study we wanted to investigate whether a value of mean permeability also had an impact on the presence of UCA. Thus, mean permeability was measured and are reported in Figure 7. A comparison between these data and the UCA reported in Figure 10a–d shows no correlation, which suggests mean permeability is not a key factor in determining UCA when initial ink transfer is not impeded. This is logical, since the removal of fount water by hydraulic impression in the printing nip defines the initial ink transfer success, but not the subsequent degree of adhesion. Local spots with low permeability, however, are more detrimental and may be regarded as a severe coating defect.

UCA in prints from C6 can only be due to ink refusal since the 6<sup>th</sup> unit was the last unit, but UCA in C5 and C2 may be caused by a combination of both ink refusal and ink-lift-off. The data in this paper show that UCA due to ink-lift-off could be as high as 1.5 % on calendered paper, while UCA due to ink-lift-off on uncalendered papers never exceeded 0.5 %. The calendered papers showed low UCA after C6, thus low ink refusal. However, UCA was significant on prints from

C5. Consequently, we consider UCA on the calendered papers to mainly be caused by the ink-lift-off mechanism, and the greater thin layer splitting force generated on the smoother calendered surface.

4.3 Print mottle in different wavelength bands

An ocular inspection of the prints revealed that prints from C5 and C6 had not only white spots but also a small-scale “blurry” pattern of variation in print density. This may be a consequence of water being emulsified into the ink, which dilutes the ink locally and gives a non-uniform distribution of ink pigment on the paper. Thus, water-induced-mottle (WIM) may be divided into two groups; UCA induced mottle and emulsified water induced mottle. In addition, back trap mottle (BTM) may show up in prints from C2 and C5.

Figure 16 show micrograph images of fulltone areas of prints from C5 with low (Figure 16a) and high (Figure 16b) amount of UCA. The mottle value is higher for the print in Figure 15b due to the high amount of UCA. Both prints show small-scale variation and a blurry small-scale pattern is obvious in the left image.

Print mottle is quantified as the print density variation in different wavelength bands. Back trap mottle (BTM) characterised in the wavelength 1–8 mm has previously shown good correlation with perceived unevenness in print density, and, thus, this wavelength band is most often used for quantification of print mottle (Johansson, 1993; Lindberg, Fahlcrantz and Forsgren, 2008). However, there is no information in the open literature about correlations between perceived and measured mottle for water interference mottle (WIM). Since the spots that formed the UCA were small, and the blurriness also appeared to be of small scale, the print mottle was measured not only in the 1–8 mm wavelength band but also in the 0.25–8 mm band in order to capture irregularities of smaller sizes. This larger wavelength interval gave higher values of mottle. Figure 17a shows a diagram where the two mottle values have been plotted against each other for all fulltone prints. The data divide into two linear master curves with very high correlation coefficients and intercepts close to the origin. When only prints on calendered papers were used to calculate the R<sup>2</sup> values, they increased to 0.98 and 0.91 for the upper and lower line, respectively (Figure 17b).

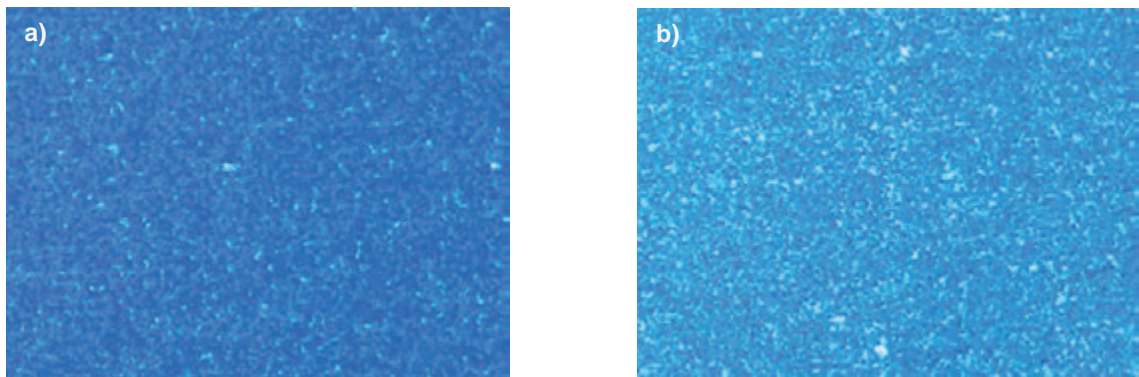


Figure 16: A micrograph image of a mottled print a) with low amount of UCA and b) with high amounts of UCA

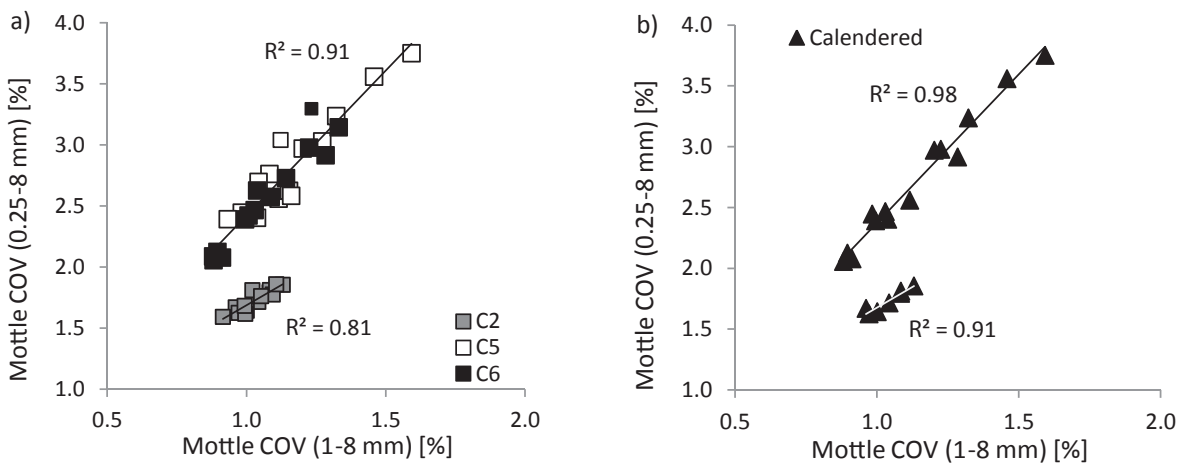


Figure 17: Print mottle COV (0.25–8 mm) [%] as a function of print mottle COV (1–8 mm) [%] on fulltone prints a) on both calendered and uncalendered paper printed at C2, C5 and C6, respectively and b) on calendered paper only

It is indeed initially surprising that the data collect into two lines (Figure 17). All data points in the lower line are from prints in C2, while all the data in the upper line are from prints in C5 and C6 where fountain solution has been in contact with rubber blankets, paper and ink in the earlier print units. The prints in the lower line have a low amount of UCA but the prints from C6 in the lower end of the upper line also have low UCA. Some papers from C2 actually have higher UCA than certain papers from C6 (see Figure 9). Thus, UCA alone cannot fully provide an explanation for the fact that the data form two groups.

In the following, mottle values measured in the larger wavelength band are referred to as “ $\frac{1}{4}^{T08}$ -mottle” and mottle values in the shorter wavelength band are referred to as “ $1^{T08}$ -mottle”. For the same value of  $1^{T08}$ -mottle (e.g. 1.0), papers from C5 and C6 have much higher  $\frac{1}{4}^{T08}$ -mottle than papers from C2, about 0.8 units higher. Thus, the small-scale mottle is much higher in C5 and C6 than in C2, which does not only come from UCA.

It is reasonable to assume that the “blurry” ink density pattern which we anticipate to be due to water emulsified into the ink prior to, or during, its transfer to the paper, contributes strongly to small-scale mottle in C5 and C6, and that the mottle in C2 mainly is due to BTM. Furthermore, when the water feed is reduced, the  $\frac{1}{4}^{T08}$ -mottle of the two prints from C2 becomes slightly reduced, from  $1.77 \pm 0.01 \%$  (mean value of the two prints) to  $1.48 \pm 0.03 \%$ ; also the  $1^{T08}$ -mottle is slightly reduced, from  $1.07 \pm 0.02 \%$  to  $0.94 \pm 0.01 \%$  (see Figure 14). But the impact on the four prints from C5 and C6 is much higher, as the  $\frac{1}{4}^{T08}$ -mottle is reduced from  $2.4 \pm 0.3 \%$  (mean value of the four prints) to  $1.4 \pm 0.1 \%$ . In the  $1^{T08}$ -mottle measured under the same conditions the reduction goes from  $1.03 \pm 0.14 \%$

to  $0.71 \pm 0.03 \%$ . The experimental data from C5 and C6 at reduced water feed collect on, or slightly above, the lower line. Thus, it is quite obvious that the upper line collects data where WIM dominates the mottle, while the lower line collects data where BTM dominates. The emulsified water induced mottle (WIM) differs from BTM in the sense that it shows a smaller-scale pattern, and it in turn differs from UCA induced mottle since the light areas have a certain non-zero print density.

A  $1^{T08}$ -mottle value  $< 1$  is regarded as low. Thus, there was no severe mottle in the C2 prints. On the other hand, the papers with the highest values will touch the limit where there is a need for improvement, and so many of the prints in C5 and C6 classify as suffering from severe mottle.

#### 4.4 Impact of UCA on print mottle

The  $\frac{1}{4}^{T08}$ -mottle values of fulltone prints were plotted as a function of UCA. The results can be seen in Figure 18. Good correlation was obtained on both calendered and uncalendered papers when all papers were included in the plot. A closer look at the correlation coefficients for prints from the different print units (Table 3) shows that high correlation coefficients are obtained for calendered papers printed in the fifth and sixth unit.

Table 3: The collected correlation coefficients ( $R^2$ ) between mottle and UCA (on a log scale) on prints from the three cyan printing units

Prints from	$R^2$	
	Calendered	Uncalendered
C2	0.44	0.01
C5	0.95	0.51
C6	0.91	0.43
C2, C5 and C6	0.93	0.79

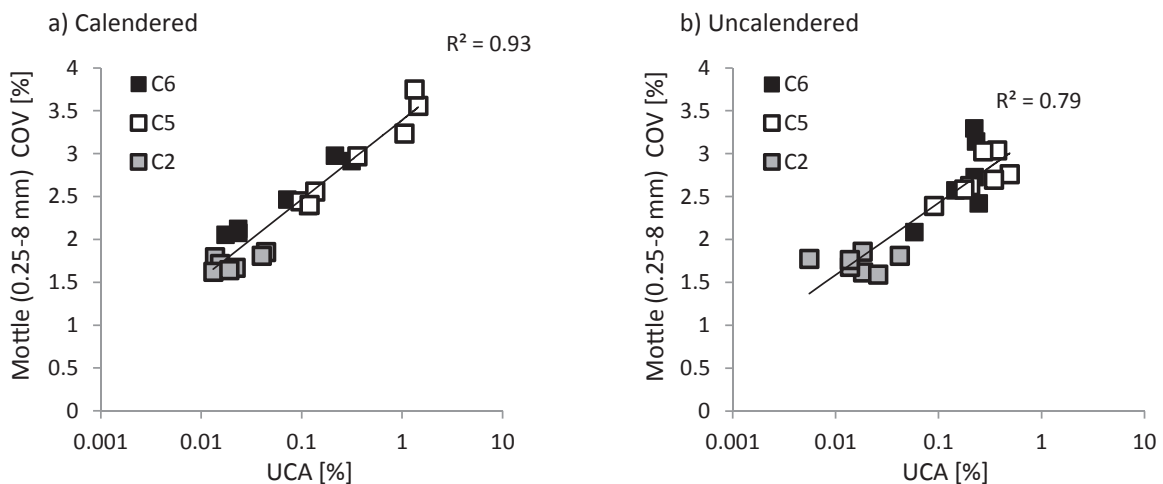


Figure 18: The print mottle COV [%] for the larger wavelength class as a function of UCA [%] on fulltone prints printed at C2, C5 and C6, respectively, a) on calendered paper and b) on uncalendered paper

Prints from the second unit and prints on uncalendered papers do not show the same high correlations. For these prints, other factors besides UCA appear to induce print mottle.

For prints in C2, BTM is regarded to be the dominant mechanism, while for uncalendered papers in C5 and C6 the “blurry” pattern from the water emulsion induced mottle may be a dominant contribution to the mottled print. This seems reasonable since uncalendered papers have a more non-uniform surface topography than calendered papers, which contributes to the transfer of an uneven thickness of the wet ink film.

Local variations in emulsified fount may amplify the variation in ink film thickness after ink setting and drying, in particular if the content of emulsified fount is high on areas where a thin wet film was transferred.

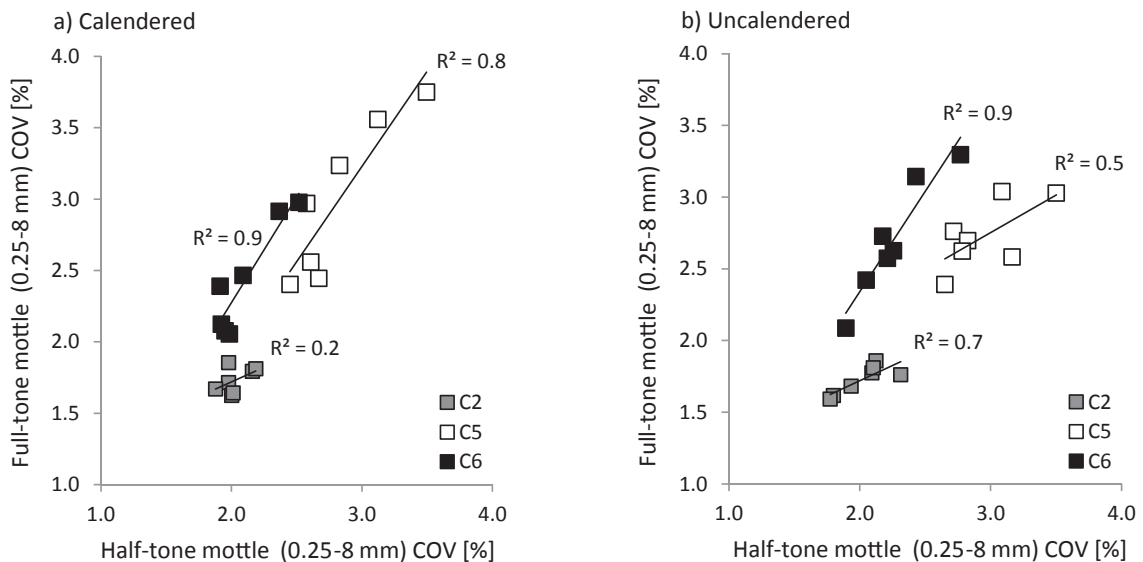


Figure 19: Fulltone mottle COV [%] for the larger wavelength class as a function of corresponding halftone mottle COV [%] on prints printed at C2, C5 or C6, respectively, a) on calendered papers and b) on uncalendered papers

## 5. Conclusion

The aim of this paper was to gain a solid understanding of the impact of dispersant content in coating colour formulations and of fountain feed level during printing on the quality of offset prints. The papers were pilot coated, calendered and printed during a full scale offset printing trial. Prints from the second, fifth and sixth unit were evaluated. They were printed only once and with cyan. The only difference in coating formulation was the amount of additional dispersant. The papers were evaluated uncalendered and calendered in order to include effects of coating structure. Excess dispersant had a detrimental effect on the printing quality. This was more pronounced at high fountain feed levels and for calendered papers.

## 4.5 Correlation between fulltone and halftone mottle

In Figure 19, fulltone mottle is plotted against halftone mottle for all prints on calendered and uncalendered papers. The experimental data are grouped into three series. The series from print unit 5 show almost the same mottle in fulltone as in halftone. Prints from C6, where UCA was only due to ink refusal (WIM), shows higher mottle in fulltone than in halftone. This suggests that ink refusal is lower in halftone, most likely because the water on the paper can be pushed away parallel to the surface when the ink dot meets the paper. This effect may well be enhanced due to higher local pressure in the halftone print, related to the smaller contact area presented by the individual ink dots. Prints from C2 show lower values in fulltone mottle. The mottle in C2 is, as already discussed, not influenced by UCA as is evident from the low correlation coefficients in Table 3.

The work showed that for prints from the fifth and sixth unit where the paper had been subjected to fount a number of times from the previous nips, the print mottle was dominated by WIM, which showed a more fine-scaled pattern compared to BTM. WIM was strongly influenced by white spots in the print, where the ink adhesion had failed. Beside the white spots, WIM showed a small-scale blurry pattern of variation in print density, which we concluded to be due to fount emulsified into the ink.

When the fount feed was reduced, the WIM character of the mottled prints from the fifth and sixth units became much reduced.

The white spots in the print are referred to as UCA and were due to a failure of the ink–paper adhesion.

We identify two origins of this failure:

- Ink-transfer failure, also referred to as ink refusal, a well-known phenomenon.
- Ink-lift-off failure, which means that the ink initially was transferred to the paper but was removed in a subsequent print unit. This mechanism appeared to be dominant for calendered papers with excess of dispersant. This is a newly reported phenomenon and further details are available in a recent report (Kamal Alm et al., 2015).

The adhesion failure, and thus formation of UCA, occurred in low amounts in absence of additional dispersant and at low water feed on both calendered and uncalendered papers. It is strongly influenced by addition of excess dispersant, water feed and calendering. Increases of 10 to 100 times were observed. This was

explained by the formation of a more hydrophilic surface induced by the dispersant, which increases the susceptibility of water molecules to become retained at the outermost surface layer, together with a disruption of coating structure and inhomogeneity through flocculation, which in turn is strongly dependent on the calcium ion to polyacrylate ratio, and formation of non-uniform compact areas induced by calendering, which reduces the transport of free water from the surface to the interior of the coating.

In the light of these findings, it can be concluded that the practice of post-adding excess anionic dispersant to combat the coater runnability-damaging effects of calcium ion release by acidic shock in calcium carbonate containing coating formulations, for example following addition of low pH binders during coating makedown or in the case of prolonged high levels of anaerobic microbiological contamination, is generally highly counterproductive in respect to subsequent print quality.

## Acknowledgment

This study was financially supported by Omya International AG and Innventia AB, and their contributions are thankfully acknowledged. Norbert Gerteiser, Maurizio Sturzo and Oliver Grossmann, amongst others, are greatly thanked for the coordination of and the assistance during both the pilot coating trial and the printing trial.

## References

- Aspler, J., 2006. Ink-water interactions in printing: An update review. In: *9<sup>th</sup> Tappi Advanced Coating Fundamental Symposium 2006 Proceedings*, February 2006, Åbo, Finland, pp. 117–146.
- Barros, G.G. and Johansson, P.-Å., 2005. The OptiTopo technique for fast assessment of paper topography – limitations, applications and improvements. *Journal of Imaging Science and Technology*, 49(2), pp. 170–178.
- Fadner, T.A. and Doyle, F.J., 1985. Real-time rates of water pickup by lithographic inks. In: *TAGA 1985 Proceedings*, pp. 309–327.
- Fowkes, F.M., 1980. Surface effects of anisotropic London dispersion forces in n-alkanes. *The Journal of Physical Chemistry*, 84(5), pp. 510–512.
- Gane, P.A.C., Kettle, J.P., Matthews, G.P. and Ridgway, C.J., 1996. Void space structure of compressible polymer spheres and consolidated calcium carbonate paper-coating formulations. *Industrial and Engineering Chemistry Research*, 35(5), pp. 1753–1764.
- Hansson, P. and Johansson, P.-Å., 1999. A new method for the simultaneous measurement of surface topography and ink distribution on prints. *Nordic Pulp & Paper Research Journal*, 14(4), pp. 315–319.
- Husband, J.C., 2000. Interactions between ground calcium carbonate pigments and polymer latices. *Nordic Pulp & Paper Research Journal*, 15(5), pp. 382–386.
- Isoard, J.C., 1983. Ink transfer and retransfer – mottling and offset picking of coated papers. In: *Tappi Coating Conference 1983 Proceedings*, San Francisco, USA, pp. 143–153.
- Johansson, P.-Å., 1993. Print mottle evaluation by band-pass image analysis. In: W. H. Banks, ed., *Advances in Printing Science and Technology: Proceedings of the 22<sup>nd</sup> International Research Conference of Iarigai*, Munich, Germany, Pentach Press, 22, pp. 403–413.
- Johansson, P.-Å. and Norman, B., 1996. Methods for evaluating formation, print unevenness and gloss variations developed at STFI. In: *Tappi Process and Product Quality Control Conference 1996 Proceedings*, Tappi Press, Atlanta, p. 139.
- Järnström, L., 1993. The polyacrylate demand in suspensions containing ground calcium carbonate. *Nordic Pulp & Paper Research Journal*, 8(1), pp. 27–33.
- Kamal, H., Ström, G., Schoelkopf, J. and Gane, P.A.C., 2010. Characterization of ink-paper coating adhesion failure: effect of pre-dampening of carbonate containing coatings. *Journal of Adhesion Science and Technology*, 24(3), pp. 449–469.

- Kamal Alm, H., Ström, G., Karlström, K., Schoelkopf, J. and Gane, P.A.C., 2010. Effect of excess dispersant on surface properties and liquid interactions on calcium carbonate containing coatings. *Nordic Pulp & Paper Research Journal*, 25(1), pp. 82–92.
- Kamal Alm, H., Ström, G., Schoelkopf, J. and Gane, P.A.C., 2015. Ink-lift-off during offset printing: A novel mechanism behind ink-paper coating adhesion failure. *Journal of Adhesion Science and Technology*, 29(5), pp. 370–391.
- Kato, Y., Fowkes, F.M. and Vanderhoff, J.W., 1982. Surface energetics of the lithographic printing process. *Industrial & Engineering Chemistry Product Research and Development*, 21(3), pp. 441–450.
- Kipphan, H., 2001. *Handbook of print media*, Heidelberg, Germany: Springer, pp. 52–53, 206, 211.
- Koivula, H., Kamal Alm, H. and Toivakka, M., 2011. Temperature and moisture effects on wetting of calcite surfaces by offset ink constituents. *Colloids and Surfaces A: Physicochemical and Engineering Aspects*, 390(1–3), pp. 105–111.
- Lidenmark, C., Forsberg, S., Norgren, M., Edlund, H. and Karlsson, O., 2010. Changes with aging in the surface hydrophobicity of coated paper. *Tappi Journal*, 9(5), pp. 40–46.
- Lie, C. and Kolseth, P., 2007. Aspects of water-induced mottle when printing on coated paper in sheet-fed lithographic offset. In: N. Enlund and A. Defrusne, eds., *Advances in Printing and Media Technology: Proceedings of the 34<sup>th</sup> International Research Conference of Iarigai*, Grenoble, France, 34, pp. 59–67.
- Lindberg, S., Fahlcrantz, C.-M. and Forsgren, G., 2008. Making subjective assessments objective – A mottle ruler for calibration of panel assessments of perceived print mottle. *PaperCon08 Tappi/PIM/Coating conference Proceedings*, Dallas, USA, pp. 39–52.
- Loiseau, J., Ladavière, C., Suau, J.M. and Claverie, J., 2005. Dispersion of calcite by poly(sodium acrylate) prepared by reversible addition-fragmentation chain transfer (RAFT) polymerization. *Polymer*, 46(19), pp. 8565–8572.
- MacPhee, J., 1979. An engineer's analysis of the lithographic printing process. *TAGA 1979 Proceedings*, pp. 237–277.
- MacPhee, J. and Lind, J., 1991. Measurement of ink film thicknesses printed by the litho process. *TAGA 1991 Proceedings*, pp. 550–573.
- McGill, W.J., 1977. Adhesion and failure of organic coatings. *Journal of the Oil and Colour Chemists Association*, 60(4), pp. 121–126.
- Ozaki, Y., Bousfield, D.W. and Shaler, S.M., 2008. Characterization of coating layer structural and chemical uniformity for samples with back-trap mottle. *Nordic Pulp & Paper Research Journal*, 23(1), pp. 8–13.
- Plowman Sandreuter, N., 1994. Predicting print mottle: A method of differentiating between three distinctively different types of mottle: back-trap mottle, water sensitive mottle and wet ink trapping mottle. *Tappi Coating Conference 1994 Proceedings*, pp. 211–228.
- Purfeest, R.D. and Van Gilder, R.L., 1991. Tall-edge picking, back-trap mottle and fountain solution interference of model latex coatings on a six-color press predicted by laboratory tests. *Tappi Coating Conf. 1991 Proceedings*, Atlanta, GA, pp. 146–472.
- Rajala, P. and Koskinen, T., 2004. Experimental and statistical investigation of drying effects on coated offset paper quality. *Tappi Journal*, 3(7), pp.19–25.
- Schoelkopf, J., Gane, P.A.C. and Ridgway, C.J., 2004. Observed non-linearity of Darcy-permeability in compacted fine pigment structures. *Colloids and Surfaces A: Physicochemical and Engineering Aspects*, 236(1–3), pp. 111–120.
- Shen, W., Hutton, B. and Liu, F., 2004. A new understanding on the mechanism of fountain solution in the prevention of ink transfer to the non-image area in conventional offset lithography. *Journal of Adhesion Science and Technology*, 18(15–16), pp. 1861–1887.
- Shen, Y., Bousfield, D.W., Van Heiningen, A. and Donigian, D., 2005. Linkage between coating absorption uniformity and print mottle. *Journal of Pulp and Paper Science*, 31(3), pp. 105–108.
- Stefan, J., 1874. Versuche über die scheinbare Adhäsion (Experiments on apparent adhesion). *Sitzungsberichte der Mathematisch-Naturwissenschaftlichen Klasse der Kaiserlichen Akademie der Wissenschaften*, LXIX, Part II, pp. 713–735.
- Stenius, P., Järnström, L. and Rigdahl, M., 1990. Aggregation in concentrated kaolin suspensions stabilized by polyacrylate. *Colloids and Surfaces*, 51, pp. 219–238.
- Ström, G. and Gustafsson, J., 2006. Physical and chemical drying in sheet-fed offset printing on coated paper. *Professional Papermaking*, 2, pp. 72–77.
- Ström, G.R. and Karathanasis, M., 2008. Relationship between ink film topography and print gloss in offset prints on coated surfaces. *Nordic Pulp & Paper Research Journal*, 23(2), pp. 202–209.

Ström, G. and Madstedt, S., 2009. Water induced irregularity of halftone dots and its impact on print mottle. In: N. Enlund and M. Lovreček, eds., 2009, *Advances in Printing and Media Technology: Proceedings of the 36th International Research Conference of Iarigai*, Stockholm, Sweden, 36, pp. 353–362.

Täg, C.-M., Toiviainen, M., Juuti, M. and Gane, P.A.C., 2010. Dynamic analysis of temporal moisture profiles in heatset printing studied with near-infrared spectroscopy. *Measurement Science and Technology*, 21(10), pp. 105602–105613.

Täg, C.-M., Toiviainen, M., Juuti, M., Ridgway, C.J. and Gane, P.A.C., 2011. Online detection of moisture in heatset printing: The role of substrate structure during liquid transfer. *Industrial & Engineering Chemistry Research*, 50(8), pp. 4446–4457.

Xiang, Y., Bousfield, D.W., Coleman, P.S. and Osgood, A., 2000. The cause of back-trap mottle: Chemical or physical? *Tappi Coating Conf. 2000 Proceedings*, Tappi Press, Atlanta, GA, pp. 45–58.

Xiang, Y., Bousfield, D.W., Hassler, J., Coleman, P. and Osgood, A., 1999. Measurement of local variation of ink tack dynamics. *Journal of Pulp and Paper Science*, 25(9), pp. 326–330.

## Appendix

### Coating process

#### Coating application parameters

<b>Coater:</b> Blade coater Modular Combi Blade (MCB) manufactured by Voith Paper	
The following trial order was used during the coating process: Ref, 0.2 NaPA, 0.4 NaPA, 0.8 NaPA, 0.2 NaCaPA, 0.4 NaCaPA and 0.8 NaCaPA.	
<b>Jetflow:</b>	
Jet gap	0.9 mm
Jet angle	37.72°
Jet position	8.03 mm
Beam angle	33.04°
<b>Blade configuration:</b>	
Blade thickness	0.38 mm
Blade tip angle	30°
Blade extension	16 mm
<b>IR drying:</b>	
15 rows of IR were used with a capacity of 510 kW	
<b>Air drying:</b>	
<b>Hood 1</b>	
Air temperature	142 ± 7 °C
Hood pressure	13 ± 3 mbar
<b>Hood 2</b>	
Air temperature	210 ± 18 °C
Hood pressure	14 ± 2 mbar
<b>Hood 3</b>	
Air temperature	128 ± 5 °C
Hood pressure	18 ± 4 mbar

### Calendering process

#### Calender parameters

<b>Supercalender:</b> SK 14/12-90 manufactured by Bruderhaus Maschinen GmbH	
<b>No. nips</b>	11
<b>Speed</b>	300 m · min <sup>-1</sup>
<b>Pressure</b>	120 N · mm <sup>-1</sup>
<b>Temperature</b>	90 °C

**Printing trial setups***Print press parameters*

<p><b>Press:</b> Manroland R706 LTTLV manufactured by Manroland sheet-fed GmbH  The calendered papers were printed first followed by the uncalendered papers.  The following trial order was used: 0.8 NaPA, 0.8 NaCaPA, 0.4 NaPA, 0.2 NaPA, Ref, 0.4 NaCaPA and 0.2 NaCaPA.</p>	
<b>Plates</b>	Agfa Alura, N30 Web, CTP negative
<b>Speed</b>	8 000 sheets/hour
<b>Ink parameters:</b>	
Ink sequence	(K, C2, M, Y, C5, C6)
Ink supplier	Epple Druckfarben
Ink series	ÖkoPlus
<b>Fountain solution parameters:</b>	
pH	5.6
Conductivity	1.228 $\mu\text{S} \cdot \text{cm}^{-1}$
Isopropyl level	4 %
Additives	5 % Substifix MGA 836509 (Huber Group)
Temperature	12.8 °C
Powder	Grafik Hitronic 3000

JPMTR 071 | 1506  
DOI 10.14622/JPMTR-1506  
UDC 582.736 – 0277.33 : 763

Original scientific paper  
Received: 2015-07-29  
Accepted: 2015-11-19

## Soybean oil based inks for enhanced deinkability of litho prints

Veronika Husovska, Jan Pekarovic, Alexandra Pekarovicova and Paul D. Fleming III

Western Michigan University, Center for Recycling,  
Center for Ink and Printability, CEAS,  
A-231 Parkview, Kalamazoo, MI 49008-5462, US

E-mail: v.husovska@pressburgllc.com  
a.pekarovicova@wmich.edu

### Abstract

Three types of food grade soybean oils were tested to determine if their byproducts could be utilized in the paper recycling industry. Free fatty acids were extracted from these commercially available soybean-oils. These acids were utilized in one loop air flotation deinking of litho-printed paper substrates. It was found that the three experimental fatty acids used in deinking differ in their chemical composition, namely Acid number and Saponification number. The effect of each of the soy-oil free fatty acid on deinking was studied, quantified and compared to the standard INGEDE 11p procedure. The INGEDE method employs commercially available oleic acid and experimental fatty acids were tested as its replacement. INGEDE method 11p was slightly modified due to unavailability of a Hobart type pulper. Therefore, a MicroMaelstrom™ Laboratory Pulper was used instead. The substrate used for deinkability study was heavily printed from both sides by sheetfed offset lithography. Due to heavy ink mileage, none of the four fatty acids had the power to deink such substrates in a one loop flotation recycling experiment. Besides INGEDE deinking evaluations, further deinking assessments were performed. Deinkability factors  $DEM_{lab}$  and  $DEM_f$  were used to express the success of ink removal from the pulp, since ERIC instrument measuring equivalent residual ink concentration, considered in INGEDE scoring, was not available. Dirt count analysis of deinked handsheets was performed by scanning them using an Epson Perfection V500 Photo scanner followed by processing of scanned images by Verity IA Color Image Analysis software. Overall, it was found that two of the three experimental fatty acids (free fatty acid from everyday pure soy oil and the one from high oleic soy oil) performed better than the standard, using oleic acid. It was also found that these free fatty acids had lower acid number than the standard oleic acid, which could improve the deinking performance.

**Keywords:** deinking, offset litho printing, recycling, acid number, deinkability factor

### 1. Introduction

In the recycling facilities, the first step of the deinking process focuses on repulping of the printed substrate. Repulping occurs in an aqueous environment, typically in a basic pH range.

Mechanical agitation allows the breaking of the fiber network. Breaking of the bonding between the fibers and the ink particles is fundamental for the ink detachment from the fibers. Addition of deinking chemicals in the repulping stage facilitates the ink detachment. In general, repulped stock will be dark with visible contaminants floating on the surface. Such pulp will produce a dark, speckled paper substrate that will be unacceptable for the customer. Therefore, the major goal of the recycling is to eliminate the ink particles and improve the optical properties of the recovered pulp (Renner, 2000). Based on studies performed by multiple researches, the strength of the fiber-ink bonding depends on pigment particle size, ink formulation, printing process, ink film thickness and ink depth penetration (Carré et al., 2000; Pekarovicova, Pekarovic and Frimova, 2003). Further, ink aging and

its raw components will also impact the deinking efforts (Angellier, Bousfield and Dimotakis, 2004; Haynes, 2000).

This experimental study was focused on deinking via INGEDE Method 11p (2009) and its modification. The deinking protocol consisted of offset printed stock repulping followed by the air flotation and further hand-sheet preparation. Free fatty acids extracted from three types of commercially available soy oils were tested as a replacement of oleic acid used in INGEDE Method 11p (2009). The objective of the study was to determine if three fatty acids coming from three types of soybean oil would produce the deinked pulp with comparable optical properties to the deinked pulp prepared using oleic acid. The effect of each of the soy-oil byproducts on deinking was observed and quantified. The main focus was to investigate whether the free acid extracted from food grade soybean oil can replace commercially available oleic acid. This work is applicable in the field of utilization of byproducts from soybean processing and also in improving deinking process as designed by the INGEDE method.

## 2. Materials and methods

### 2.1 Analysis of soy oils

The Michigan Soybean Promotion Committee provided three commercially available soybean oils. Their typical use is found in the food industry. The differences in their internal structure were analyzed via saponification and acid number testing (ASTM D94-07, 2012; ASTM D664-11a, 2011). Sodium soaps were prepared from each of the three soy-oils. In order to replace oleic acid used in INGEDE protocol, it was necessary to extract free fatty acids from the soy oils. The extraction of fatty acids was performed by use of Method IV from Standard methods for the analysis of oils, fats and derivatives (Hautfenne, 1982).

### 2.2 Offset sheetfed printed substrate

The offset sheetfed litho printed substrate was obtained from North American Color, Kalamazoo, MI. The substrate was heavily color-printed in multicolor offset lithography from both sides, with dual picture on one side, see Figure 1. Physical and optical properties of the unprinted sheet are illustrated in Table 1.

Table 1: Properties of unprinted base sheet used for deinking

Physical properties of Unprinted Base Sheet	
Grammage (g/m <sup>2</sup> )	115
Thickness (µm)	75.0
Ash content (%) @ 525 °C	45.0
Optical properties of Unprinted Base Sheet	
Brightness	86.7
Luminance (Y-value)	83.1
L*	92.9
a*	1.24
b*	-2.52

### 2.3 Deinking

Prior to the deinking, printed and unprinted substrates were aged for 72 hours at 60 °C as per INGEDE Method 11p (2009). After aging, printed and unprinted substrates, respectively, were torn to 2 cm × 2 cm pieces and were conditioned in the paper laboratory for 24 hours, 23 ± 1 °C at 50 ± 2 % relative humidity.

Due to the unavailability of a Hobart type pulper used in INGEDE Method 11p, a MicroMaelstrom™ Laboratory Pulper type of slush-maker was used instead. Repulping parameters (rpm – revolutions per minute and repulping time) versus particle dirt count and diameter size were examined prior this experimental study. The most suitable conditions were selected and they are listed in Table 2. Dilution water hardness was adjusted as per INGEDE requirement. INGEDE protocol lists the homogenization process as optional. During our experimental study, all of the pulps were homogenized using a TAPPI disintegrator. A total of eight repulping and flotation experiments were conducted using the four fatty acids.

The goal of the repulping is to break the bonds between ink and fibers. It was achieved first by applying shear forces, secondly by addition of deinking chemicals. Pulping time was constant for all experiments and its length was 10 min. The speed of the MicroMaelstrom™ Laboratory Pulper was set to 500 rpm and the temperature was adjusted to 45 °C by using the built in thermostat. After defibration, repulped stock was diluted to 6 % consistency using dilution water with fixed hardness value of 128 mg Ca<sup>2+</sup>/L. Next, repulped stock was stored for an hour in the water bath at 45 °C. After storage, TAPPI disintegrator was used to disintegrate fiber bundles for 1 minute. Prior to the air flotation, undeinked stock was taken for preparation of 2 filter



Figure 1: Sheetfed offset litho printed paper side 1 and side 2

papers and 10 handsheets. The rest of the undeinked pulp was taken and was subjected to flotation deinking. A small 2 L laboratory flotation cell was used for all deinking trials. Due to the volume of the cell, each of the experiments was repeated twice. This way, larger amounts of deinked pulp suitable for handsheets and filter pads formation were obtained. “Filter pad” was filtration paper Whatman 1, through which pulp slurry was filtered to obtain filtrate as well as the fibers from slurry without washing needed for further study. Variable amount of fibers was trapped on filter paper. The flotation cell aeration was fixed to flow rate of 1 L/min. The

duration of flotation deinking was 12 minutes. A paddle scraper was used for froth removal over the course of flotation. The removed froth was collected in a reject tank. The yield of the flotation was calculated once the reject was dried and deducted from the original floated slurry weight. The final consistency of the deinked stock was calculated and the deinked stock was subjected to preparation of the handsheets, filter pads and membrane filters. 2 filter pads and 10 handsheets were formed from undeinked pulp, as well as from deinked pulp. 2 membrane filters were prepared from water obtained after 2 filter pads were formed.

Table 2: Repulping, storage and disintegration process parameters

<b>Re-pulping recipe</b>	Sodium hydroxide	0.6 %
	Sodium silicate	1.8 %
	Hydrogen peroxide	0.7 %
	Oleic acid/Acid from soy oil A or B or C	0.8 %
<b>Re-pulping conditions</b>	Water hardness	128 mg Ca <sup>2+</sup> /L
	Temperature	45 °C
	pH	9.5 ± 0.5
	Consistency	6 %
	Mixing speed	500 rpm
	Re-pulping time	10 min
<b>Storage</b>	Consistency	5 %
	Duration	60 min
	Temperature	45 °C
<b>Disintegration</b>	Consistency	4 %
	Duration	1 min
	Temperature	45 °C
<b>Flotation</b>	Consistency	0.8 %
	Duration	12 min
	Temperature	45 °C
	Aeration flow rate	1 L/min

### 3. Results and discussion

In order to better understand the differences between three soy-based oils, determination of Saponification number of oils and Acid number of free fatty acids was performed. Saponification number allowed identifying the amounts of free and bound acid groups per gram of tested oils, while the Acid number determines amount of free acid groups per gram of tested oil or fatty acid. The slight differences in amounts of Saponification numbers were found for soybean oil B (199.40) and soybean oil C (197.71). Slightly higher saponification values were determined for soy oil A (201.19). Further processing of oils A, B and C resulted in their free fatty acids, further designated as FFA-A, FFA-B and FFA-C,

respectively. Their Acid numbers were determined and are represented in Table 3 with that of oleic acid.

Table 3: Acid numbers of free fatty acids

Free fatty acid	Acid number
FFA-A	202.6
FFA-B	196.2
FFA-C	194.8
Oleic acid	200.3

Deinkability evaluation parameters according to INGEDE Method 11p focus on pulp and process parameters. The objective of pulp parameters are high reflection of deinked pulp represented by luminance value  $Y$ , high cleanliness of deinked pulp characterized by low dirt particle area  $A$  and no discoloration of deinked pulp depicted by  $a^*$  coordinate of CIELAB space, where three axes,  $L^*$ ,  $a^*$  and  $b^*$ , evaluate the color in three dimensional color space (CIE Proceedings, 1932; Fleming, 2003). The goal of process parameters is to assure good ink removal represented by ink elimination and lastly the cleanliness of circuit water characterized by filtrate darkening  $\Delta Y$ . Due to unavailability of the instrument capable of measuring the effective residual ink concentration (ERIC), deinking evaluation assessment by  $DEM_{I,lab}$  factor (Rao and Stenius, 1998) was done. The  $DEM_{I,lab}$  factor uses the color difference between unprinted deinked pulp (US) and printed deinked pulp (DS) in relation to the color difference between unprinted deinked pulp (US) and printed undeinked pulp (BS). Technidyne Brightness Meter S-5 with  $C/2^\circ$  geometry of light source was used. The  $DEM_{I,lab}$  factor was calculated according to following Equation [1]:

$$DEM_{I,lab} = \left( 1 - \frac{\sqrt{(L^*_{US} - L^*_{DS})^2 + (a^*_{US} - a^*_{DS})^2 + (b^*_{US} - b^*_{DS})^2}}{\sqrt{(L^*_{US} - L^*_{BS})^2 + (a^*_{US} - a^*_{BS})^2 + (b^*_{US} - b^*_{BS})^2}} \right) \quad [1]$$

where US represents unprinted deinked pulp, DS represents printed deinked pulp, and BS represents printed undeinked pulp.

In general, the deinkability factor is presented on a scale from 0 to 100 %. A deinkability factor closest to the 100 % will represent the sample that was flawlessly deinked. The color difference of a sample to a reference sample as a vector in the CIELAB color system was used to develop  $DEM_{I,lab}$  deinkability factor.

During the evaluation, deinkability factor  $DEM_f$  developed by Papiertechnische Stiftung (PTS) in Munich, Germany was used. Deinkability factor  $DEM_f$  considers brightness difference between the deinked pulp and pulp before deinking. It is calculated (Equation [2]) using averaged brightness values of unprinted deinked pulp, printed deinked pulp and printed undeinked pulp (Renner, 2000).

$$DEM_f = \frac{Brightness(DS) - Brightness(BS)}{Brightness(US) - Brightness(BS)} 100 [\%] \quad [2]$$

Based on both deinkability factors ( $DEM_{I,lab}$  and  $DEM_f$ ), FFA-C has the highest deinking efficiency, while FFA-A resulted in the least deinked pulp (Table 4). FFA-B was somewhat less efficient than FFA-C, but still provided better results than oleic acid.

In the present study, the main focus was not necessarily to obtain perfectly deinked pulp, but to determine if the free fatty acid extracted from food grade soybean oil can replace commercially available oleic acid.

In addition, the paper substrate was heavily printed. In order to achieve more progressive deinkability results, deinked pulp would have to undergo multi-looped deinking systems, rather than one step deinking flotation.

Table 4: Deinkability efficiency of various free fatty acids

Acid type used for deinking	Deinkability $DEM_{I,lab}$ [%]	Deinkability $DEM_f$ [%]
Oleic acid	40.1	36.8
FFA-A	31.6	29.1
FFA-B	50.2	45.9
FFA-C	59.2	56.4

Additionally, the deinking evaluation focused on the dirt count. Handsheets were scanned using Epson Perfection V500 Photo scanner. Evaluation of the scanned handsheets was done with the help of Verity IA Color Image Analysis software (VERITY IA Light and Dark Dirt, 3.4.0). Scanning resolution was set to 1200 ppi. The inspected area was set to 13000 mm<sup>2</sup>. Dirt count is illustrated in Table 5.

Optical properties of handsheets from deinked pulps, including the deinking yield, are summarized in Table 6. The highest deinking yield was obtained with FFA-A from low linoleic soy oil. Standard oleic acid and FFA-B from high oleic acid resulted in the similar deinking yields, while FFA-C from everyday pure soy oil gave the lowest yield.

Table 5: Handsheets Dark Objects Count (in ppm) of different pulps

Acid type used for deinking	Unprinted deinked (US)	Printed undeinked (BS)	Printed deinked (DS)
Oleic acid	34	108774	37188
FFA-A	15	101993	46005
FFA-B	60	94165	22690
FFA-C	27	108721	15362

Table 6: Optical properties of handsheets from deinked pulp (average and standard deviation  $\sigma$ )

Free acid type	Statistics	Y	$\Delta Y$	A	L*	a*	b*	Brightness	Yield [%]
Oleic acid	Average	66.3	3.87	37 188	85.1	1.26	-2.92	69.7	86.6
	$\sigma$	0.8	–	1633	0.4	0.09	0.18	0.7	0.1
FFA-A	Average	65.0	2.64	46 005	84.5	1.37	-2.79	68.2	92.9
	$\sigma$	1.1	–	1581	0.6	0.24	0.12	1.1	0.1
FFA-B	Average	70.3	1.73	22 690	87.2	1.34	-2.30	73.2	86.6
	$\sigma$	0.9	–	1029	0.5	0.24	0.20	0.89	0.2
FFA-C	Average	72.7	0.67	15 362	88.3	1.33	-2.68	76.1	84.1
	$\sigma$	0.9	–	1 653	0.4	0.18	0.32	1.0	0.1

#### 4. Conclusion

The deinkability efficiency of three experimental fatty acids obtained by extraction from three types of soybean oil A, B and C was studied. The deinkability potential of experimental fatty acids was compared to the deinkability power of oleic acid that is used as a standard fatty acid in INGEDE 11p method. The substrate used for deinkability study was heavily printed from both sides and therefore none of the four fatty acids had power to deink such a substrate in one flotation loop experiment. Overall, it

was found that two of the three experimental fatty acids from soybean oils (FFA-C and FFA-B) performed better than in standard used oleic acid. One of the fatty acids was found to perform poorer than oleic acid. Based on acid number analysis characterizations performed on the fraction of fatty acids from soy, it was assumed that the lower Acid number of fatty acid is more beneficial in ink removal. However, further study will be required to statistically confirm this assumption.

#### Acknowledgement

The authors would like to thank the Michigan Soybean Promotion Committee for the donation of soybean oils and for the financial support.

#### References

- Angellier, H., Bousfield, D.W. and Dimotakis, E.D., 2005. Lithographic ink setting on uncoated paper. *TAGA Journal of Graphic Technology*, (1), pp. 35–42.
- ASTM D94-07, 2012. *Standard test methods for saponification number of petroleum products*. West Conshohocken, PA, USA: ASTM International.
- ASTM D664-11a, 2011. *Standard test method for acid number of petroleum products by potentiometric titration*. West Conshohocken, PA, USA: ASTM International.
- CIE Proceedings, 1932. *Commission Internationale de l'Éclairage, Proceedings, 1931*, Cambridge University Press, Cambridge.
- Carré, B., Magnin, L., Galland, G. and Vernac, Y., 2000. Deinking difficulties related to ink formulation, printing process and type of paper. *TAPPI Journal*, 83(6), p. 60.
- Fleming, P.D., 2003. Issues in color measurement and need for new SWOP guidelines to address these issues. In: *Printing & Converting Common Interest Group Luncheon Presentation, TAPPI Spring Technical Conf. & Trade Fair*, Chicago.
- Hautfenne, A., ed., *Standard Methods for the analysis of oils, fats and derivatives*, 1982. *Pure & Appl. Chem.*, 54(6), p. 1269.
- Haynes, R.D., 2000. The impact of the summer effect on ink detachment and removal. *TAPPI Journal*, 83(3) pp. 56–65.
- INGEDE Method 11p, 2009. Bietigheim-Bissingen, INGEDE.
- Pekarovicova, A., Pekarovic, J. and Frimova, A., 2003. Particle size of commercial inks and their deinkability. In: *Proceedings of the Technical Association of the Graphic Arts Conference*, TAGA, Montreal, pp. 64–65.
- Rao, R.N. and Stenius, P., 1998. Mechanisms of ink release from model surfaces and fibre. *Journal of Pulp and Paper Science*, 24(6), pp. 183–187.
- Renner, K., 2000. Deinkability of printing inks. In: L., Götttsching and H., Pakarinen, eds., *Recycled Fiber and Deinking*. Fapet Oy and TAPPI, Helsinki, pp. 267–301.



JPMTR 072 | 1435  
DOI 10.14622/JPMTR-1435  
UDC 655.1 – 024.25 : 621.38

Research paper  
Received: 2014-09-01  
Accepted: 2015-09-24

## Self-supported printed multi-layer capacitors

*Michael James Joyce, Ali Eshkeiti, Paul D. Fleming III, Alexandra Pekarovicova and Massood Zandi Atashbar*

Western Michigan University,  
Center for the Advancement of Printed Electronics (CAPE),  
4601 Campus Drive, Room A217,  
Kalamazoo MI, 49008

E-mails: Michael.Joyce@wmich.edu,  
Ali.Eshkeiti@wmich.edu  
Dan.Fleming@wmich.edu  
A.Pekarovicova@wmich.edu  
Massood.Atashbar@wmich.edu

### Abstract

The increasing demand for miniaturized electronic devices has elevated the need for rechargeable micro-power sources. While lithium and lithium ion batteries have been utilized in these applications since the late 1990s, other energy harvesting technologies, such as mechanical, thermal and solar, are now being used to augment batteries to enable systems to be self-powered. However, the lifetime of any battery is finite, which may be a major problem when the application is in a permanent structure or medical implant device. For power or significant energy storage applications, printed multilayer capacitors or supercapacitors are being explored as an enhancement, or replacement of micro-batteries.

The printing of multilayer capacitors offers an inexpensive manufacturing process for these devices. Though the ability to print supercapacitor electrodes, supercapacitors, and batteries on rigid and flexible substrates is well known, having a device supported by a substrate is not always advantageous. This is especially true for cases where the rigidity of the substrate limits the extent to which the device can be bent or wound, or where substrate compatibility issues to the surface to which it is to be attached is faced. The ability to bend or wind devices can improve the attachment to surfaces; enable its placement in confined spaces and advance efforts to further miniaturize devices. In this research, a sacrificial water-soluble polymer layer was used to produce self-supported (substrate free) printed conductive and dielectric ink films of different thicknesses, as well as a completed capacitor. The electrical and mechanical properties of these films and the capacitor were measured. Such measurements have not yet been reported and should therefore advance our understanding of properties at different thicknesses.

**Keywords:** supercapacitor, printed electronics, screen printing, alginate, silver electrode

### 1. Overview

The increasing demand for miniaturized electronic devices has grown the need for rechargeable micro-power sources. Though lithium and lithium ion batteries have been utilized in these applications since the late 1990s, other energy harvesting technologies such as thermal, mechanical and solar, are now being used (Pech et al., 2010). The benefit of using energy harvesting technologies to recharge batteries is that they enable systems to be self-powered. However, the useful life of a battery is limited, which may be a serious problem when placed in a permanent structure, such as a concrete support structure, engine or biomedical implant (Kang, 2006). Batteries also cannot provide the peak power for some portable electronic devices without increasing the bulkiness or weight of the device. With developing electronic markets searching for thinner, lighter weight, lower cost and more conformable solutions, printed electronics offers a possible solution to meeting these goals, but a complementary energy source to batteries is still missing (Kaempgen et al., 2009).

Electronic capacitors are used to provide charge storage. Their ability to endure millions of cycles and fast charge/discharge rates enables energy densities to be maintained for the balancing of circuitry in electronic devices (Miller and Simon, 2008; Simon and Gogotsi, 2008). For power or significant energy storage applications, multilayer capacitors or supercapacitors can be used to enhance battery performance, which would help batteries fill current and future energy needs (Kaempgen et al., 2009).

The printing of multilayer capacitors offers an inexpensive manufacturing process for producing such devices and the ability to print supercapacitor electrodes, supercapacitors, and batteries are well documented (Simon and Gogotsi, 2008; Kaempgen et al., 2009; Kiebele and Gruner, 2007; Grande et al., 2012). However, everything reported to date has involved the printing of various functional inks on rigid or flexible substrates. The type of

substrate used is often dictated by the processing temperature requirements of the functional materials printed and flexibility requirements of the end product. This study focused on the fabrication and testing of self-supporting printed multilayer capacitors. The roughness, flexibility and density of the printed layers were characterized. A completed capacitor, consisting of four alternating layers of silver and dielectric, was printed and tested. The

## 2. Introduction

### 2.1 Capacitor and supercapacitor technologies

The direct printing of passive (electrodes, resistors, capacitors) and active (thin film transistors, photovoltaics, organic light emitting diodes) devices has gained significant attention as a low cost manufacturing method for flexible electronics. As the global need for energy continues to rise, the risk of facing a supply imbalance also grows. Concerns on how the world will keep pace with growing energy demands have led to increased efforts to find new technologies for harvesting and storing energy. Some of the energy harvesting technologies being explored are light, human movement, vibration and heat, based on technologies such as photovoltaics (Swanson, 2009), electrodynamics (Sterken et al., 2007), and piezoelectronics (Challa et al., 2008).

The harvesting of renewable energy offers just one part of the needed solution. Once harvested, efficient technologies to store the energy are required. Batteries are the most predominant technology used (Linden, 1984), but other technologies such as eutectic systems (Smith and Hashemi, 2006) or mechanical methods, such as flywheel (Ruddell, 2003) and hydroelectric storage (Jog, 1989) can be used.

The two most significant criteria for the performance of an electrical energy storage device are power and energy density. Power density is a measure of how fast energy can be transferred per unit mass into a device ( $\text{J} \cdot (\text{kg} \cdot \text{s})^{-1}$ ). Energy density is the amount of energy stored per unit mass ( $\text{J} \cdot \text{kg}^{-1}$ ). Both of these criteria are especially important when device portability is needed (Jiang, 2007).

Two major types of energy storage devices are batteries and capacitors. Batteries directly convert chemical energy to electrical energy through the generation of charge from redox reactions that take place at the electrodes of the battery. The generated charge creates a voltage between the battery's cell terminals. The concentration and chemical species within the battery determines the voltage output. In contrast, capacitors store energy by charge separation. A basic capacitor consists of a dielectric material sandwiched between two parallel electrodes capable of establishing an electrical potential. The dielectric material can be either an ionic

capacitor was also wound to demonstrate the feasibility of producing a multi-stacked capacitor. The benefits of this research include defining the design and commercial potential for self-supported printed energy storage devices, and advancing the technical knowledge for self-supported printed electronic devices. The findings of this study should also greatly advance work being performed in printed sensors and active transistor devices.

solution (electrolyte) or solid material. When a closed circuit between the two electrodes is formed the electrical potential is released generating a power density (Bird, 2010). The two main functions of a capacitor are to charge or discharge electricity and to block the flow of direct current (DC). The function of charging or discharging energy is used in smoothing the circuits of power supplies and backing-up circuits of microcomputers. The function of blocking DC flow enables them to be used as filters to block undesirable frequencies in a circuit. In general, capacitors do not efficiently utilize the material from which they are fabricated so their energy densities are typically low (Bird, 2010).

Electrolytic capacitors evolved from the basic capacitor design. They are similar to batteries, but have an anode and cathode composed of the same materials. There are aluminum, tantalum and ceramic capacitors (Jayalakshmi and Balasubramanian, 2008).

The next evolution in capacitor technology was the creation of electric double layer capacitors, EDLCs, which store electrical charge at a metal/electrolyte interface. The main component of these devices is activated carbon, which is used in the electrode construction of these capacitors. This technology served the needs of industry for many years, then experienced resurgence as interests in electrical storage technology for medical devices, miniature electronic devices and applications requiring very short high power pulsed devices. EDLCs complement batteries by supplying a high power density and low energy density when needed, while lasting longer than batteries. In comparison to conventional capacitors, they have higher energy densities. The disadvantage to EDLCs is that they suffer from low energy density. To address these problems, researchers have explored mixing transition metal oxides with the activated carbon used as the electrode material. This mixing enhanced the specific capacitance by a factor of 10–100, depending on the type of metal oxide used (Halper and Ellenbogen, 2006). The increased performance brought about by this technology introduced a new class of capacitors called supercapacitors or pseudocapacitors.

Supercapacitors have been the focus of much research over more than past 10 years (Butler, Miller, and Taylor,

2002). The difference in performance between a supercapacitor and capacitor can be seen through a comparison of the specific power and specific energy rates as shown in Figure 1.

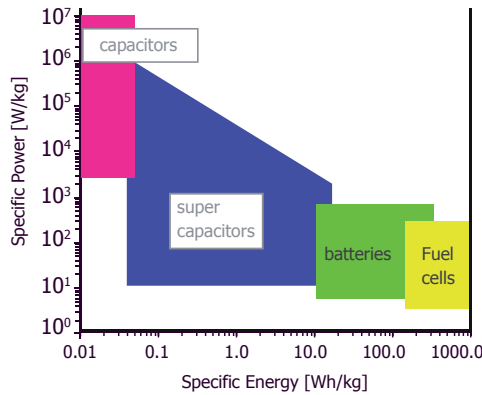


Figure 1: Comparison of different storage devices, modified from Winter and Brodd (2004)

The general equations for capacitance, Equation [1], and energy storage, Equation [2], were first proposed by Helmholtz (1853):

$$C = (A\varepsilon_0\varepsilon)/d \tag{1}$$

$$E = \frac{1}{2} CV^2 \tag{2}$$

where  $C$  is capacitance (F),  $E$  is the energy stored (J or Ws),  $\varepsilon_0$  is the permittivity of free space, equaling  $8.8541 \cdot 10^{-12}$  F/m,  $\varepsilon$  is the relative permittivity of the dielectric layer, or dielectric constant,  $A$  is the total surface area of the electrodes ( $m^2$ ),  $d$  is the distance between the two parallel electrodes (m),  $V$  is the established potential between the electrodes (V).

From Equation [1], it is clear that to achieve very high supercapacitor performance, a combination of maximizing the plate area, minimizing the distance between plates and selecting a dielectric material to maximize the effective permittivity is needed. For printed capacitors, the distance between plates is limited by the thickness of the printed dielectric layer, which is often determined by the printing method used. The permittivity is based on the properties of the dielectric material, which can be deposited/printed, or the original substrate itself. Using a number of geometric techniques, such as stacking alternating plates or winding up a flat device, can result in a flexible capacitor, which can effectively manipulate the area.

By combining these equations from above, the peak energy density per unit mass can be written as Equation [3]:

$$\text{Energy Density} = E\rho = (\varepsilon_0/2)(A/d)(\varepsilon V_b^2 \rho) \tag{3}$$

where  $\rho$  is the device density and  $V_b$  is the breakdown voltage of the dielectric material.  $V_b$  is used instead of

$V$  in order to allow the properties of different dielectric materials to be compared.

A close examination of Equation [3] shows three parts: a constant term ( $\varepsilon_0/2$ ), a geometrical term ( $A/d$ ) and a materials property term ( $\varepsilon V_b^2 \rho$ ). Hence, the energy density of a capacitor can be achieved by altering the geometry and properties of the materials used (Pollet, Marinel and Desgardin, 2004).

The most sophisticated types of ultracapacitors are electrochemical capacitors, ECCs, and electric/electrochemical double layer capacitors, EDLCs. Both devices have capacitance values that are orders of magnitude higher than traditional capacitors, hence, the prefixes super and ultra. An ECC consists of two electrodes immersed in an ionic solution, which enables the accumulation of charge at the double layer interface. The most common uses of ECCs are in hybrid electrical vehicles and in solar and wind power facilities where they are used to supply intermittent energy. EDLCs store charge from ions supplied from an electrolytic solution in contact with high surface area electrodes, typically made from activated carbon. These unique properties enable them to fill the gap between batteries and conventional capacitors.

Both ECC and EDLC technologies are commercially available. The main use of EDLCs are in applications where energy conservation, electrical power load leveling, and high power millisecond long pulse delivery is needed, for example to start an engine or automotive braking system (Jayalakshmi and Balasubramanian, 2008).

The basic differences between the design and construction of two types of ultracapacitors are shown in Figure 2.

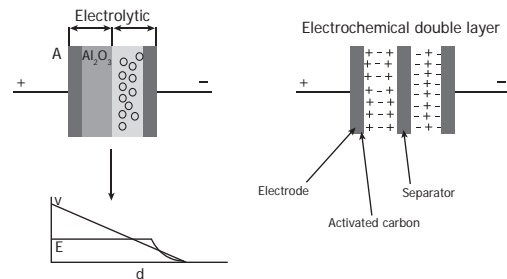


Figure 2: Schematic presentation of electrolytic capacitor and electrical double layer capacitor, recreated from Jayalakshmi and Balasubramanian (2008)

Two other types of capacitors are ceramic and film capacitors. Ceramic capacitors are constructed from alternating layers of metal and ceramic, with the ceramic serving as the dielectric. Multilayer ceramic capacitors (MLCs) typically contain around 100 alternating layers encased in two ceramic layers. They are fabricated by

screen-printing both the conductive and dielectric layers, and subsequently, co-sintering them together. The most commonly used material for the conductive (electrodes) and dielectric layers is Ag-Pd and BaTiO<sub>3</sub>, respectively (Pollet, Marinel and Desgardin, 2004).

Since the year 2000, when the communications market began to flourish, the demand for MLCs has increased to keep pace. Other ceramic materials that have been identified are CaZrO<sub>3</sub>, MgTiO<sub>3</sub>, and SrTiO<sub>3</sub>. Mn and Ca are some of the other electrode materials being used. Film capacitors, just as the name suggests, are made using thin films of polyester or polypropylene. These materials are used with the dielectric and meta-glazed capacitors, which consist of Al electrodes created by the vapor deposition of Al onto a polyester, polypropylene, or polycarbonate film (Nagata et al., 2006; Keskinen et al., 2012).

Recent printed electronics research has examined nano-gold, graphene, nano-silver, nano-copper, single-wall and multi-wall carbon nanotubes (CNT) as electrode materials (Grande et al., 2012; Keskinen et al., 2012; Le et al., 2011; Hartman, 2011). A comparison of a few different conductive inks for use in printed electronics is shown in Table 1.

In addition to the conductive inks listed above, graphene has also been heavily studied as a conductive material for pseudocapacitors. Graphene is a non-toxic nano-material, which is readily dispersible; it is the most conductive form of carbon. It does not require high temperature sintering and therefore can be used with plastic film and paper substrates. It also gives the ability to be deposited as very thin layers, and is less expensive than silver, copper, and CNT inks.

A comprehensive review of recent research performed using graphene in energy harvesting/storage devices and printed electronics was recently performed by Grande et al. (2012) and Nair et al. (2008), showed graphene to be a feasible alternative to indium tin oxide (ITO) in OPVs, due to the ability of a single layer of graphene to transmit 98 % of total incident light. Blake et al. (2008), reported films of graphene having a sheet resistivity of approximately 6 kΩ/sq. This corresponds to a bulk resistivity of about  $2 \cdot 10^{-6}$  Ωm. The sheet resistance of graphene

was found to depend on the quality of the graphene sheets. The fewer the defects in the sheets, the lower the sheet resistance. Several reports have also shown the method of synthesis greatly impacts the sheet resistance of graphene.

The use of graphene to produce supercapacitors with specific energy densities comparable to Ni metal hydride batteries for hybrid vehicles was recently demonstrated by Liu et al. (2010). The supercapacitors produced have the advantage of being rechargeable in less than 2 minutes, which is faster than what can be obtained with current hybrid battery technologies. Wang et al. (2009) and Yu, Davies and Chen (2010) synthesized 25 nm thick graphene/graphite sheets using a vacuum filtration method, which enabled a capacitance of 135 F/g to be realized. The graphene sheets produced by this method were found to be flexible and transparent, thus capable of being used in applications where transparent supercapacitors would be needed.

The use of hybrid CNT/graphene composites in polyethyleneimine (PEI) and polyaniline (PANI) in supercapacitors was explored by Yu, Davies and Chen (2010) and Wang et al. (2009), respectively. Capacitances of 120 F/g and 210 F/g, respectively, at a current density of 0.3 A/g were achieved. Han, Ding and Shang (2010) used polypyrrole (PPy) and obtained a capacitance of 223 F/g at a current density of 0.5 A/g. PPy has the advantage of being more stable under ambient conditions in comparison to PANI.

Jari et al. (2012) explored the use of graphene to create supercapacitors. In their work, supercapacitor electrodes of 2 cm<sup>2</sup> and 0.5 cm<sup>2</sup> using activated carbon were prepared. They showed standard 2 cm<sup>2</sup> capacitors to have typical capacitance values of 30–35 F/g with only the activated carbon mass taken into account. They also compared electrodes printed from 3 commercial silver inks to graphene electrodes and found no practical differences in their conductivity values with typical sheet resistances of 0.03–0.05 Ω/sq for 20–30 μm thick layers (Keskinen et al., 2012).

Graphene oxide (GO) has also been studied. Although, alone it is not electrically conductive, the addition of thermal, chemical, and photothermal processes reduces

Table 1: Comparison of conductive inks for PE applications (Grande et al., 2012)

Ink	Conductivity	Oxide	Film cohesion	Process concerns
Silver	Excellent	Conductive	Good	Long drying times
Carbon	Average	Does not form	Poor	None
Copper	Good	Non-conductive	Good	Ink stability
Polymer	Average	Does not form	Good	Low solubility
CNT	Excellent	Does not form	Poor	Toxic

it to graphene. A recent study by Le et al. (2011) showed the ability to inkjet print a mass fraction of 0.2 % water based GO ink with a viscosity of 1.06 mPa·s and surface tension of 68 mN/m on a Dimatix inkjet printer. Once printed, GO electrodes were thermally reduced under N<sub>2</sub> atmosphere at 200°C to graphene. Even though these ink characteristics were outside the recommended ranges for normal inkjet printing (i.e., 10–12 mPa·s and 28–32 mN/m), Le et al. (2011) found that by manipulating the firing voltages of the nozzles as a function of time spherical ink droplets without clogging could be produced. A spatial resolution of ~ 50 μm was achieved. Titanium foils from Sigma Aldrich (100 μm thick, 99.99 % purity) were used as a comparison for electrochemical performance. The use of two identical electrodes clamped with a Celgard separator produced a specific capacitance of 48–132 F/g in the scan range of 0.5 to 0.01 V/s for the graphene electrodes, and were able to retain 96.8 % of the capacitance over 1 000 cycles. It was also shown that graphene electrodes prepared by conventional powder based methods were similar in performance to the inkjet printed electrodes (Wu et al., 2010).

Although graphene and carbon nanotube inks are good alternative electrode materials to silver, the printing of these nano-materials can be difficult. The difficulty in printing these materials is due to their hydrophobic nature, which causes them to segregate in water, unless surfactants are added, or their surfaces are functionalized (Le et al., 2011).

Silver inks, on the other hand, are well established in the market place. Inkjet, screen, flexo, and gravure Ag inks are readily available and have been used as electrode materials in many printed electronics applications. Solvent based silver inks are of special interest to this study, due to their high water resistance, which is required to allow for lifting off the printed layer through the use of a sacrificial water-soluble base layer.

Printed supercapacitors need to be flexible and capable of being printed or attached onto multiple substrates. To be useful, the performance of the storage device should meet the life expectancy of the product. Low cost and ease of production would increase their acceptance. Printed energy sources that could be integrated into a printed device in line would greatly reduce the fixed production costs of supercapacitor systems.

## 2.2 Lift-off processes

Several methods for the lift-off of printed electronic devices have been reported (Ogier, Veres and Yeates, 2003; Greer and Howard Jr., 1989; Haskal, McCulloch and Broer, 2010; Rogers et al., 2010). Ogier, Veres and Yeates (2003) describe the use of a lift-off ink to enable the printing and lift-off of organic electronic devices, mainly organic light emitting displays, OLEDs. The lift-off ink is printed as a negative image and then sequential device layers are printed on top. To lift-off the device, a lift-off solution, which dissolves the lift-off ink, but not the device layers, is applied. The process requires the use of ultrasonic agitation, stirring, a spray liquid medium and/or heat to be used. Haskal, McCulloch and Broer (2010) describe a laser lift-off process that uses the wet casting of a plastic coating, containing a UV absorbing additive, to a substrate followed by the screen or inkjet printing of thin film electronic elements to fabricate an active display matrix. The laser is used to lift-off the plastic layer after it has been printed from the carrier substrate. Greer and Howard Jr. (1989) describe a lift-off process to remove any unwanted areas from a metallization layer to form a layer of masking material over a semiconductor device. Lift-off occurs upon heating of the device to a temperature where the metal melts on the masking layer and forms globules when it cools, which can be removed. Rogers et al. (2010) described a carrier layer coated with a sacrificial layer to which a stretchable substrate is attached. The stretchable substrate is printed with electronic devices, and removed to produce a self-supporting stretchable device. This process can presumably make strain-independent electronic devices (Rogers et al., 2010).

This study focused on the feasibility of screen-printing a self-supported capacitor. The capacitor was fabricated using a commercially available solvent-based silver and UV dielectric ink. Information on the conductive (silver), and dielectric (acrylate) inks is listed in Table 2.

The novelty of this work is that a newly discovered lift-off process was used for the first time to obtain a self-supported capacitor. The work demonstrates that a self-supported fully printed capacitor could be wound, resulting in multi-stacked conductive and dielectric layers. The findings suggest that it may be possible to create a supercapacitor by winding a self-supported dielectric-conductive-dielectric-conductive printed stack.

Table 2: Commercial inks used

Supplier	Ink type	Commercial name
Sun Chemical	Thermal flake silver	AST 6200
Henkel	UV dielectric	Electrodag PF-455B

### 3. Experimental methods

#### 3.1 Creation of sacrificial layer

A water-soluble solution of sodium alginate was applied to sheets of Melinex ST 506 PET film (DuPont, Chester, VA) using different Byrd applicators to obtain films of different thicknesses. The alginate (S-160-QD, SNP Inc., Durham NC) was applied to the PET as a 6 % aqueous solution. Alginate solutions were prepared by slowly sprinkling the appropriate amount of dried alginate into a pre-weighted amount of deionized water under agitation. Once all alginate was added, the solution was allowed to mix for 60 minutes to ensure complete hydration. The solution was then placed in a closed container in a refrigerator overnight to enable it to degas. After 24 hours, the solution was removed and brought to room temperature, approximately 21 °C, before applying it to the PET film. The PET film was cleaned with isopropyl alcohol just prior to application of the alginate solution. While preparing the alginate films of different thickness from the 6 % solution, it was observed that during drying the alginate films were cracking. To alleviate this problem, glycerol was added to the solution of alginate to help plasticize the film. The addition level of glycerol that was found to give the most uniform alginate film was a mass fraction of 20 % of dry alginate. From this solution, films were then prepared using #0.5, 1.0, 6.0, 8.0 and 10 mil Byrd applicators. Unfortunately, these films were very thin and could not be easily removed and handled. To create films that could be more readily handled Meyer rods were used instead. After experimenting with several different rods, #14 and #20 rods were chosen. The films produced using these rods were strong enough to handle without tearing, and readily dissolved in water when rewetted. The thicknesses of these films were found to be 6.88 and 14.41  $\mu\text{m}$ , respectively.

After coating, the samples were placed in a conditioned room at 50 % RH and 23 °C (allowing for reproducible and consistent drying conditions). The roughness ( $S_a$ ) and thicknesses of the films were then measured with a Bruker GT-K white light interferometer microscope at a magnification of 50 $\times$  giving a sample area of approximately 0.125 mm  $\times$  0.098 mm. Three measurements were taken on each film sample prepared (for both roughness and thickness). Two films for each condition were tested. After the initial roughness measurements were obtained, it was apparent that the amount of particulate matter in the air throughout the building and within the conditioning room was significant, so handling procedures were adjusted to minimize contamination. All coated samples were placed in an enclosed (“clean”) environmental chamber to dry, and kept in closed containers during transport to and from the print stations and drying/curing stations. The environmental chamber used was a Carron RH chamber maintained at a temperature of approximately 21 °C and 50 % RH for

24 hours. Drying refers to the thermal treatment of the applied silver ink, while curing refers to the UV treatment of the dielectric ink. The thermal treatment of the silver ink is required to evaporate the solvents allowing the silver particles to create a more intimate, uniform, and continuous layer. The UV treatment is used to initiate and propagate a polymerization reaction, which in turn forms the “dried” dielectric film.

After characterizing the properties of the alginate films, single and multilayer prints were prepared according to Figure 3. The two different thicknesses of alginate and ink layers are denoted by the +1 and –1 conditions as shown and explained in the figure caption. Ink films of different thicknesses were obtained by printing single and double layers of the ink. The ink films were dried/cured in between prints, allowing for measurements to be taken. Samples were prepared in this way to allow for the characterization of the alginate films and single layer prints alone, before characterizing the multilayer prints. This methodology also allowed the impact of each layer on the final device performance to be better understood.

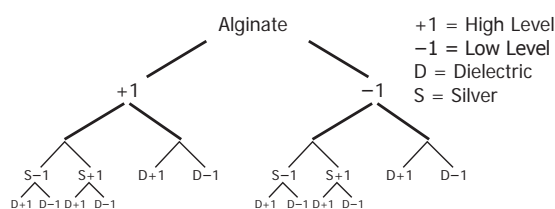


Figure 3: Sequence of sample preparation: –1 for alginate obtained using a #14 Meyer rod and +1 obtained using a #20 Meyer rod, S–1 and D–1 refer to single layer silver and dielectric, and S+1 and D+1 refer to double layer silver and dielectric, respectively

#### 3.2 Printing

The print pattern used is shown in Figure 4. Figure 4a shows each individual layer and how they were overlaid onto one another, while Figure 4b depicts the completed final device.

The inks were screen-printed onto the alginate coated PET samples using an AMI MSP-485 semi-automated screen printer. Double layer samples were accomplished by first printing and drying/curing the first layer prior to printing the second layer on top of the first. The samples were then cured/dried using a Fusion UV curing unit equipped with a D bulb (Peak Radiated Power at approximately 375 nm, FusionUV, 2015). The samples were passed through the Fusion UV curing unit at 75 m/min, until fully cured (no longer tacky to the touch), which took anywhere from 3 to 4 passes. Using an IR tempera-

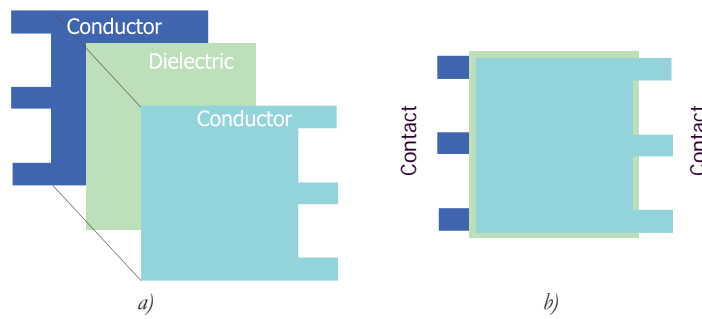


Figure 4: Three layer structure in a) exploded view, b) top view

ture probe, the curing unit temperature within the Fusion UV drier was measured to be 54.4 °C, which was sufficient to fully dry the silver ink after 3–4 passes. The pattern printed for each ink was a 5 cm × 5 cm solid block. The specifications for the screen used are given in Table 3. After drying/curing, the roughness ( $S_a$ ) and thickness of the printed films were measured.

Table 3: Screen specifications

Manufacturer	Specifications
Microscreen (South Bend, IN)	230 lpi mesh 0.0011" wire diameter at 45° wire angle 10 μm thick emulsion

### 3.3 Removal of the sacrificial layer

After measuring all the desired properties of the PET printed samples, the samples were wetted with room temperature (21 °C) deionized (DI) water to dissolve the sacrificial layer of sodium alginate and the printed layers lifted-off the PET. After retrieving the self-supported films from the water, the films were blotted dry and retained for further measurement.

### 3.4 Characterization of film properties

The Young (1805) equation has been known for over two centuries. Its modified form (Equation [4]) is as follows:

$$\gamma_{LV} \cos \theta = \gamma_{SV} - \gamma_{SL} \quad [4]$$

where  $\gamma_{LV}$  is the liquid-vapor interfacial tension or surface energy,  $\gamma_{SV}$  is the solid-vapor interfacial tension,  $\gamma_{SL}$  is the solid-liquid interfacial tension, and  $\theta$  is the contact angle.

This equation and the measured value of the contact angle are still being used as the basis for calculating the surface free energies of the films. However since its inception, as the result of further studies, other contact angle measurement methods for the determination

of the surface free energy of polymeric materials have evolved. These methods have been widely adopted as they are relatively easy to perform and of high accuracy. One such method is the Owens–Wendt method. In this method, the surface free energy of a solid is determined from the following Equation [5]:

$$\sqrt{\gamma_s^d \gamma_L^d} + \sqrt{\gamma_s^p \gamma_L^p} = 0.5 \gamma_L (1 + \cos \theta) \quad [5]$$

where  $\gamma_s^d$ ,  $\gamma_L^d$ ,  $\gamma_s^p$ ,  $\gamma_L^p$  are dispersion and polar components and  $\gamma_L$  is the surface free energy of measuring liquid. Because  $\gamma_s^d$  and  $\gamma_L^p$  are both unknowns, this equation is insufficient to determine the surface free energy of a solid. Thus, the contact angle of two liquids of known surface tension must be measured. By making these measurements, two linear equations in the form below, with different values of the constant coefficients are obtained (equations [6a] and [6b]).

$$x + ay = b(1 + \cos \theta_1) \quad [6a]$$

$$x + cy = d(1 + \cos \theta_2) \quad [6b]$$

where  $x = \sqrt{\gamma_s^d}$ ,  $y = \sqrt{\gamma_s^p}$ , and  $\theta_1$  and  $\theta_2$  are the contact angle values of the two known liquids, and  $a$ ,  $b$ ,  $c$ ,  $d$  are the coefficients dependent on the kind of liquids used. For this method, one liquid with a dominant polar component and one liquid with a dominant dispersive component should be used. By using such liquids, the solution of the system of above linear equations is affected as little as possible by the errors accompanying the determination of the  $\gamma_L^d$  and  $\gamma_L^p$  values.

The Owens-Wendt method is one of the most common methods used for calculating the surface free energy of solids and the two most frequently used measurement fluids used are water and methylene iodide (diiodomethane). This method was used to determine the surface energies of the films. The contact angles of water and methylene iodide were measured with a First Ten Ångstrom dynamic contact angle measurement device, which captures the change in contact angle with time with a high-speed video camera (FTA, 2015; Owens and Wendt, 1969). Once captured, the change in contact angle with time was plotted, and the equilibrium contact

angle obtained and used in the calculation of the surface energy of the solid to which the liquids were applied. Five equilibrium contact angles were obtained for each fluid from which five surface free energy values were calculated. The equilibrium contact angle is the angle where no further change in contact angle with time was observed. The average surface free energies (total, polar and dispersive) for each sample are reported.

The resistance of the conductive ink layers and capacitance (using the dielectric ink films as the insulating layer with dielectric test fixture) were measured with the instruments listed in Table 4. The dielectric constant of the dielectric layers was then calculated from the capacitance measurements using Equation [1]. The sheet resistivities of the samples were obtained using a four point probe sensing station consisting of a Keithley 2602 Dual Source Meter with a SMR Probe Head from Bridge Technology. The two outer probes are used for sourcing the current, and the two inner probes are used for

measuring the voltage across the layer. The sheet resistivity is calculated from the measured voltage, applied source current, and dimensions of the conducting layer. After printing all the layers of the capacitors, the capacitance was measured using an LCR meter (Agilent E4980A) over a range of frequencies (1 Hz to 1 MHz), and the impedance response was measured. Based on the response, the capacitance values were calculated. Attempts to measure the electrical properties while being flexed on a Mark-10 instrument and attached to a Keithley 2602 Dual Source Meter failed, due to the inability of the samples to survive the test without tearing. To determine the densities of the films, the weights, thicknesses, and areas of the printed free films were measured. The areas were measured using an ImageXpert image analyzer. The weights were obtained using a Mettler digital balance. Attempts to determine the stiffness of the films with a Gurley Stiffness test instrument failed due to the stiffness of the films being below the detectable limits of the instrument.

Table 4: Electrical characterization equipment and measurement parameters

Test Equipment	Measurement Parameters
Keithley 4200-SCS Semiconductor Characterization System	Capacitance (for final device only), Resistance, Effective Dielectric Constant
Keithley 2602 Dual Source Meter	1 $\Omega$ to 1 M $\Omega$ Surface Resistance
Keithley 6517A High Impedance Test Set and ASTM D257 Resistivity Test Fixture	> 1 M $\Omega$ Surface Resistance
Agilent 4338B m $\Omega$ Meter	< 1 $\Omega$ Surface and Bulk Resistance
Agilent E4980A LCR Meter	Capacitance (for final device only), Effective Dielectric Constant

#### 4. Results

The surface free energies of the alginate coated PET films are shown in Table 5. As shown, the surface free energy increased with increasing film thickness. This could be because at the higher alginate film thickness, the lower surface free energy PET did not influence the measurement, but for the thinner alginate film, it did. This is reasonable explanation when one considers the high solubility of alginate in water. It should be noted that observations were made, after running the test,

showing less of the thinner alginate film remained on the area where the water made contact in comparison to the thicker alginate film (testing took approximately 30 seconds).

The high surface free energy of the alginate film is due to the large number of carboxyl and hydroxyl groups in the polymer (Figure 5) (visit-alginate, 2015). The polar groups attract the polar components of the test

Table 5: Influence of alginate film thickness on surface free energy

Substrate (Alginate Film Thickness)	PET	+1* (14.41 $\mu\text{m}$ )	-1* (6.88 $\mu\text{m}$ )
Polar [ $\text{m}$ ] $\cdot$ $\text{m}^{-2}$ ]	2.3 $\pm$ 0.2	30.3 $\pm$ 0.2	15.5 $\pm$ 0.2
Dispersive [ $\text{m}$ ] $\cdot$ $\text{m}^{-2}$ ]	41.5 $\pm$ 0.2	29.7 $\pm$ 0.5	31.3 $\pm$ 0.5
Surface free energy [ $\text{m}$ ] $\cdot$ $\text{m}^{-2}$ ] (polar + dispersive)	43.8 $\pm$ 0.5	60.0 $\pm$ 0.7	46.8 $\pm$ 0.7

\*Refer to Figure 3

fluid (i.e., water, H<sub>2</sub>O), pulling the fluid’s molecules away from one another and toward those contained on the substrate causing the fluid to spread. This increased spreading then lowers the contact angle at which the fluid contacts the substrate’s surface decreasing the fluid’s thickness (e.g. water, ink, etc.).

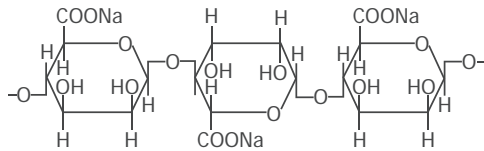


Figure 5: Molecular structure of sodium alginate (FP-Chem, 2011)

The surface roughnesses of the +1 and -1 alginate films (which are the 14.41 and 6.88 μm thick alginate films, respectively) are shown in Figure 6. The average roughnesses, S<sub>a</sub>, of the +1 and -1 films are 0.44 and 0.28 μm, respectively. The higher roughness of the thicker alginate film could be the result of the coarser grooves on the #20 Meyer rod or greater film shrinkage.

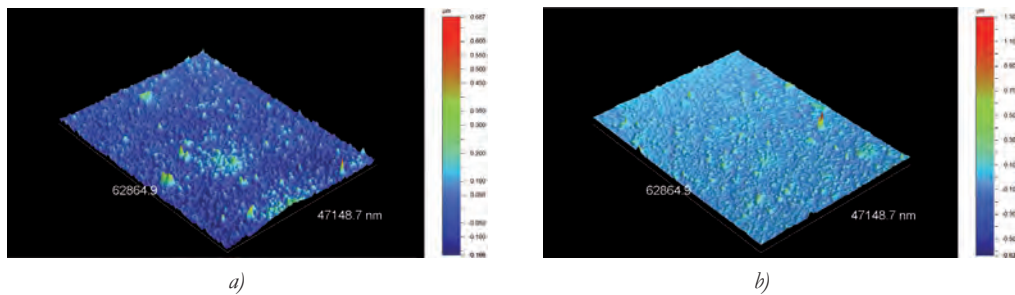


Figure 6: Surface roughness a) of the +1 (14.41 μm) alginate film, b) of the -1 (6.88 μm) alginate film

After fully characterizing the alginate layers, the roughness and thickness of the dielectric and conductive layers printed over the alginate films, according to the experimental setup, were measured. The results are shown in Figures 7 and 8.

The roughness values of the silver layers were significantly higher than the dielectric layers due to the presence of silver flakes in this ink. The roughness of the alginate layers had little or no effect on the roughness of either the conductive or dielectric layers. This would indicate that the thickness of these layers, as a result of the properties of the ink, screen-printing or drying processes, was sufficient to overcome the roughness of the alginate film. Since the roughness of the alginate film was related to its thickness, it can be concluded that the thickness of the alginate film had no influence on the roughness of the printed layers.

A comparison of the 14.41 μm (+1) and 6.88 μm (-1) alginate printed samples shows an influence of these layers on ink film thickness of both the single and double layer printed conductive and dielectric ink films. All

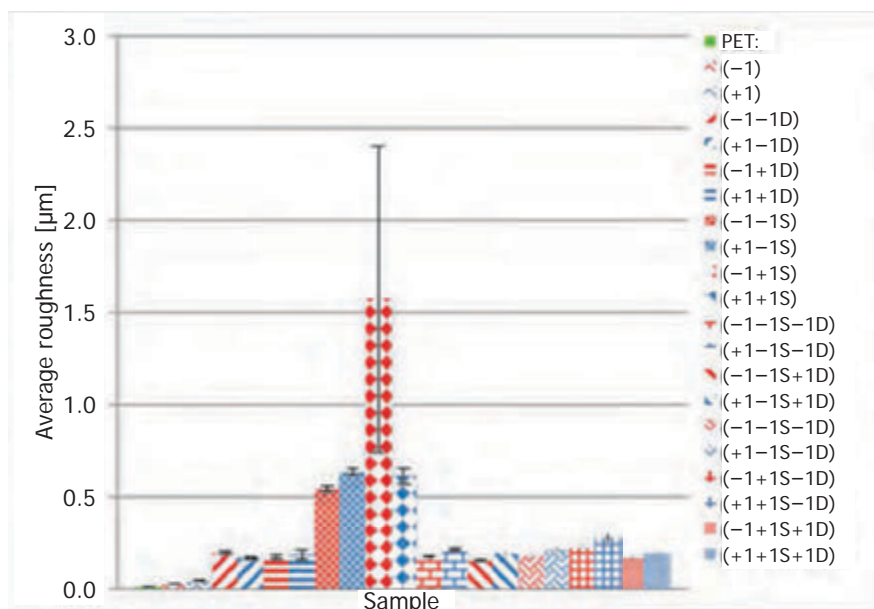


Figure 7: Variations in alginate and ink film roughness with printed and coated layer thicknesses

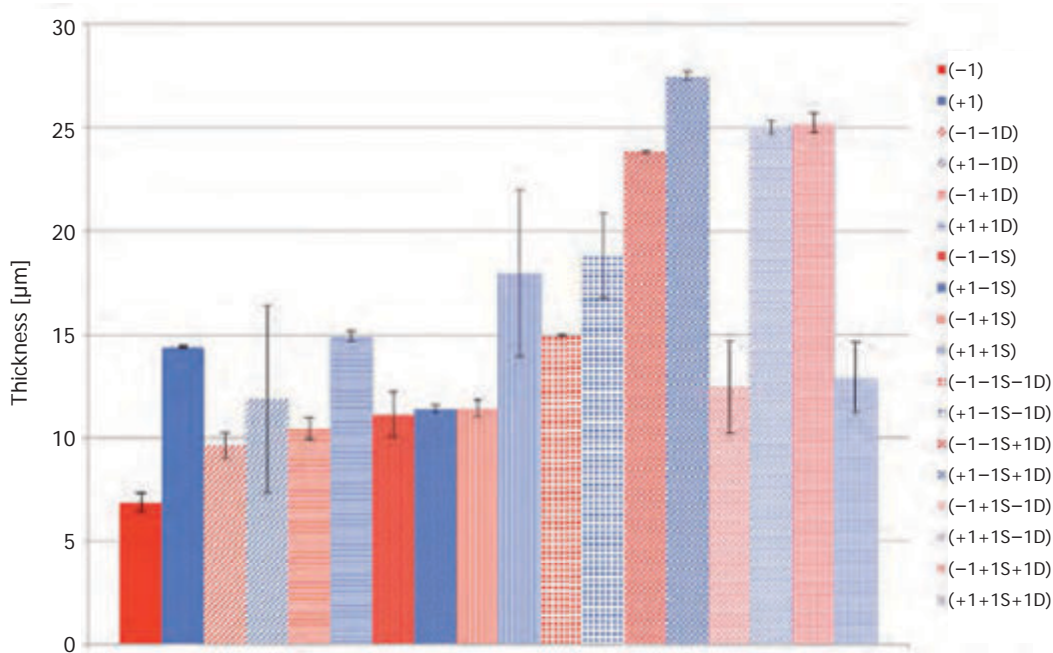


Figure 8: Comparison of film thickness values

dielectric ink films (single and double, -1D and +1D respectively) were thinner than the conductive ink films. It is also seen that all ink films printed on the 6.88 µm (-1) alginate films are thinner in comparison to the 14.41 µm (+1) films, with the exception of the (+1-1S-1D) sample. This could be attributed to the differences in surface free energies of the alginate films. The higher polarity (due to the presence of carboxyl and hydroxyl groups on the alginate, Figure 5) of the 14.41 µm (+1) alginate film could prevent the dielectric and conductive inks from spreading, consequently producing a thicker ink film.

Due to edge effects, the thicknesses of the single and multilayer films were difficult to measure. Edge effects are common with all printed samples, due to ink spreading. The contact angle is a measure of liquid wetting and spreading, the lower the contact angle, the more liquid (ink) wetting that occurs. The amount of spreading that occurs can also be influenced by how quickly the ink film is dried. Since the samples were printed on film, spreading would be expected to be greater, than if printed on a porous substrate. As shown in Figures 9 and 10, the thicknesses of the printed layers were lower at the edges, where more spreading occurred. This can be seen in both the 2D topographical image in Figure 9, and from the representative topographical profile of the x-profile in Figure 10, where the slope of the line decreases from left to right. The high magnification of the Bruker GT-K objective (only a 50× objective was available for use) also increased the difficulty of this measurement by minimizing the area of view to approximately 0.125 mm × 0.09 mm.

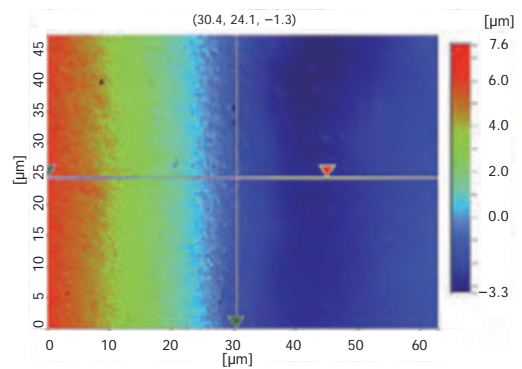


Figure 9: Topographical image of -1D ink on +1 alginate edge effect

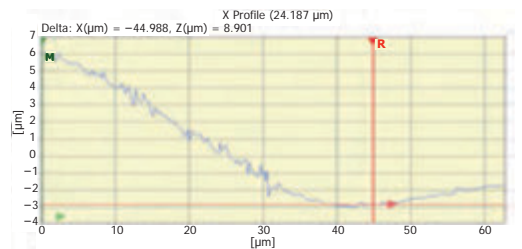


Figure 10: Profile of -1D ink on +1 alginate edge effect

The sheet resistivities of the conductive printed layers are shown in Figure 11. All measurements were made on PET. Figure 11 shows the importance of reporting sheet resistivity versus alginate layer thickness. The large deviations show the unreliability of this test method. The bulk resistivities of the samples are shown in

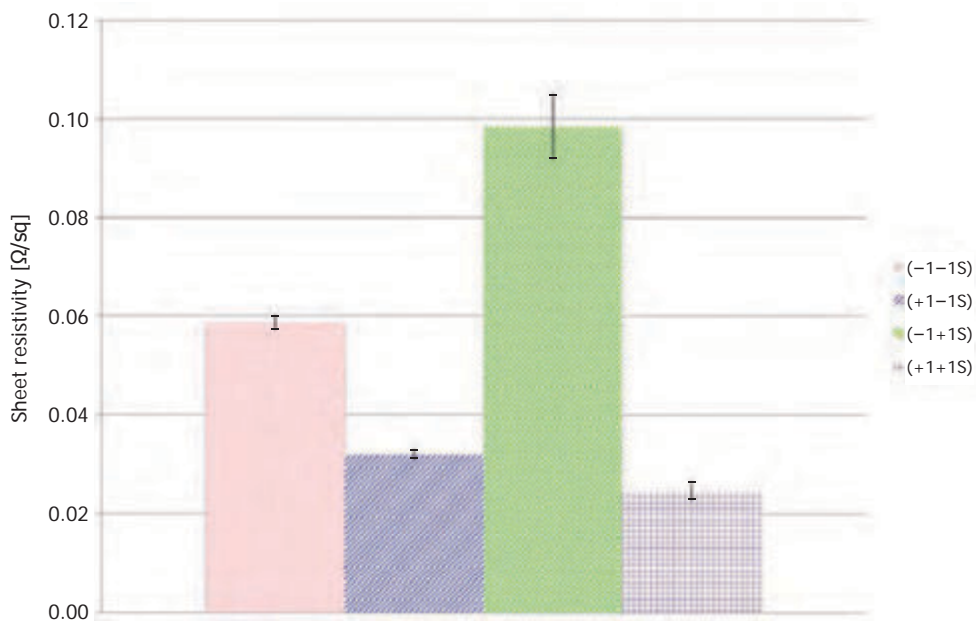


Figure 11: Changes in sheet resistivity of single and double printed silver ink layers as a result of altering the thickness of the sacrificial alginate coating layer

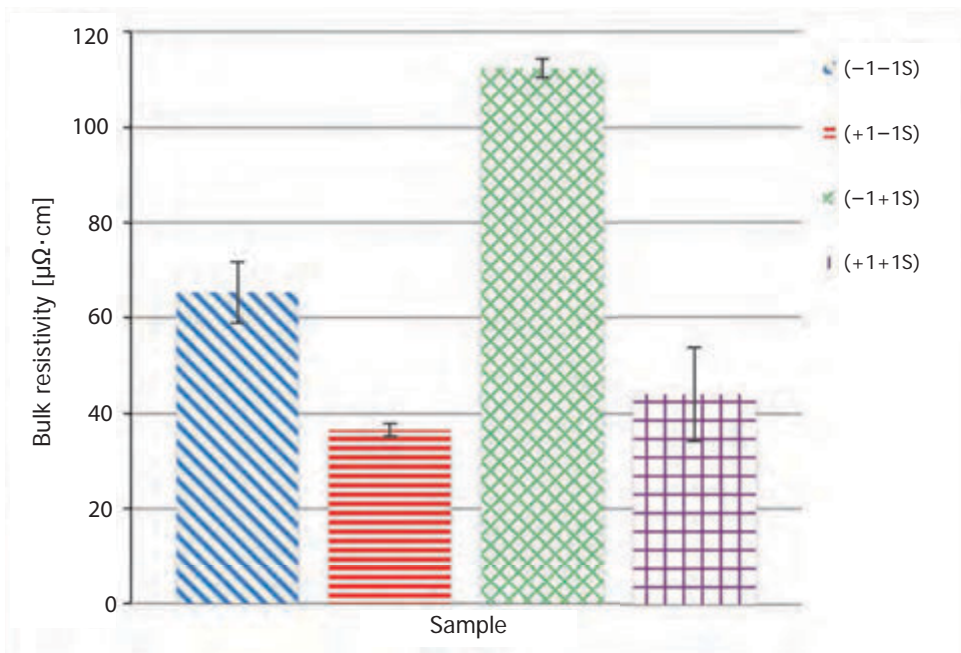


Figure 12: Changes in bulk resistivity of single and double printed silver ink layers as a result of altering the thickness of the sacrificial alginate coating layer

Figure 12. Bulk resistivity (e.g., units  $\Omega \cdot \text{cm}$ ) accounts for the thickness of the ink film within its calculation, while sheet resistance does not. It does this by multiplying the sheet resistance by the thickness, giving a resistance times length. The performances of the thicker ink films are significantly better due to the additional thickness. For this reason, the sheet resistivities of the dou-

ble layer conductive samples are lower than the single layer samples. The thickness of the alginate layer had a greater effect on the sheet resistivity of the thinner conductive film in comparison to the thicker one.

As seen in Figure 13, the dielectric constants are lower for the ink films lifted-off the thinner alginate coated

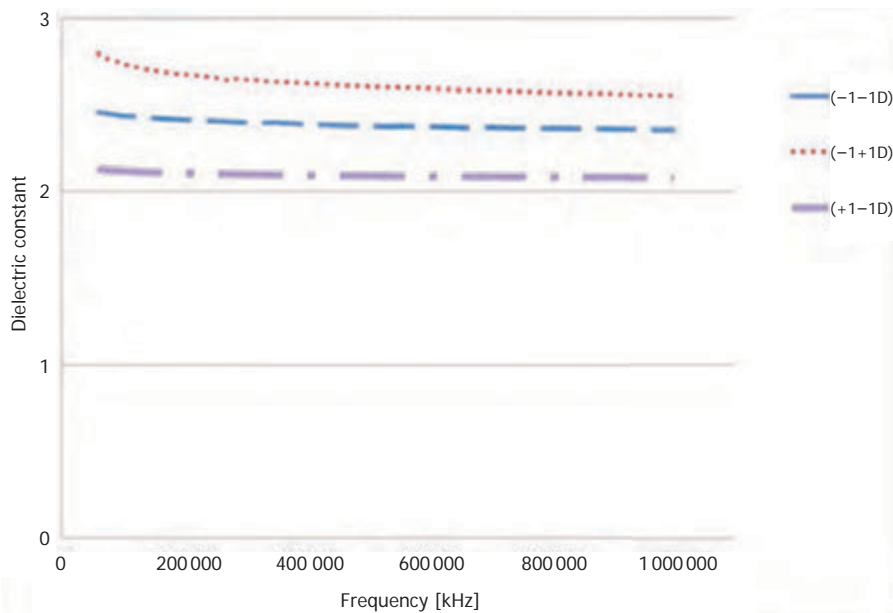


Figure 13: Comparison of the dielectric constants of single and double layer printed dielectric ink layers over alginate films of varying thicknesses

PET samples in comparison to the dielectric film printed on the thicker alginate sample. The +1+1D sample was not reported because its values were repeatedly measured as being negative, indicating that the thickness values for these samples were wrong. Unfortunately, the measurements could not be repeated without reprinting all the samples for consistency of the results.

Ink film densities were able to be determined after removal of the films from the PET. Figure 14 shows the results obtained by measuring the weight and caliper of the samples of known dimensions. From Figure 14

it may be seen that the density of the second layer is higher than that of the first layer (for both the silver and dielectric inks). This could be due to an incomplete removal of solvents in the first layer, or due to inaccuracies of the thickness measurements incurred by the edging effects. By having solvent left in the first layer prior to drying of the second layer the second layer during curing acts as a solvent trap on the solvents trying to escape from the first layer. If the same percentage of solvent was removed, all the silver films would have the same density and all the dielectric films would have the same density.

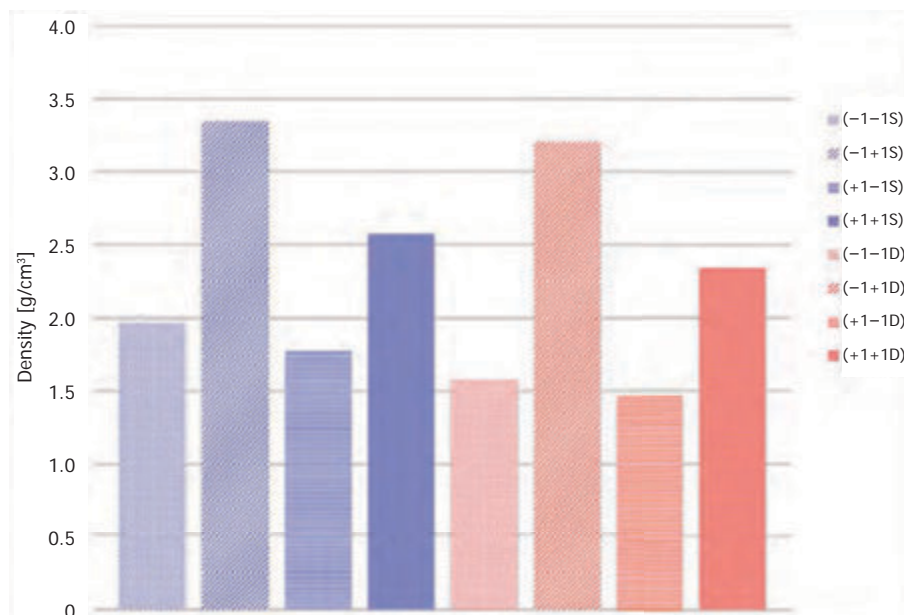


Figure 14: Changes in ink film density resulting from the printing of a second silver and dielectric layer

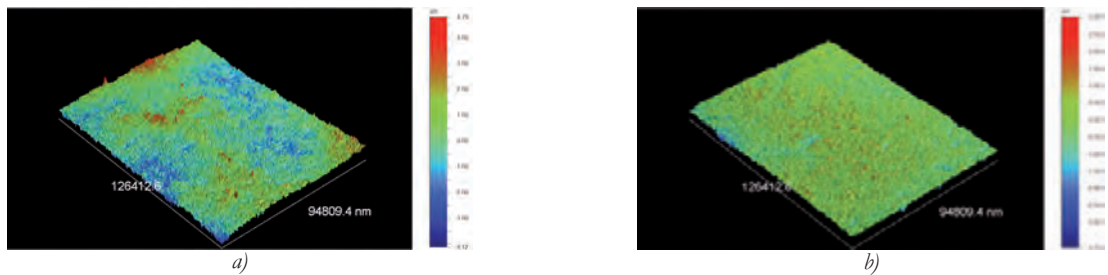


Figure 15: Roughness of the self-supported ink films for a)  $-1+1S$  top side ( $S_a=0.74 \mu\text{m}$ ), b)  $-1+1S$  bottom side ( $S_a=0.342 \mu\text{m}$ )

In Figure 15 the top and bottom side roughness of the self-supported conductive (silver) ink films are compared (these are free films, no substrate supporting them). As shown, the roughness of the topside (the side that was not in contact with the PET film) is nearly twice as rough as the side of the film, which was in direct contact with the alginate coated PET film prior to its removal in water.

Similar differences can be seen between the top side and bottom side for all the silver films in Figure 16.

The difference in surface topography of the top and bottom surface of the films is attributed to the difference in the smoothness of the surfaces in which they are in contact. That is, the top side is the side that contacts the printing screen, which is highly rough due to the mesh openings, as well as being exposed to the particulate matter within the environment during drying. In opposite, the bottom side of the ink film is in direct contact with the highly smooth (in relation to the printing screen) alginate coated PET film, and is protected from the environment during drying. This difference in roughness is apparent when looking at the differ-

ences between the top and bottom  $S_a$  statistical values. The  $S_a$  value depicts the average roughness averaged over an area (a 3D parameter) (Olympus-IMS, 2015; Cohen, 2013). The differences in topography of the top and bottom side of the conductive ink films shows an approximate 50 % reduction in  $S_a$  values.

One of the main objectives of this research was to determine if the self-supported films (combined to create a capacitor) could be wound without damage to the ink layers and capacitor itself. This objective was successfully achieved. A single stacked, self-supported capacitor was successfully created as seen in Figure 17, and successfully wound without damage, as seen in Figure 18. The gain in device flexibility as a result of not having a carrier substrate layer is obvious. These encouraging results show promise for the use of this technology as a means to produce a supercapacitor by winding a multi-stacked device or to minimize the size of a device to fit into tight places or where substrate compatibility issues to the surface to which it is to be attached is faced. The ability to bend devices can improve the attachment to surfaces, enabling its placement in confined spaces and advancing efforts to further miniaturize devices. It has also been shown that

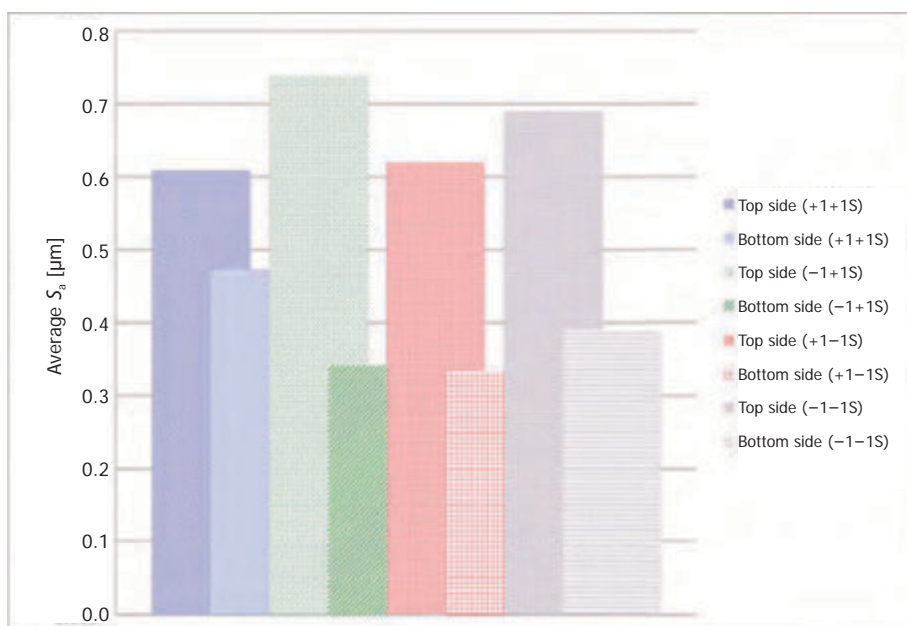


Figure 16: Comparison of top side and bottom side roughness of self-supported single layer silver ink films

the side of the printed film lifted off the rigid substrate is much smoother. This can be advantageous for multi-layer prints by requiring less ink to achieve complete surface coverage. So in practice, a printed film could be lifted from a smooth surface, flipped, and printed with



Figure 17: Self-supported unwound capacitor

minimal ink for coverage. By demonstrating that the self-supported layers could be rolled, it is feasible that a supercapacitor could be created through the addition of an insulating layer to prevent shorting upon winding. This work is currently in progress.

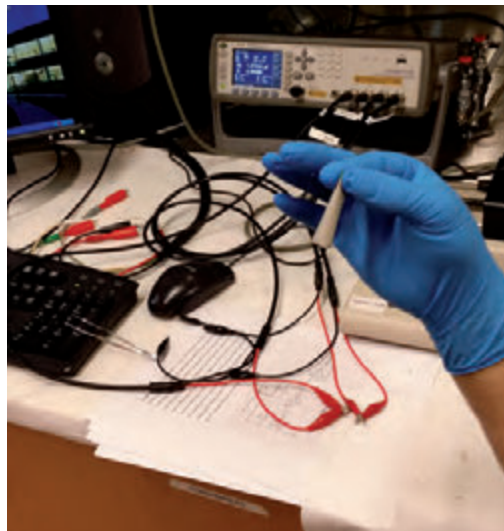


Figure 18: Self-supported wound capacitor

## 5. Conclusions

A process to produce self-supported electrically functional ink layers was demonstrated. Smooth alginate films on a PET substrate (sacrificial substrates) were produced by coating a 6% solution of alginate with a mass fraction of 20% of glycerol. This film served as a sacrificial layer for enabling the lift-off of screen-printed thermal conductive and UV dielectric ink films from a PET film after immersion of the printed samples in distilled water. The thickness of the alginate film was found to influence the thickness of the printed dielectric and conductive layers, which impacted their electrical performance. The ability to produce self-supported films to determine the dielectric constant of a dielectric ink film at different thicknesses was demonstrated. This is further supported by the fact that the final dielectric measurement of 3.81 (dielectric constant), calculated (using

Equation [1]) from the final capacitance measurements (from the fully printed capacitor) was within range of what the manufacturer (Table 2) reported (which is about 4). This was also true for the conductive inks' sheet resistivity measurements, which were reported as being between 0.015–0.020  $\Omega/\text{sq}$ . The finding of the differences from the top to bottom side conductive film roughness is of great interest. The ability to use the bottom side of a printed layer, for use when high smoothness is required may prove to be valuable. The density measurements also proved to be highly useful when calculating for the bulk resistivity and will be highly useful for any situation where accurate densities need to be accomplished. The ability to wind a fully printed self-supported capacitor was demonstrated and holds promise for the creation of supercapacitors by this technique.

## References

- Bird, J., 2010. *Electrical and Electronic Principles and Technology*, New York: Routledge.
- Blake, P., Brimicombe, P.D., Nair, R.R., Booth, T.J., Jiang, D., Schedin, F., Ponomarenko, L.A., Morozov, S.V., Gleeson, H.F., Hill, E.W., Geim, A.K. and Novoselov, K.S., 2008. Graphene-based liquid crystal device. *Nano Letters*, 8(6), pp. 1704–1708.
- Butler, P., Miller, J.L. and Taylor, P.A., 2002. *Energy Storage Opportunities analysis: Phase II Final Report, A Study for the DOE Energy Storage Systems Program*. Albuquerque, New Mexico, Sandia National Laboratories.
- Challa, V.R., Prasad, M.G., Shi, Y. and Fisher, F.T., 2008. A vibration energy harvesting device with bidirectional resonance frequency tunability. *Smart Materials and Structure*, 17(1), pp. 1–10.

- Cohen, D.K., 2013. *The connection between surface texture and sliding friction*. [online] Available at: <[https://www.bruker.com/fileadmin/user\\_upload/8-PDF-Docs/SurfaceAnalysis/AFM/Webinars/Bruker-SlidingFriction-presentation-07262013.pdf](https://www.bruker.com/fileadmin/user_upload/8-PDF-Docs/SurfaceAnalysis/AFM/Webinars/Bruker-SlidingFriction-presentation-07262013.pdf)> [Accessed 16 August 2015].
- FP-Chem, 2011. *Sodium Alginate*. [online]. Available at: <<http://www.fp-chem.com/index.php?c=msg&id=373&>> [Accessed 17 August 2015].
- FTA, 2015. *Owens-Wendt Surface Energy Calculation*. [online] Available at: <<http://www.firsttenangstroms.com/pdfdocs/OwensWendtSurfaceEnergyCalculation.pdf>> [Accessed 16 August 2015].
- FusionUV, 2015. *An Electrodeless Bulb for Consistency and Long Life* [online]. Available at: <[http://www.fusionuv.com/uv\\_bulbs.aspx](http://www.fusionuv.com/uv_bulbs.aspx)> [Accessed 16 August 2015].
- Grande, L., Chundi, V.T., Wei, D., Bower, C., Andrew, P. and Ryhänen, T., 2012. Graphene for Energy Harvesting/Storage Devices and Printed Electronics. *Particuology*, 10(1), pp. 1–8.
- Greer, S.E. and Howard Jr., R.T., 1989. *Lift-off process for terminal metals*. U.S. Pat. 4,861,425.
- Halper, M.S. and Ellenbogen, J.C., 2006. *Supercapacitors: A Brief Overview*. MITRE Nanosystems Group, MITRE Corporation, McLean, Virginia, USA.
- Han, Y., Ding, B. and Shang, X., 2010. Preparation of graphene/polypropyrole composites for electrochemical capacitors. *Journal of New Materials for Electrochemical Systems*, 13(4), pp. 315–320.
- Hartman, A., 2011. *Printing Carbon Nanotube Based Supercapacitors for Packaging*. Master thesis, Clemson University.
- Haskal, E.I., McCulloch, D.J. and Broer, D.J., 2010. *Active matrix displays and other electronic devices having plastic substrates*. U.S. Pat. 2010/0163,878.
- Helmholtz, H.v., 1853. Über einige Gesetze der Vertheilung elektrischer Ströme in körperlichen Leitern mit Anwendung auf die thierisch-elektrischen Versuche. *Annalen der Physik und Chemie*, 89(6), pp. 211–233.
- Jayalakshmi, M. and Balasubramanian, K., 2008. Simple capacitors to supercapacitors – an overview. *International Journal of Electrochemical Science*, 3, pp. 1196–1217.
- Jiang, Z., 2007. *Technology Assessment and Market Analysis of Solid State Ultracapacitors*. Master thesis, Massachusetts Institute of Technology.
- Jog, M.G., 1989. *Hydroelectric and Pumped Storage Plants*. New Delhi: New Age International.
- Kaempgen, M., Chan, C.K., Ma, J., Cui, Y. and Gruner, G., 2009. Printable thin film supercapacitors using single-walled carbon nanotubes. *Nano Letters*, 9(5) pp. 1872–1876.
- Kang, J.Y., 2006. Micropower for Medical Application. In: J.G., Webster, ed., *Encyclopedia of Medical devices and Instrumentation*. New Jersey: Wiley-Interscience.
- Keskinen, J., Sivonen, E., Jussila, S., Bergelin, M., Johansson, M., Vaari, A. and Smolander, M., 2012. Printed Supercapacitors on Paperboard Substrate. *Electrochimica Acta*, 85, pp. 302–306.
- Kiebele, A. and Gruner, G., 2007. Carbon nanotube based battery architecture. *Applied Physics Letters* 91(14), p. 144104.
- Kinaret, J., Falko, V., Ferrari, A., Helman, A., Kivioja, J., Neumaier, D., Novoselov, K., Palermo, V. and Roche, S., 2012. *Coordination Action for Graphene-Driven Revolutions in ICT and Beyond*. Graphene Flagship: Deliverable 6.3 “Publishable flagship proposal report”, EC grant n°284558.
- Le, L.T., Ervin, M.H., Qiu, H., Fuchs, B.E., Zunino, J., and Lee, W.Y., 2011. Inkjet-printed graphene for flexible micro-supercapacitors. In: *11<sup>th</sup> International Conference on Nanotechnology*. Portland, Oregon, USA.
- Linden, D., 1984. *Handbook of batteries and fuel cells*. New-York: McGraw-Hill.
- Liu, C., Yu, Z., Neff, D., Zhamu, A. and Jang, B.Z., 2010. Graphene-based supercapacitor with an ultrahigh energy density. *Nano Letters*, 10(12), pp. 4863–4868.
- Miller, J. R. and Simon, P., 2008. Electrochemical capacitors for energy management. *Science*, 321(5889), pp. 651–652.
- Nagata, H., Ko, S.W., Hong, E., Randall, C.A., Trolier-McKinstry, S., Pinceloup, P., Skamser, D., Randall, M. and Tajuddin, A., 2006. Microcontact printed BaTiO<sub>3</sub> and LaNiO<sub>3</sub> thin films for capacitors. *Journal of the American Ceramic Society*, 89(9), pp. 2816–2821.
- Nair, R.R., Blake, P., Grigorenko, A.N., Novoselov, K.S., Booth, T.J., Stauber, T., Peres, N.M.R. and Geim, A.K., 2008. Fine structure constant defines visual transparency of graphene. *Science*, 320(1308), p. 1308.
- Ogier, S.D., Veres, J. and Yeates, S.G., 2003. *Organic electronic devices*, EP 1529317 A2.

- Olympus-IMS. 2015. *Roughness (3D) parameter*. [online] Available at: <[http://www.olympus-ims.com/en/knowledge/metrology/roughness/3d\\_parameter/](http://www.olympus-ims.com/en/knowledge/metrology/roughness/3d_parameter/)> [Accessed 16 August 2015].
- Owens, D.K. and Wendt, R.C., 1969. Estimation of surface free energy of polymers. *Journal of Applied Polymer Science*, 13(8), pp. 1741–1747.
- Pech, D., Brunet, M., Taberna, P.L., Simon, P., Fabre, N., Mesnilgrente, F., Conédéra, V. and Durou, H., 2010. Elaboration of a microstructured inkjet-printed carbon electrochemical capacitor. *Journal of Power Sources*, 195(4), pp. 1266–1269.
- Pollet, M., Marinel, S. and Desgardin, G., 2004. CaZrO<sub>3</sub>, a Ni-co-sinterable dielectric material for base metal-multilayer ceramic capacitor applications. *Journal of the European Ceramic Society*, 24, pp. 119–127.
- Rogers, J.A., Huang, Y., Ko, H.C., Stoykovich, M., Choi, W.M., Song, J., Ahn, J.H. and Kim, D.H., 2010. *Stretchable and foldable electronic devices*. U.S. Pat. 2010/0002402.
- Ruddell, A. 2003. *Investigation on Storage Technologies for Intermittent Renewable Energies: Evaluation and recommended R&D strategy*. Storage Technology Report: WP-ST6: Flywheel.
- Simon, P. and Gogotsi, Y., 2008. Materials for electrochemical capacitors. *Nature Materials*, 7(11), pp. 845–854.
- Smith, W.F. and Hashemi, J., 2006. *Foundations of materials science and engineering*, Boston: McGraw-Hill.
- Sterken, T., Fiorini, P., Van Hof, C. and Puers, R., 2007. A Hybrid Electrodynamical Vibration Harvester. In: *Proceedings of Power MEMS 2007*, pp. 85–88.
- Swanson, R.M., 2009. Photovoltaics Power Up. *Science*, 324(5929), pp. 891–892.
- visit-alginate, 2015. [online] Available at: <<http://www.visit-alginate.com/sodium-alginate-chemical-properties.html>> [Accessed 16 August 2015].
- Wang, Y., Shi, Z., Huang, Y., Ma, Y., Wang, C., Chen, M. and Chen, Y., 2009. Supercapacitor devices based on graphene materials. *The Journal of Physical Chemistry C*, 113(30), pp. 13103–13107.
- Winter, M. and Brodd, R.J., 2004. What are batteries, fuel cells, and supercapacitors? *Chemical Reviews*, 104(10), pp. 4245–4270.
- Wu, Q., Xu, Y., Yao, Z., Liu, A. and Shi, G., 2010. Supercapacitors based on flexible graphene/polyaniline nanofiber composite films. *ACS Nano*, 4(4), pp. 1963–1970.
- Young, T., 1805. An essay on the cohesion of fluids. *Philosophical Transactions of the Royal Society of London*, 95, pp. 65–87.
- Yu, A., Roes, I., Davies, A. and Chen, Z., 2010. Ultrathin, transparent, and flexible graphene films for supercapacitor application. *Applied Physics Letters*, 96(25), p. 253105.

# Topicalities

*Edited by Markéta Držková*

## Contents

News & more	303
Bookshelf	305
Events	311



# News & more

## The online ticket shop for drupa 2016 opens on 2<sup>nd</sup> January



During the few months remaining until May 31<sup>st</sup> when drupa 2016 opens its doors, the plenty of information about the printing industry and related fields is provided by the drupa organizers to all of us through several news channels and also reflected in reports and expert articles.

## Second drupa Global Insights report

More than a year after the publication of the first report focused on strategic shifts in the international print and media sector, 'The Impact of the Internet on Print – The Digital Flood', the second report named 'Touch the future – Applications that can create growth' is available now. Underlying survey on the implementation of so called fresh print applications was conducted in spring 2015 and gained almost 750 respondents, 170 of which offered also their personal experience of implementing such applications. Success stories as well as failures or least major setbacks were reported. The importance of careful planning, effective implementation, integration and marketing for exploiting the potential of print applications allowed by digital technology for turnover growth and profitability was demonstrated.

In spite of recessions and the impact of digital communications, the demand for print is expected to continue to grow thanks to growing world's population, improving literacy and living standards amongst the developing nations and the rise in trade. Over the last five years, print consumer expenditure is falling much more slowly than print advertising (compound annual rate –1.5 % versus –6 %, respectively). An investment in integrated print applications capable to meet evolving customer demands is favoured as a key to improved and sustainable performance. Being aware of fast and fundamental changes driven by digital technology, the report predicts that the success of different printing sectors and their applications will depend on the integration of printed products with web and mobile communication platforms underpinned by data services and automated workflows.

To quote some numbers included in the report, those adopting good management practices invested on average an additional \$70,235 but were rewarded by an additional \$175,623 of annual turnover and \$63,330 of annual profit. However, regardless of the implementation quality and the size of the original investment, some applications outperformed the others in terms of a quicker payback. When comparing on-demand with short-run batch book production and multichannel marketing with business stationery applications, the latter had on average over double the payback period. In case of comparison of digitally printed flexibles with digitally printed corrugated applications, it was even four times longer.

## Expert articles in brief

Four drupa 2016 expert articles were published since the first one, which we have shortly introduced in summer issue. The second one, written by Des King, is entitled 'Package Printing' and cites the top brand owners and branding experts in the world. Today, numerous advances enable the production of an eye-catching and innovative printed packaging, facilitating

## New market reports from Smithers Pira

The Future of Printer Demographics to 2020 released by the end of November builds on historic and current company and employment situation and examines trends in terms of company size, printer revenues and other key indicators, offering almost 400 tables and figures for individual industries and countries. In the 60 monitored countries, the number of commercial printing enterprises raised by 3 % to 720,000 and the number of employees by 6 % to 7.2 million between 2010 and 2014. However, this growth was limited mainly to the Asia, with little or slow growth in transitional economies and decline in regions with developed printing markets.



The Future of Global Printing to 2020 published now in December forecasts annual growth of 2 % per year from now to 2020. As its drivers, growth in package printing, continued growth in emerging economies, and added-value opportunities associated with digital print are identified. The report includes numerous tables and figures, analysing the global markets for new print equipment, colorants, printing ink, plates and substrates, as well as different end-use sectors, printing processes and individual national markets. In the last chapter, leading printing groups are introduced.

## Colour multi-material 3D printed models enhance complex kidney cancer surgery planning

Medical applications of 3D printing are not limited just to the extensive research in bioprinting. Stratasy's transparent VeroClear material helps in CHU Bordeaux, France, to better locate kidney tumors and estimate their depth. The 3D printed models also increase patient understanding of procedures and are beneficial for education and training purposes.

### Em Software solutions for editorial work and creation of fully formatted documents

WordsFlow and DocsFlow plugins enable placing of



Microsoft Word and Excel or Google Drive documents, respectively, with live links in Adobe InDesign; this way the authors and editors can continue working on the original documents while the production of final file proceeds. Changes on either side are merged, with automatic notification of any conflicts. Efficiency further increases because all involved in the process work in their native tools.

Similarly, InCatalog InDesign plugin and Xcatalog QuarkXPress XTension connect prepress documents to the source data stored in database or spreadsheet, thus avoiding the need for manual updating if data change.

InData for InDesign and Xdata for QuarkXPress are so called software robots, which turn raw structured data from spreadsheets and databases into finished documents based on predefined template, ranging from the simple layouts up to the complex ones, incorporating any number of graphics, and even variable page layouts using master pages. Likewise, Xtags can be used both with InDesign and QuarkXPress when data are in an appropriate simple tagged text format. A great amount of time is saved especially in case of repetitive and extensive publishing tasks.

Plugins as well as XTensions supporting several versions of layout applications up to InDesign CC 2015 and QuarkXPress 2015 are available.

### Access to PDF files in Dropbox using the Adobe applications

The possibility to access PDF files stored in Dropbox Basic, Pro or Business accounts through the Acrobat or Acrobat Reader desktop and mobile applications (at the moment on iOS and in 2016 on Android devices) is a good news for all their users, but especially for cooperations where an investment into professional prepress workflow tools wouldn't pay-off.



greater engagement between a brand and a consumer – in particular, the adoption of online-oriented technologies to highlight the overall concept, add fun and at the same time reduce the extent of information required to be displayed on-pack, technologies which increase product security and brand integrity, along with traditional contribution of well-executed creative design and special decorative effects, supported by appropriate colour management technologies and web-based workflow platforms linking all components within the packaging print supply chain.

In the third drupa 2016 expert article, the question 'Inkjet – State of the Art or Sci-fi Fantasy Print?' is raised and discussed by Sean Smyth. Same as in case of other technologies, really successful application of inkjet printing needs to focus on market with large potential, invest in simple employing or even inventing appropriate materials, equipment and systems, and still develop new business models. The inkjet technology continues to evolve, including the availability of more flexible inks with increased colour gamut, thus enabling to reduce the need for special substrates and increase the productivity. Decrease in ink cost is still required to make inkjet printing competitive for medium to long runs with high ink coverage. In general, well utilized inkjet as the only non-contact, high quality, high performance printing process is expected to provide higher return on investment for many products – besides traditional printing and graphics also in various industrial decoration applications.



Fourth expert article is 'Crossing the finish line – a Cinderella story' contributed by Cary Sherburn. The title suggests that this time the focus is on the postpress step, i.e. binding and finishing in commercial print, packaging, sign and display graphics and other sectors. While both prepress and printing processes are nowadays highly automated, significant opportunities for improving throughput and productivity as well as reducing costs are seen in postpress departments of many companies. Although the machine setup can be often automated based on job ticketing information, bar codes, marks and the like, reducing the risk of errors and the number of oversheets significantly and allowing to utilise less skilled workers, time consuming and error prone manual machine set-up, is still common. Further, modular finishing solutions are crucial for greater flexibility and better utilisation. The second part discusses each segment and its individual characteristics, covering direct mail with emphasis on automation and inspection systems, high added value finishing and converting with special effects applicable to wide range of printed products including packaging, as well as advanced and versatile binding solutions for book printers.

Finally, the fifth one by Laurel Brunner deals with 'Print and Sustainability'. Environmental regulations and green expectations add to all factors mentioned above, making the situation in today's printing industry even more complex and confusing for both printers and their customers. On the other hand, these circumstances speeded up the development and implementation of automation and standardisation to allow efficient production and controlling colour quality and ink consumption across substrates as well as for digital output, accompanied by cutting waste and emissions, while increasing the use of renewable resources and materials optimised for recycling. Standards like ISO 14001 Environmental management systems or ISO 16759 Calculating the carbon footprint of print help to manage these issues. The author points out that for successful and sustainable future, printers must reshape their businesses to help clients leverage channels and align commercial and environmental goals.

# Bookshelf

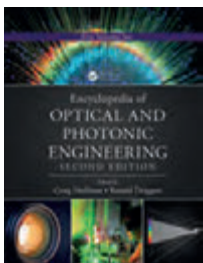
## Encyclopedia of Optical and Photonic Engineering

Shortly after the 3<sup>rd</sup> edition of the Encyclopedia of Surface and Colloid Science presented in previous issue, CRC Press has published also the 2<sup>nd</sup> edition of the Encyclopedia of Optical and Photonic Engineering in a five-volume set. Besides the printed edition, online subscription to this reference work is offered by Taylor & Francis Group.

The first edition covered devices or systems that generate, transmit, measure, or detect light, and partly the basic interaction of light and matter. This edition is claimed to have a half of the articles revised, with 25 % of new material. Benefiting from the addition of a second editor, it offers the fundamentals of a diverse portfolio of technologies and discoveries in areas ranging from x-ray optics to photon entanglement and beyond. For each topic, a general discussion for non-specialists is presented together with an expert content supported by extensive references to primary literature and other sources.

Among basic topics can be listed e.g. aberrations, antireflection coatings, backscatter, coherence, collimation testing techniques, diffractive optics, distortion, etching, filters, f-number, numerical aperture and depth of focus, Fresnel equations, holography, illumination optics, interference, lenses, mirrors and prisms, liquid crystals, lithography, optical amplifiers, optical design and fabrication, optical fibers, paraxial optics, piezoelectric effect, polarization, scattering, surface roughness, thin film deposition, wavelets and optical elements for x-rays. Automatic target detection and recognition, compression transforms, digital image restoration, enhancement, processing, redundancy and segmentation, pattern recognition, ray tracing, or eye movements and accommodation, human vision and colour, psychophysical measurement and nonlinear dynamic approaches to vision are also covered. Cavity quantum electrodynamics, high power femtosecond pulses, nanophotonics for photovoltaics or numerous entries on nonlinear optics and quantum optics can serve as an examples of the more advanced ones.

Characterization methods comprise film thickness measurement, fluorescence microscopy, Fourier transform infrared spectroscopy, interferometry, microscopy, photometry, polarization measurements, radiometry, a number of spectroscopic methods, 3D noncontact sensing and others. From biology and medicine, e.g. biomedical spectroscopy, optical biopsy, optical manipulation of living cells, microscopy of living cells, tissues and organs, ophthalmic optics, tissue spectroscopy, tissue–laser interactions, and medical applications of x-rays can be found. General applications include e.g. communication networks, data storage, detectors, display systems, disk drives, electro-optical imaging systems, integrated optical circuits, lasers, light emitting diodes, liquid crystal displays, optical heads, optical modulators, optical neural networks, optical parametric oscillators and amplifiers. In relation to astronomy and remote sensing, entries on galaxies, Milky Way, scintillation, Solar System, stellar characteristics, Sun, distribution of matter in Universe, atmospheric optics, lidar (light detection and ranging) or ocean optics applications are presented.



Encyclopedia of Optical and Photonic Engineering  
 Editors: *Craig Hoffman, Ronald Driggers*  
 Publisher: CRC Press  
 2<sup>nd</sup> ed., September 2015  
 ISBN: 978-1-4398-5097-8  
 4088 pages  
 Hardcover

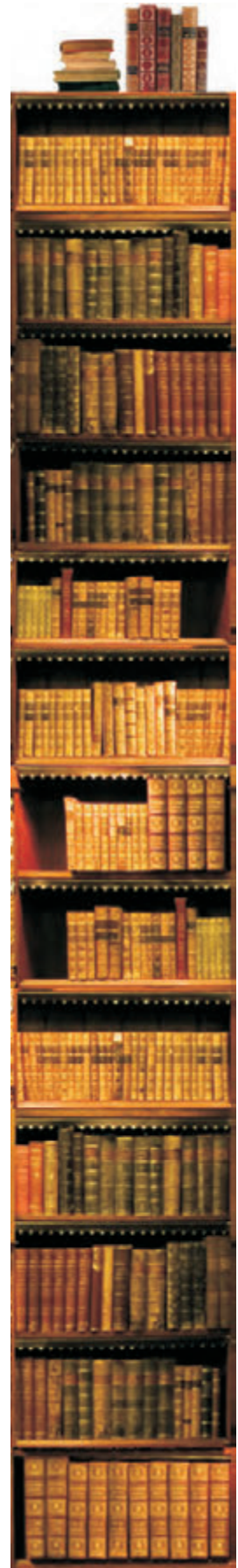


### Image Resolution: Deconstructing Hollywood's Zoom and Enhance

Author: Robert D. Fiete

Publisher: SPIE  
Publications  
1<sup>st</sup> ed., February 2015  
ISBN: 978-1628416466  
46 pages  
eBook



SPIE Spotlights is a new eBook series. This one examines the results of a typical zooming and enhancing process, assuming real capabilities of a digital camera and image processing. The example explored is the capability of crime scene investigators to zoom and enhance on the reflection of an eye in an image to reveal the identity of an assailant. Optics, sensors, and processing challenges are considered, leading to a definition of a camera able to provide the required resolution.

### Optical Sensing: Microstructured Fibers, Fiber Micromachining, and Functional Coatings

Authors: Minghong Yang,  
Dongwen Lee, Yu-Tang Dai

Publisher: SPIE  
Publications  
1<sup>st</sup> ed., May 2015  
ISBN: 978-1628417937  
23 pages  
eBook



Integration of the most recent enabling technologies based on either the longitudinal or transverse structuring of fibers for optical sensing is presented along with example applications of e.g. sapphire or photonic crystal fiber.

### Optimization Techniques for Diffraction Spectrometers

Author: Elena A. Sokolova

Publisher: SPIE  
Publications  
1<sup>st</sup> ed., June 2015  
ISBN: 978-1628418439  
62 pages  
eBook



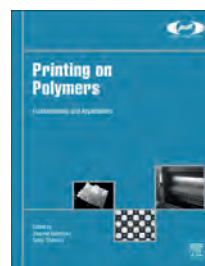
Optical design methods are applied to diffraction grating fabrication with the aim to improve diffraction

### Printing on Polymers: Fundamentals and Applications

The knowledge built during many decades of development of printing on polymeric substrates, as well as current research in this field and its new challenges, are presented in this book, intended as a one-stop reference resource for an audience ranging from plastics, resin and ink manufacturers over packaging, automotive, aerospace and consumer goods industry to scientists involved in materials and printing. Problems that can be caused by physical, chemical and thermal interactions, such as cracking, peeling or dulling, are addressed, helping to choose the correct way of decorating a particular polymer. Furthermore, necessary quality, safety, environmental sustainability and cost considerations are presented.

The introduction brings a short history of printing and a brief overview of all techniques used for polymer printing and decorating along with their suitability for selected polymeric and packaging materials – simple or multilayer films, semirigid and rigid plastic sheets, molded products, synthetic papers, and polymer-coated boards. Surface free energy is explained, being a key factor that determines material wettability and adhesion of ink to the substrate and thus its printability. Some facts about the plastic printing industry are included too. All aspects related to materials are detailed in next chapters on the structure, properties and applications of polymeric materials, printing ink types, formulations and components, including additives and advanced nanoscale materials, rheology of printing inks, and finally various modifications of polymer surface – plasma assisted or corona treatment, chemical modification and other methods. Following chapters describe individual printing techniques: flexographic, gravure, offset, inkjet, screen and pad printing, stamping, 3D printing and other. Last part of the book encompasses theory, modelling and simulation of printing, characterization of colorimetric aspects and mechanical properties of prints, their ageing and degradation, applications of printed polymeric materials, and also the safety and environmental aspects of polymer printing, concluded by the recyclability and life cycle analysis of printed materials.

Printing on Polymers:  
Fundamentals and Applications  
Editors: Joanna Izdebska, Sabu Thomas  
Publisher: William Andrew  
1<sup>st</sup> ed., October 2015  
ISBN: 978-0-323-37468-2  
444 pages  
Hardcover  
Available also as an eBook



### Adhesives Technology Compendium 2015

This comprehensive overview of German suppliers, research facilities and service providers, the latest legislation, standards, testing methods and statistics is available also at <http://www.adhesivetechnologycompendium.de>.

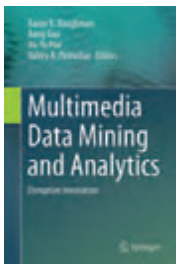
Adhesives Technology Compendium 2015  
Edited by: Industrieverband Klebstoffe e.V.  
Publisher: Springer Vieweg  
1<sup>st</sup> ed., October 2015  
ISBN: 978-3-658-10331-6  
316 pages  
Softcover



## Multimedia Data Mining and Analytics: Disruptive Innovation

The book describes the impact of innovations in mobile, social, cognitive, cloud and organic based computing on the multimedia data processing, and the corresponding shift of the research focus towards networked social communities, mobile devices and sensors. It pays attention to the practical implementation of frameworks, libraries and open source software that enables the development from research to practical, real-world applications.

Privacy issues in multimedia social environments and large-scale biometric data processing, as well as content and concept based multimedia search and various advanced algorithms for representation, processing and visualization of multimedia data, are included. To name a few examples, sentiment analysis or mining popular routes using social multimedia, detection of demographics and identity in spontaneous speech and writing, content based image search, concept detection in video by combining visual and textual cues and mining videos for attention-driving features are explored within 19 chapters of the book, along with the explanation of fast binary embedding for high-dimensional data or musical representation of time-dependent data for listening to the sound of data.



Multimedia Data Mining and Analytics: Disruptive Innovation  
 Editors: Aaron Baughman, Jiang Gao, Jia-Yu Pan, Valery A. Petrushin  
 Publisher: Springer  
 1<sup>st</sup> ed., April 2015  
 ISBN: 978-3-319-14997-4  
 454 pages  
 Hardcover  
 Available also as an eBook

## Marketing Analytics: Practitioner's Guide to Marketing Analytics and Research Methods

The digital age and especially the almost permanent use of internet-based services on smart devices has transformed the way the customers communicate, shop and buy, and thus the very nature of marketing. The methods of collecting, processing, analysing and disseminating market intelligence has changed as well, enabling marketers to respond with much greater speed and accuracy at lower costs.

Intended for business management students as well as marketing professionals, the book brings a comprehensive overview of market analytic techniques and market research processes. It is divided into parts discussing brand, consumer, product, advertising, price and promotion, and retail, accompanied by seven case studies. In addition, sampling and gain-loss algorithms are explained in appendices. Further content including lecture presentations and case study datasets is available at book's website.

Marketing Analytics: Practitioner's Guide to Marketing Analytics and Research Methods  
 Author: Ashok Charan  
 Publisher: World Scientific Publishing Co.  
 1<sup>st</sup> ed., October 2015  
 ISBN: 978-981-4641-36-4  
 720 pages  
 Hardcover  
 Available also as an eBook



efficiency, tolerance analysis, and optimization techniques. Performance testing of gratings and modification of classical spectrometers using modern design and fabrication techniques is also covered.

## International Colloquium of Art and Design Education Research (i-CADER 2014)

Editors: Oskar H. Hassan, Shahrizan Z. Abidin, Rafeah Legino, Rusmadiyah Anwar, Muhamad F. Kamaruzaman



Publisher: Springer  
 1<sup>st</sup> ed., October 2015  
 ISBN: 978-9812873316  
 709 pages  
 Hardcover  
 Also as an eBook

This collection offers variety of contributions, ranging from microscopic image and text examination of conventional and digital printouts through a formal proposition of graphics analysis of comics, infographics as a tool for facilitating learning, preventing childhood obesity through poster design or the behaviour patterns towards printed colour medium for students with hearing disabilities to an overview of book printing and publishing industry in Malaysia and many more.

## Becoming a Graphic and Digital Designer: A Guide to Careers in Design

Authors: Steven Heller, Veronique Vienne



Publisher: Wiley  
 5<sup>th</sup> ed., May 2015  
 ISBN: 978-1118771983  
 336 pages  
 Softcover  
 Also as an eBook

The 5<sup>th</sup> edition of this successful guide has been substantially reworked and offers to those interested in a graphic design career the content with an emphasis on portfolio requirements and job opportunities, supported by numerous images, interviews and essays showcasing work, opinions and experiences of leading designers. The book is organized into parts on graphic design, design genres, transitional design, digital design and design education.

### 3D Bioprinting and Nanotechnology in Tissue Engineering and Regenerative Medicine

Authors: Lijie Grace Zhang,  
John P. Fisher, Kam Leong

Publisher: Academic Press  
1<sup>st</sup> ed., February 2015  
ISBN: 978-0128005477  
392 pages, Hardcover  
Also as an eBook



This book aims to provide a summary of the suitability, sustainability and limitations of each technique for specific applications. Basic principles are explained, followed by biomaterials and applications (e.g. for blood vessels, neural, vascular or dental tissue, skin, craniofacial bone and cartilage, up to organ printing) and also intellectual property aspects.

### Bioprinting in Regenerative Medicine

Editor: Kursad Turksen

Publisher: Springer  
1<sup>st</sup> ed., September 2015  
ISBN: 978-3319213859  
140 pages  
Hardcover  
Also as an eBook



Second book on bioprinting presented here belongs to the Stem cell biology and regenerative medicine series and introduces basics as well as latest developments in laser-assisted bioprinting for engineering different types of tissue.

### Bioprinting: Principles and Applications

Authors: Chee Kai Chua, Wai Yee Yeong

Publisher: World Scientific Publishing Co.  
1<sup>st</sup> ed., January 2015  
ISBN: 978-9814612104  
296 pages, Hardcover  
Also as an eBook



Research in bioprinting is summarized also by these authors active in the field, from the concept of tissue engineering over various approaches including computational design and simulation to potential applications.

### Electrochemistry of Carbon Electrodes

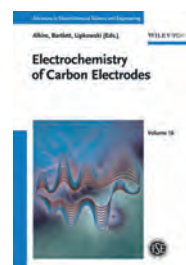
The goal of this book was to summarize the preparation techniques and specific characteristics of carbon-based electrodes together with their established as well as potential applications. First, a brief overview of carbon properties is given. Next chapters explore the state of the art in electrochemistry at highly oriented pyrolytic graphite, carbon nanotubes (including preparation of carbon nanotube paste electrodes with screen printing), graphene and conducting diamond. Remaining chapters are dedicated to various related technologies – namely to modification of carbon electrode surfaces, use of carbon materials in low-temperature polymer electrolyte membrane fuel cells, electrochemical capacitors based on carbon electrodes in aqueous electrolytes, utilization of carbon electrodes in electrochemical technology and in molecular electronics, carbon paste electrodes, and also screen-printed carbon electrodes.

This last chapter is written by Stephen Fletcher. After the introduction, the conductivity of composites, carbon polymorphs, oxygen functionalities, activated carbons, binder–solvent combinations, PVDF properties and solubility are described. Next sections introduce requirements on flexible substrates, screen printing process and materials, ink flow, substrate wetting, commercial ink additives and binder percentage. Finally, the multilayered electrodes, overcoming the IR drop (voltage drop due to energy losses in a resistor), areal capacitance and equivalent circuit are discussed.

Electrochemistry of Carbon Electrodes

Editors: Richard C. Alkire,  
Philip N. Bartlett, Jacek Lipkowski

Publisher: Wiley  
1<sup>st</sup> ed., October 2015  
ISBN: 978-3-527-33732-3  
472 pages  
Hardcover  
Available also as an eBook



### Handbook of Carbon Nano Materials

Volume 7: Synthetic Developments of Graphene and Nanotubes

Volume 8: Characterization, Conducting Polymer and Sensor Applications

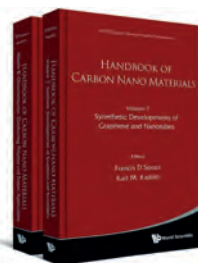
World Scientific Series on Carbon Nanoscience continues with Volume 7, dealing with synthesis of graphene, nanocarbon and multifunctional carbon nanostructures along with their appropriate characterization and applications, graphene quantum dots prepared by chemical vapour deposition, and synthesis and modification of the electronic structure of single-walled carbon nanotubes. Volume 8 contains five chapters on characterization, conducting polymer and sensor applications. The second one, written by S. Lawes, Q. Sun and X. Sun, is dedicated to the printing of graphene and carbon nanotubes for energy storage and conversion applications – lithium-ion batteries, supercapacitors, hydrogen fuel cells and solar cells.

Handbook of Carbon Nano Materials: Volume 7&8

Editors: Francis D'Souza (also an author), Karl M. Kadish

Publisher: World Scientific Publishing Co.

1<sup>st</sup> ed., October 2015  
ISBN: 978-981-4678-90-2  
500 pages  
Hardcover  
Available also as an eBook



# Bookshelf

## Academic dissertations

### Towards Industrial Viability of Organic Solar Cells: ITO-free, Green Solvents and Technological Aspects for Upscalability

The motivation for this dissertation, which builds upon recent extensive research of organic photovoltaics (OPV), is named in its title along with three key issues solved by the author. The presented approaches are intended to the broadest possible range of materials. After an overview of organic solar cells fundamentals and state-of-the-art, experimental methods and materials are introduced. The investigation toward large-scale processing and post-processing deals with inkjet printing as a roll-to-roll compatible technique. When aiming to achieve a suitable layer morphology, the drying kinetics has been found to be the most critical. A new method to determine appropriate printing patterns for active layer deposition was developed and the so called vapour printing was demonstrated as an alternative post-processing treatment that allows faster annealing of the active layer. Next part is focused on replacing halogenated solvents by 'green' formulations in active layer processing. In order to find suitable solvent systems, the Hansen solubility parameters analysis was successfully extended for small molecule based devices and later adapted to low band gap polymers. Finally, the replacement of indium-tin-oxide (ITO) to lower the cost of an OPV module and improve the flexibility and conductivity of its transparent electrode is investigated. The fabrication and optimization of devices with current collecting Ag grids is described, including the adapted model for determination of suitable grid geometries through estimated shadowing and resistive losses, and the preparation of grid structures using two different techniques, showing the inkjet printing as more robust for this application. Efficient ITO-free devices based on metallic grids were demonstrated.

Doctoral thesis – Summary

Author:  
*Ignasi Burgués Ceballos*

Speciality field:  
*Experimental Sciences*

Supervisors:  
*Mariano Campoy Quiles*  
*Paul Lacharmoise*

Defended:  
*17 June 2014*  
*at UAB / Department of Chemistry*  
*Barcelona, Spain*

Contact:  
*ignasi.burgues@cut.ac.cy*

### Color-Image Quality Assessment: From Metric to Application

This thesis contributes to the research in the field of image quality assessment, which is important for most image-processing systems. At present, mainly objective methods that utilize the image-difference metric are employed, predicting the perceived difference between a distorted image and a reference, while working only on the monochromatic intensity level to increase the computation speed. Color distortions and the influence of viewing conditions are thus neglected, although their impact on the perceived image quality may be significant.

First, the knowledge on visual psychophysics and color spaces is presented, as well as an overview of image quality and its objective assessment. Next, visual experiments needed to collect subjective data in order to gain information about perceived image quality are described. The image quality assessment databases are divided into two groups according the applied distortions – conventional and gamut-mapping ones. The main goal of the thesis was the development of a new image-difference metric with a modular framework which accounts for viewing conditions and color information. The images are normalized to standard viewing conditions using image-appearance model and represented in a working color space. The characteristic values for local image differences with respect to human perception are then extracted from lightness, chroma, and hue attributes. In the last step, these image-difference features are combined into Color-Image-Difference (CID) metric, yielding the best prediction performance

Doctoral thesis – Summary

Author:  
*Jens Preiss*

Speciality field:  
*Mechanical engineering*

Supervisors:  
*Philipp Urban*  
*Edgar Dörsam*  
*Michael Gesele*

Defended:  
*17 December 2014*  
*at TU Darmstadt / Institute of*  
*Printing Science and Technology*  
*Darmstadt, Germany*

Contact:  
*doersam@idd.tu-darmstadt.de*

for gamut-mapping distortions. Further increase of prediction accuracy on conventional distortions was achieved with an improved version denoted as iCID, which addresses individual artifacts occurring in CID-based gamut-mapping optimization (lightness inversion, chromatic ringing, chromatic edges, and lightness banding) by adjustment of CID metric parameters. Moreover, the modified metric did not require parameter training on an image quality assessment database. Resulting iCID-based gamut-mapping optimization significantly outperforms a state-of-the-art spatial gamut-mapping algorithm on a small newspaper gamut. The optimized images benefited from the preservation of local contrast, structure, and color of the original image to a great extent. The final part of the work deals with the concept of transforming high-dynamic-range images into low-dynamic-range devices' gamuts in a single step called high-dynamic-range gamut mapping. For this, an existing high-dynamic-range color space was adapted to an almost perceptually uniform color space called *hdr-LAB2000HL*.

Doctoral thesis – Summary

Author:  
*Janneke Adema*

Speciality fields:  
*Media Studies, Cultural Studies,  
Book History*

Supervisors:  
*Gary Hall  
Sarah Kember*

Defended:  
*7 April 2015 at Coventry University  
Coventry, United Kingdom*

Contact:  
*ademaj@uni.coventry.ac.uk*

### Knowledge Production Beyond The Book? Performing the Scholarly Monograph in Contemporary Digital Culture

The main argument made throughout this thesis is that there is a need to pay more attention to the way our scholarship, and the scholarly book specifically, is currently cut together-and-apart, or reconfigured, and for what reasons. Academics themselves are appealed to examine and critique their entanglement with the book, both through their scholarly communication practices and the systems that sustain them. Scholars should start thinking and performing the apparatus of the book otherwise, in a potentially more ethical way, as part of a reconceptualisation of the book to come, and alongside an ongoing review of scholarly identity.

Current experiments with forms of unbinding, such as remix, openness and liquidity, and their potential to cut the book together-apart differently on the basis of alternative values and criteria, are analysed. The thesis itself is an experiment in making affirmative incisions into the book apparatus, following a methodology of critical praxis. Instead of simply conforming to and repeating established practices with respect to writing a thesis – without analysing the assumptions and perceptions upon which they are based – the author has adopted a digital and open research practice to focus on the processual nature of the research. Different ways of versioning the thesis during its development have included – and will include – the use of a weblog, various open archiving media and a hypermedia platform. Versioning the research in this way serves as a critique of the continued emphasis on the end-result of research as well as the object-centred publication approach promoted by publishers, universities and funders alike.

The thesis shows why it is important at this specific point in time to imagine a different future for the scholarly book. First of all, because monographs are endangered at the moment – and certain specialised, experimental and difficult instantiations of the monograph in particular. Hegemonic communication power structures play an important part here, focusing more on increasing reputation and reward for their stakeholders than on promoting access to and reuse of scholarly research for the public at large. Furthermore, this is also a key moment to imagine a different future for the book because the digital provides an opportune context in which to re-examine print-based and humanist communication systems, practices and discourses. This is the case especially with respect to how these humanist systems and practices continue to determine authorship practices, material systems of knowledge production, and conceptions of the inherent affordances or essential material features of the book (i.e. fixity, authority, originality and trust).

# Events

## SPIE Applications of 3D Printing 2016

**SPIE. PHOTONICS WEST 3D PRINTING** San Francisco, California, USA  
13–18 February 2016

This event, aimed on innovative ways to apply the multidimensional and multidisciplinary technology of 3D printing, is a part of SPIE Photonics West and highlights almost 100 papers from numerous conferences being part of BiOS, LASE, and OPTO co-located events. Presentations topics include additive manufacturing, selective laser melting, maser sintering, laser photopolymerization, novel materials, protean materials, and laser interactions, software that increases efficiencies and speed, in-situ sensors or probes to verify and quantify additive manufacturing processes in real time, and conformal photonics/electronics. Among the industry events, the session '3D printing: A manufacturing revolution' is organized as well.

## IS&T International Symposium on Electronic Imaging 2016

San Francisco, California, USA  
14–18 February 2016

**IS&T International Symposium on Electronic Imaging**  
SCIENCE AND TECHNOLOGY

The program of the 28<sup>th</sup> annual Electronic Imaging Symposium of the Society for Imaging Science and Technology consists of 20 technical conferences with 12 planned joint sessions, complemented by 17 short courses, technology demonstrations, and a focused exhibition. For the first time, all accepted full papers will be available for free download via the IS&T Digital Library on the IngentaConnect platform.

Human vision and electronic imaging 2016 will focus on human perception and cognition for emerging technologies. Various aspects of image capture systems will be covered by Digital photography and mobile imaging XII, Image sensors and imaging systems 2016, and Mobile devices and multimedia: enabling technologies, algorithms, and applications 2016 conferences. Image reproduction and material appearance issues will be discussed within Color imaging XXI: displaying, processing, hardcopy, and applications as well as Measuring, modeling, and reproducing material appearance 2016. Another two conferences, Document recognition and retrieval XXIII and Media watermarking, security, and forensics 2016, will aim at document processing and media security. Even four conferences are dedicated to image and video processing, quality, and systems – Computational imaging XIV, Image processing: algorithms and systems XIV, Image quality and system performance XIII, and Visual information processing and communication VII. Virtual and augmented reality, 3D, and stereoscopic systems will be covered by three conferences – 3D image processing, measurement (3DIPM), and applications 2016, The engineering reality of virtual reality 2016, and Stereoscopic displays and applications XXVII. Image processing: machine vision applications IX and Intelligent robots and computer vision XXXIII: algorithms and techniques are reserved for real-time image and video. Finally, web and mobile imaging and visualization will be the topic of Imaging and multimedia analytics in a web and mobile world 2016, Video surveillance and transportation imaging applications 2016, and Visualization and data analysis 2016.

## Gravure at Your Fingertips

Stuttgart, Germany  
10–12 February 2016

HOCHSCHULE DER MEDIEN



The European Rotogravure Association (ERA) in cooperation with Stuttgart Media University organizes again a seminar providing an introduction to gravure cylinder preparation and printing with demonstrations as well as practical exercises. Stuttgart Media University operates a complete gravure line, allowing to experience all aspects of gravure from the galvanics for copper plating of a cylinder, through surface processing and finishing, preparation of a layout and the subsequent electromechanical engraving process, to printing on several papers with different ink viscosities, and to test the quality of all production steps with special measuring methods.

## Colour Management Symposium

Munich, Germany  
18–19 February 2016



The latest information about current trends and

challenges in the area of colour communication will be presented at the fifth Colour Management Symposium organized by Fogra.

One of the main topics will be the migration from FOGRA39 to FOGRA51 based workflows related to the revision of ISO 12647-7:2013 'Graphic technology – Process control for the production of half-tone colour separations, proof and production prints – Part 7: Proofing processes working directly from digital data', which is at the moment in the stage of registered draft International Standard (DIS). During the social evening event, Karl Gegenfurtner will give a keynote introducing the visual and mental aspects of colour perception.

## WAN-IFRA Events



### Ad Blocking Action Day

Frankfurt, Germany  
11 February 2016

This one-day conference will feature case studies on actions taken by publishers to improve user experience and create quality ad content, along with economic implications. Ad blocking is a challenge to online business models, but if appropriately addressed, it is also an opportunity to increase the audience trust.

### Digital Media India 2016 Conference

New Delhi, India  
22–23 February 2016



The 5<sup>th</sup> edition of Digital Media India will pay attention to engaging the mobile audience, the audience data analytics that enables to serve the readers better, digital advertising and ad blockers, social media challenges, and online video situation in India.

### WAN-IFRA Middle East Conference 2016

Dubai, UAE  
24–25 February 2016



WAN-IFRA's 11<sup>th</sup> Middle East Conference will enable publishing executives to discover the Internet of Things, virtual reality, ad blocking, wearables, or 3D printing, with new and emerging business models for newspaper printing companies. The best practices from newspapers around the globe related to the diversification of revenue streams will be shared, as well as experiences with inkjet printing of newspapers, print outsourcing and value added printing.

In regard to virtual and augmented reality, the use of sensor technology in interactive and immersive storytelling will be explored, utilizing e.g. registration of movements

## VISIGRAPP 2016

Rome, Italy  
27–29 February 2016

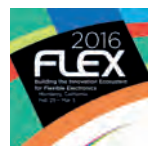


The purpose of VISIGRAPP annual event is to network researchers and practitioners interested in both theoretical advances and applications of computer vision, computer graphics and information visualization. VISIGRAPP is composed of three international conferences – GRAPP on computer graphics theory and applications, IVAPP on information visualization theory and applications, and VISAPP on computer vision theory and applications. Besides regular research papers and so called position papers, presenting an arguable opinion about an issue the author considers relevant, the program offers workshops, special sessions, tutorials and also four keynote lectures, including that on 'Trends and challenges of augmented reality' by Dieter Schmalstieg.

Another co-located event is PHOTOPTICS 2016 conference featuring tracks on optics, photonics and lasers. The topics include e.g. vision and colour, display technology and holography, or semiconductor lasers and LEDs.

## 2016FLEX

Monterey, California, USA  
29 February to 3 March 2016



This conference & exhibition is aimed at the latest breakthroughs and developments in flexible, printed and hybrid electronics and their applications. Its 15<sup>th</sup> volume starts on Monday with short courses; in the technical program, two plenary sessions are followed by 24 sessions in three tracks.

Participants can choose from five three-hour courses. The first will introduce printed electronics – related market segments, manufacturing strategies, technologies used for printed electronics production – and how to become a functional printer. The concurrent one is named 'Getting ready for readiness levels: fundamentals of TRLs and MRLs', which are abbreviations of Technology Readiness Levels pioneered by NASA to assess stages of development for emerging technologies, and Manufacturing Readiness Level built by the Air Force as a complimentary assessment tool to evaluate stages of manufacturing readiness, respectively. This course will teach participants to perform a detailed TRL/MRL assessment of emerging technologies to enhance and accelerate transition to prototypes and products. The afternoon courses are dedicated to basics of hybrid electronics, stretchable textiles and fibers plus electronics, and workshop on 3D printing of engineering thermoplastics.

The lectures of the Flex conference will cover a wide range of topics – the technology and roadmaps, flexible materials, dielectrics, substrates, barriers, encapsulation, patterning, modelling, simulation, and applications like displays, lighting, photovoltaics, batteries, sensors or backplanes. Sessions dealing with flexible and hybrid electronics will discuss related technology, opportunities, applications, design and manufacturing. Similarly, the topics on printed electronics will focus on tools, methods, in-line processing, and energy harvesting, radio frequency and bio applications. Within plenary lectures, e.g. 'Building self-diagnostic fly-by-feel vehicles with stretchable, flexible sensors and electronics network' can be highlighted.

## Forum & INFO\*FLEX



Fort Worth, Texas, USA  
6–9 March 2016

Annual Forum of Flexographic Technical Association builds upon its long tradition and strives to provide conference attendees with the tools, techniques and knowledge to remain competitive. Forum 2016 offers ten technical sessions as well as one free preconference session.

In the preconference session, the roles and activities of brand owners, design artists, prepress and press personnel will be explained and demonstrated. Further, simplification of ISO 16761-2 combined with CRPC (Characterized Reference Printing Condition) profiles and implementing the PDF workflow using standard procedures will be introduced.

The first technical session aims to provide an understanding of FIRST (Flexographic Image Reproduction Specifications & Tolerances) and what the print buyers expect in terms of print quality. After the 'Hall of fame' panel discussion, new tools for prepress workflows will be presented in the last Sunday session. Next day, '2016 flexo game changers' session will focus on technologies enabling to maintain the innovative edge in flexography, and then the FQC (Flexo Quality Consortium) session will highlight current research, including evolving industry standards. The third day will start by the session on enhancing digital print with flexography and continue with two panel discussions – 'Flexo international: 60 minutes around the world' and 'Direct engraving: yesterday, today & tomorrow'. The last two sessions will provide fundamental concepts and core terminology of the flexographic process, as well as the steps necessary to take control over the print quality – through calibration, optimization, fingerprinting, and characterization.

Nearly 300 exhibitors, ranging from press manufacturers over converting equipment providers to process control experts, will showcase their solutions at the co-located INFO\*FLEX exhibition through large-scale as well as one-on-one demonstrations to prospective customers.

## FESPA Digital 2016

Amsterdam, Netherlands  
8–11 March 2016



Same as the FTA's Forum mentioned above, FESPA Digital is scheduled earlier in 2016 due to drupa. FESPA celebrates the 10<sup>th</sup> year anniversary of the show for wide format digital and textile print, which is returning to Amsterdam. Presented industry sectors include inkjet technology, 3D printing, industrial printing, sublimation and transfer printing with wide and narrow format machinery, consumables and inks, as well as pre-press, design, print and business management software or trade services.



FESPA Digital Textile Conference 2016 will be organized on March 8<sup>th</sup> and a celebration gala dinner of FESPA Awards 2016 the day after. During all four days of FESPA Digital, joint events European Sign Expo, FESPA Textile, and Printeriors can be attended.

and even current emotional state of mind. The Internet of Things will be discussed from the perspective of marketing transformation due to digital innovation and best practices, highlighting how technology, creativity and new media combine to actively engage the changing consumer.

## Publish Asia 2016

Manila, Philippines  
29–31 March 2016



Since 2000, Publish Asia gathers the Asian newspaper and news publishing industry. Besides standard topics covered by other World Association of Newspapers and News Publishers conferences, also the investigative journalism in Asia will be considered, including challenges to press freedom and journalists' safety.

## ETRA 2016 – Symposium on Eye Tracking Research & Application



Charleston,  
South Carolina, USA  
14–17 March 2016

The 9<sup>th</sup> biennial symposium focusing on all aspects of eye movement research across a wide range of disciplines is organized to bring together computer scientists, engineers and behavioural scientists. In addition to presentation of full or short papers and posters, ETRA offers three full-day tutorials: 'Eye-tracking and visualization', 'Mining scanpath sequences with R and TraMineR packages: A hands-on introduction', and 'Eye data quality: measuring, calculating, and reporting'.

## Laval Virtual



Laval, France  
23–27 March 2016

Since 1999, Laval Virtual introduces the advances in technology behind virtual and augmented reality, which enable innovations in a number of business sectors, including industry, medicine, training and marketing. VRIC 2016 conference will feature presentations and six workshops.

## Packaging Innovations Birmingham 2016

Birmingham, UK  
24–25 February 2016



In its 10<sup>th</sup> year, the Packaging Innovations show again features several co-located events for the packaging industry, which is expected to deliver ever more highly visible, exciting and engaging packaging while being more environmentally friendly. Ecopack area is dedicated to environmentally responsible packaging, while Contract Pack exhibition organized since 2008 is aimed on the contract packing and manufacturing industry.

Empack 2016 showcases packaging machinery, equipment, logistical and transit packaging, industrial packaging and robotics and automation. Label&Print 2016 tracks the latest developments in digital printing, flexography, labelling equipment, 3D print, labels and labelling, offset, gravure and active or intelligent packaging, serving to major growth areas of the packaging industry.

## Printing South China and Sino Label 2016

Guangzhou, China  
2–4 March 2016



The major keywords of this year's fair, which aims to lead the upgrading and innovation of Chinese printing industry, are automation, intelligence, efficiency and green.

Sino Label is an international exhibition covering the label printing, decoration, processing and technological applications.

## TAGA 68<sup>th</sup> Annual Technical Conference

Memphis, Tennessee, USA  
20–23 March 2016

The main scope of this traditional conference, organized by the Technical Association of the Graphic Arts, rests in graphic arts systems, software, and computer technology developments or evaluation, as well as innovative applications in the more traditional areas of press, ink, and paper engineering. The event encompasses a range of diverse topics, such as colour management, data management, workflow, materials, packaging, curing, process control, security, micro- and nanotechnology, printed electronics, and fundamental science, presented through scientific and technical innovation papers, reporting laboratory research as well as pressroom studies or software and systems engineering projects. TAGA's agenda aims on managers, material specialists, manufacturers, publishers, educators, researchers and engineers active in the area of graphic arts and related fields.



To date, the program offers three keynotes, with the fourth to be determined. In the first one, Mike D'Angelo will present web offset as the dominant unknown printing process for converting and packaging. Web offset, which has proven as a high quality, consistent print process, did recently step aside because converters' interest was captured by high speed digital printing. However, it has not delivered on the promise; therefore, it's seen as worth to take another look at web offset, offering more solutions through evolutions in ink and colour technology than ever. Next, continuous progress of inkjet printing that migrates and gains acceptance into all segments of print production will be reported by Don Schroeder. The goal of the third keynote is clearly expressed by its title – 'Down the rabbit hole: Chasing the Internet of Things' (IoT). Kevin Berisso will share his attempts to better determine this wide ranging concept that often means different things to different people, with tens of differing definitions and the potential to touch every aspect of our existence and impacting everything from the power grid to healthcare, manufacturing processes to communications and everything in between.

Scientific and technical innovation papers will be organized in two parallel tracks, both days framed by plenary sessions and concluded by so called technical focus sessions. The latter will be dedicated to colour on Monday and to ink and paper on Tuesday. As the examples illustrating the diversity of presented topics, the contributions on 'Evaluating the impact of printing, color reproduction, and screening technologies on image preference', 'A model for the cost analysis of inkjet, flexographic, offset and electrophotographic printing processes', 'Color management with OBAs – theory and practice', 'Metrology for 3D printing: assessing methods for the evaluation of 3D printing products', 'Resistive gravure inks made with soy protein', and 'Using wide format UV ink-jet printing for digital package prototyping' can be mentioned.

TAGA also supports high-quality student publications. Competition deadlines are set like this: 15 January 2016 for Harvey Levenson Undergraduate Student Paper Award and the Dusty Rhodes Graduate Student Paper Award; in case of Helmut Kipphan Student Publication Award it is 29 January 2016 for formatted PDF of journal, electronic publication, eBook, interactive PDF or web page, and 20 March 2016 for submission of printed journals for final judging on the first day of the TAGA Annual Conference.

# Call for papers

The Journal of Print and Media Technology Research is a peer-reviewed periodical, published quarterly by **iarigai**, the International Association of Research Organizations for the Information, Media and Graphic Arts Industries

JPMTTR is listed in Index Copernicus, PiraBase and PaperBase (by Smithers Pira) and NSD – Norwegian Register of Scientific Journals, Series.

Authors are invited to prepare and submit complete, previously unpublished and original works, which are not under review in any other journals and/or conferences.

The journal will consider for publication papers on fundamental and applied aspects of at least, but not limited to, the following topics:

- ⊕ Printing technology and related processes  
Conventional and special printing; Packaging; Fuel cells and other printed functionality; Printing on biomaterials; Textile and fabric printing; Printed decorations; Materials science; Process control
- ⊕ Premedia technology and processes  
Color reproduction and color management; Image and reproduction quality; Image carriers (physical and virtual); Workflow and management
- ⊕ Emerging media and future trends  
Media industry developments; Developing media communications value systems; Online and mobile media development; Cross-media publishing
- ⊕ Social impact  
Environmental issues and sustainability; Consumer perception and media use; Social trends and their impact on media

Submissions for the journal are accepted at any time. If meeting the general criteria and ethic standards of scientific publishing, they will be rapidly forwarded to peer-review by experts of high scientific competence, carefully evaluated, selected and edited. Once accepted and edited, the papers will be printed and published as soon as possible.

There is no entry or publishing fee for authors. Authors of accepted contributions will be asked to sign a copyright transfer agreement.

Authors are asked to strictly follow the guidelines for preparation of a paper (see the abbreviated version on inside back cover of the journal). Complete guidelines can be downloaded from:

<http://www.iarigai.org/publications/>

Papers not complying with the guidelines will be returned to authors for revision.

Submissions and queries should be directed to:

[journal@iarigai.org](mailto:journal@iarigai.org)

# Vol.5, 2016

## Prices and subscriptions

Journal of Print and Media Technology Research  
A peer-reviewed quarterly ISSN 2223-8905

Starting with 2016 the journal is published in digital form.  
Print version is available on-demand and at additional price.

Please, find below the prices of the Journal as well as of a single paper.  
Use the opportunity to benefit from the Subscriber's discount price!

By ordering a publication or by subscription a password will be provided to you  
for downloading. The password protection of every issue is active during  
the six months period. After this period the publications will be available for free.

**iarigai** members will get the download password for free!

---

### Regular prices

Four issues, digital JPMTR, (password protected)	300 EUR
Single issue, digital JPMTR, (password protected)	100 EUR
Single paper from JPMTR, (pdf file)	20 EUR
Four issues, print JPMTR, (on-demand)	400 EUR
Single issue, print JPMTR, (on-demand)	100 EUR

---

### Subscription prices

Annual subscription, four issues, digital JPMTR, (password protected)	240 EUR
Annual subscription, four issues, print JPMTR, (on-demand)	400 EUR

---

### Prices for **iarigai** members

Four issues, digital JPMTR, (password protected)	Free of charge
Single paper from JPMTR, (pdf file)	Free of charge
Four issues, print JPMTR, (on-demand)	400 EUR
Single issue, print JPMTR, (on-demand)	100 EUR

---

Place your order online at:

<http://www.iarigai.org/publications> (open: Order/Subscribe here)

or send an e-mail order to: [journal@iarigai.org](mailto:journal@iarigai.org)

## Guidelines for authors

Authors are encouraged to submit complete, original and previously unpublished scientific or technical research works, which are not under review in any other journals and/or conferences. Significantly expanded and updated versions of conference presentations may also be considered for publication. In addition, the journal will publish reviews as well as opinions and reflections in a special section.

Submissions for the journal are accepted at any time. Papers will be considered for publishing if meeting the general criteria and ethic standards of the scientific publication. When preparing a manuscript for JPMRT, please strictly comply with the journal guidelines, as well as with the ethic aspects. The Editorial Board retains the right to reject without comment or explanation manuscripts that are not prepared in accordance with these guidelines and/or if the appropriate level required for scientific publishing cannot be attained.

### A - General

The text should be cohesive, logically organized, and thus easy to follow by someone with common knowledge in the field. Do not include information that is not relevant to your research question(s) stated in the introduction.

Only contributions submitted in English will be considered for publication. If English is not your native language, please arrange for the text to be reviewed by a technical editor with skills in English and scientific communication. Maintain a consistent style with regard to spelling (either UK or US English, but never both), punctuation, nomenclature, symbols etc. Make sure that you are using proper English scientific terms.

Do not copy substantial parts of your previous publications and do not submit the same manuscript to more than one journal at a time. Clearly distinguish your original results and ideas from those of other authors and from your earlier publications - provide citations whenever relevant. For more details on ethics in scientific publication, please consult:

<http://www.elsevier.com/ethicguidelines>.

If it is necessary to use an illustration, diagram, table, etc. from an earlier publication, it is the author's responsibility to ensure that permission to reproduce such an illustration, diagram etc. is obtained from the copyright holder. If a figure is copied, adapted or redrawn, the original source must be acknowledged.

Submitting the contribution to JPMTR, the author(s) confirm that it has not been published previously, that it is not under consideration for publication elsewhere and - once accepted and published - it will not be published under the same title and in the same form, in English or in any other language. The published paper may, however, be republished as part of an academic thesis to be defended by the author. The publisher retains the right to publish the printed paper online in the electronic form and to distribute and market the Journal (including the respective paper) without any limitations.

### B - Structure of the manuscript

**Title:** Should be concise and unambiguous, and must reflect the contents of the article. Information given in the title does not need to be repeated in the abstract (as they are always published jointly).

**List of authors:** i.e. all persons who contributed substantially to study planning, experimental work, data collection or interpretation of results and wrote or critically revised the manuscript and approved its final version. Enter full names (first and last), followed by the present address, as well as the e-mail addresses.

Separately enter complete details of the corresponding author - full mailing address, telephone and fax numbers, and e-mail. Editors will communicate only with the corresponding author.

*The title of the paper and the list of authors should be entered on a separate cover page (numbered as 0). Neither the title nor the names of authors can be mentioned on the first or any other following page.*

**Abstract:** Should not exceed 500 words. Briefly explain why you conducted the research (background), what question(s) you answer (objectives), how you performed the research (methods), what you found (results: major data attained, relationships), and your interpretation and main consequences of your findings (discussion, conclusions). The abstract must reflect the content of the article, including all the keywords, as for most readers it will be the major source of information about your research. Make sure that all the information given in the abstract also appears in the main body of the article.

**Keywords:** Include three to seven relevant scientific terms that are not mentioned in the title. Keep the keywords specific. Avoid more general and/or descriptive terms, unless your research has strong interdisciplinary significance.

*Abstract and keywords should be entered on a separate page, numbered as page 1. Do not continue with the main body of the text, regardless of the possible empty space left on this page.*

### D - Submission of the paper and further procedure

Before sending your paper, check once again that it corresponds to the requirements explicated above, with special regard to the ethic issues, structure of the paper as well as formatting. Once completed, send your paper as an attachment to: [journal@iarigai.org](mailto:journal@iarigai.org). You will be acknowledged on the receipt within 48 hours, along with the code under which your submission will be processed. The editors will check the manuscript and inform you whether it has to be updated regarding the structure and formatting. The corrected manuscript is expected within 15 days. At the same time the first (or the corresponding) author will be asked to sign and send the Copyright Transfer Agreement.

Your paper will be forwarded for anonymous evaluation by two experts of international reputation in your specific field. Their comments and remarks will be in due time disclosed to the author(s), with the request for changes, explanations or corrections (if any) as demanded by the referees. After the updated version is approved by the reviewers, the Editorial Board will consider the paper for publishing. However, the Board retains the right to ask for a third independent opinion, or to definitely reject the contribution. Printing and publishing of papers once accepted by the Editorial Board will be carried out at the earliest possible convenience.

**Introduction and background:** Explain why it was necessary to carry out the research and the specific research question(s) you will answer. Start from more general issues and gradually focus on your research question(s). Describe relevant earlier research in the area and how your work is related to this.

**Methods:** Describe in detail how the research was carried out (e. g. study area, data collection, criteria, origin of analyzed material, sample size, number of measurements, equipment, data analysis, statistical methods and software used). All factors that could have affected the results need to be considered. Make sure that you comply with the ethical standards, with respect to the environmental protection, other authors and their published works, etc.

**Results:** Present the new results of your research (previously published data should not be included). All tables and figures must be mentioned in the main body of the article, in the order in which they appear. Do not fabricate or distort any data, and do not exclude any important data; similarly, do not manipulate images to make a false impression on readers.

**Discussion:** Answer your research questions (stated at the end of the introduction) and compare your new results with the published data, as objectively as possible. Discuss their limitations and highlight your main findings. At the end of Discussion or in a separate section, emphasize your major conclusions, specifically pointing out scientific contribution and the practical significance of your study.

**Conclusions:** The main conclusions emerging from the study should be briefly presented or listed, with the reference to the aims of the research and/or questions mentioned in the Introduction and elaborated in the Discussion.

*Introduction, Methods, Results, Discussion and Conclusions - as the scientific content of the paper - represent the main body of the text. Start numbering of these sections with page 2 and continue without interruption until the end of Conclusions. Number the sections titles consecutively as 1, 2, 3 ..., while subsections should be hierarchically numbered as 2.1, 2.3, 3.4 etc. Use Arabic numerals only.*

**Note:** Some papers might require different structure of the scientific content. In such cases, however, it is necessary to clearly name and mark the appropriate sections.

**Acknowledgments:** Place any acknowledgments at the end of your manuscript, after conclusions and before the list of literature references.

**References:** The list of sources referred to in the text should be collected in alphabetical order on a separate page at the end of the paper. Make sure that you have provided sources for all important information extracted from other publications. References should be given only to documents which any reader can reasonably be expected to be able to find in the open literature or on the web. The number of cited works should not be excessive - do not give many similar examples. Responsibility for the accuracy of bibliographic citations lies entirely with the authors.

Please use only the Harvard Referencing System. For more information consult, e. g., the referencing guide at:

<http://libweb.anglia.ac.uk/referencing/harvard.htm>.

**List of symbols and/or abbreviations:** If non-common symbols or abbreviations are used in the text, you can add a list with explanations. In the running text, each abbreviation should be explained the first time it occurs.

**Appendix:** If an additional material is required for better understanding of the text, it can be presented in the form of one or more appendices. They should be identified as A, B, ... etc., instead of Arabic numerals.

*Above sections are supplementary, though integral parts of the Scientific content of the paper. Each of them should be entered on a separate page. Continue page numbering after Conclusions.*

### C - Technical requirements for text processing

For technical requirement related to your submission, i.e. page layout, formatting of the text, as well of graphic objects (images, charts, tables etc.) please see detailed instructions at <http://www.iarigai.org/publications/journal>.

# 4-2015

## Journal of Print and Media Technology Research

A peer-reviewed quarterly

The journal is publishing contributions  
in the following fields of research:

- ⊕ Printing technology and related processes
- ⊕ Premedia technology and processes
- ⊕ Emerging media and future trends
- ⊕ Social impacts

For details see the Mission statement inside

JPMTR is listed in

Index Copernicus International

PiraBase and PaperBase  
(by Smithers Pira)

NSD – Norwegian Register for  
Scientific Journals, Series and Publishers

Submissions and inquiries  
[journal@iarigai.org](mailto:journal@iarigai.org)

Subscriptions  
[office@iarigai.org](mailto:office@iarigai.org)

More information at  
[www.iarigai.org/publications/journal](http://www.iarigai.org/publications/journal)



### Publisher

The International Association of Research  
Organizations for the Information, Media  
and Graphic Arts Industries  
Magdalenenstrasse 2  
D-64288 Darmstadt  
Germany

Printed in Slovenia by Collegium Graphicum, d. o. o. Ljubljana

